



Ss. Cyril and Methodius University – Skopje  
Faculty of Civil Engineering - Skopje



Candidate: Aleksandra Chubrinovska

Dossier No: 1055

# ANALYSIS OF COMPOSITE BOX GIRDER IN BRIDGES WITH DISTORTION EFFECTS

Master's Thesis

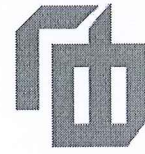
Mentor,  
Assoc. Prof. Denis Popovski PhD

Skopje, 06.2023





Ss. Cyril and Methodius University – Skopje  
Faculty of Civil Engineering - Skopje



Candidate: Aleksandra Chubrinovska

Dossier No: 1055

# ANALYSIS OF COMPOSITE BOX GIRDER IN BRIDGES WITH DISTORTION EFFECTS

Master's Thesis

Mentor,  
Assoc. Prof. Denis Popovski PhD

Skopje, 06.2023





## DATA AND INFORMATION ABOUT THE MASTER'S STUDENT

---

Name and surname	Aleksandra Chubrinovska
Date and place of birth	27.09.1993, Skopje, Macedonia
Title of completed studies, study program and year of completion	First cycle of studies at the Faculty of Civil Engineering in Skopje, Civil Engineering, 2010

---

## INFORMATION ON THE MASTER'S THESIS

---

Title of studies, study program	Second cycle of studies at the Faculty of Civil Engineering in Skopje, Structures
Title of the Master's Thesis	Analysis of composite box girder in bridges with distortion effects
Faculty where the Master's Thesis is submitted	Faculty of Civil Engineering in Skopje
Date of application of the Master's Thesis	03.04.2023
Committee for Eligibility Evaluation of Master's Thesis and Candidate	Assoc. prof. Denis Popovski PhD Prof. Goran Markovski PhD Asst. prof. Mile Partikov PhD
Committee for defense of the Master's Thesis	Assoc. prof. Denis Popovski PhD Prof. Goran Markovski PhD Asst. prof. Mile Partikov PhD
Mentor	Assoc. prof. Denis Popovski PhD
Date of Master's Thesis defense	00.06.2023

---



## FOREWORD: EXPRESSION OF APPRECIATION OR DEDICATION

Initially, I extend my gratitude to God for bestowing both evident and concealed blessings and endowments. Subsequently, I convey my deep appreciation for the moral support and technical help during the preparation of this Master's Thesis. My heartfelt acknowledgements are directed towards my parents, the guiding presence of my mentor Prof. Denis Popovski, the esteemed professors Goran Markovski, Toni Arangjelovski, Mile Partikov and my colleagues and friends.

Sincerely,

Aleksandra Chubrinovska



## АПСТРАКТ

---

„Ние градиме премногу сидови, а нема доволно мостови“ - Исак Њутн.

Симболот на мостовите е поврзан со човечките желби и аспирации да се поврзат, да истражуваат, да достигнуваат... сето тоа на крајот го означува внатрешниот татнеж на вечната потрага по смислата на животот. По кој од двата моста ќе одлучи да оди Човекот, ако не по оној вистинскиот-вербата. Бидејќи вербата преставува мост, мост помеѓу она каде сум сега и каде Бог ме води и каде сака да сум...Дали ова не е доволно за да се направи првиот чекор низ невидливиот сид на непознатото? Зборувајќи во инженерска смисла, оваа мисла ќе ја осветли желбата да се постигне се повеќе и повеќе.

Некако слеано со горе кажаното мостовските конструкции општо а особено оние со сандачести главни носачи од секогаш биле многу популарни, пред сè поради нивната подобност, подобност која произлегува од високиот степен на торзиона и флексиона крутост. Но, не бивајќи совршени, како што и ништо овоземно не е совршено, несиметричното натоварување кај сандачестите носачи предизвикува појава не само на подолжно свиткување туку и на торзија и дисторзија, двете придружени со појава на витоперење. За тенкосидни носачи, причински последично поврзано со нивната „физиономија“ дисторзијата претставува значајна појава која има влијание врз севкупниот одговор на конструкцијата. Сепак, истражувањата на тема дисторзионен одговор кај сандачестите спрегнати носачи се во лимитиран број поради комплексноста на проблематиката. Инспирирани од комплексноста и од кажаното „Сè што некогаш си посакувал се наоѓа од другата страна на стравот, и сè што треба е да го поминеш мостот!“, се дава практичен пристап пристап за истражување на дисторзиониот одговор кај спрегнатите сандачести носачи. Следствено, бидејќи станува збор за спрегнат носач ќе биде земена и соодветно вклучена во анализата разликата во крутосните карактеристики помеѓу горниот бетонски појас и долниот челичен појас, преку дефинирање на два различни дисторзиони агли, агли кој логички произлегуваат од деформацијата напречна на пресекот. А, што преставува друго деформацијата ако не вистинскиот одговор на конструкцијата за кој се пропишуваат параметри со цел негово појаснување. Како се стига до одговорот на сандачестиот носач? Преку два пристапи. Едниот е оној таканаречениот аналитички во кој се изнесуваат фундаменталните равенки за дисторзија, детерминирани преку теоријата за тенкосидни носачи и аналогитата-Beam on Elastic Foundation. Се дефинира деформираните облик и дистрибуцијата на напрегања предизвикани од самата појава на дисторзија. Вториот пристап пак се базира на метод на конечни елементи, каде користејќи ги можностите на софтверскиот пакет „ABAQUS“ се доаѓа до деформираната состојба на разгледуваниот сегмент од носачот, при што се добиваат и распределбите на напрегања. Сето ова се спроведува на еден спрегнат сандачест носач дефиниран како проста греда и се порврдува преку тридимензионална анализа со конечни елементи.

Извршена е споредби помеѓу двата методи во однос на теоретската позадина и добиените резултати. При тоа, се предлага нов, практичен метод за истражување на дисторзионото одневање на спрегнатите сандачести носачи, и за согледување на распределбата на напрегањата кај носачите земајќи го предвид влијанието на различната крутост која ја дава бетонската плоча. И како резултат на сето ова се дава инспирација за натамошни истражувања на „реални“ лабораториски мини модели за да се добија поверодостојна критичка споредба на резултатите добиени преку теоритски, нумерички пристап и оние од испитувањето.

Клучни зборови: спрегнати сандачести носачи; агол на дисторзија; витоперење; можданици; носивост на смолкнување; BEF аналогитата.



## ABSTRACT

---

"We build too many walls and not enough bridges."-Isaac Newton.

The symbol of bridges is associated with human desires and aspirations to connect, to explore, to achieve... all of which ultimately signify the inner rumbling of the eternal search for the meaning of life. On which of the two bridges will Man decide to go, if not on the right one - faith. Because faith is a bridge, a bridge between where I am now and where God is leading me and where He wants me to be...

Is this not enough to make the first step through the invisible wall of the unknown? Talking in engineering sense this thought shall light up the desire of achieving more and more.

Somewhat merged with the above, bridge constructions in general and especially those with box main girders have always been very popular, first of all because of their suitability, suitability resulting from the high degree of torsional and flexural stiffness. But not being perfect, just as nothing on earth is perfect, the asymmetric loading of box girders causes not only longitudinal bending, but also torsion and distortion, both accompanied by warping. For thin-walled beams, causally related to their "physiognomy", distortion is a significant phenomenon that has an impact on the overall response of the construction. So, asymmetrical loads on box girder bridge decks cause not only bending but also torsion with warping and distortion of the cross-section. The latter two may prove to be relevant for the longitudinal analysis and design of the deck but their effects within the overall structural behaviour are difficult to assess using shell finite element models. However, the researches on the distortional behavior of composite box girders are limited due to its complexity. Inspired by the complexity and knowing that everything we've ever wanted is on the other side of fear, and all we have to do is cross the bridge, a practical approach to investigating the distortion response of coupled box girders is given. This study is to propose a practical approach to investigate the distortional behavior and get the accurate stress distribution of composite box girders. Considering the differences of stiffness between the top concrete plate and the bottom steel flange, two different distortional angles  $\Theta$  are assumed at the top and bottom corners of the composite cross section, respectively. Then, the fundamental differential equations of distortion are derived by using energy methods based on the thin-walled beam theory and solved with BEF (Beam on Elastic Foundation) analogy. Both the deformation and the accurate stress distribution of the composite box girder due to distortion are obtained. And to approve the reliability of the analytical approach, a simply supported composite box girder is analyzed and verified by three-dimensional finite-element analyses in software package "ABAQUS". That has been made to shown the simplicity and economical aspect of the analytical approach which provides a distinct insight into the structural response of composite box girders due to distortion.

Comparisons were made between the two methods in terms of the theoretical background and the results obtained. In doing so, a new, practical method is proposed for investigating the distortional behavior of the composite box girders, and for understanding the distribution of stresses in the girders, taking into account the influence of the different stiffness provided by the concrete slab. And as a result of all this inspiration is given for further research on "real" laboratory mini-models to obtain a more reliable critical comparison of the results obtained through a theoretical, numerical approach and those of the test

Keywords: composite box girder, distortional angle, warping, shear connectors, shear capacity, BEF analogy.



## TABLE OF CONTENTS

---

Foreword: Expression of appreciation or dedication.....	<b>Error! Bookmark not defined.</b>
Анстракт .....	V
Abstract .....	VI
Table of contents.....	VII
List of symbols .....	<b>Error! Bookmark not defined.</b>
Latin letters .....	X
Greek letters.....	XVI
List of figures .....	XX
List of tables .....	XXI
1. Introduction.....	1
1.1 Scientific justification of the topic.....	1
1.2 Aim of the research .....	2
1.3 Research methodology.....	4
1.4 Brief content of the paper .....	4
2. Methods of analysis for box girders bridges .....	6
2.1 General overview of the problem .....	6
2.1.1 Box girders under construction.....	6
2.1.2 Experimental studies on elastic response of box girders.....	7
2.1.3 Limit state of load capacity of box girders .....	8
2.1.4. Dynamic response of box girders .....	10
2.1.5. Distribution and redistribution of loads and stresses in box girders, defined load distribution codes.....	12
2.2 Analytical approach .....	16
2.3 Finite element method .....	18
3. Analytical approach .....	20
3.1 Analytical approach - Introduction .....	20
3.2 Bending analysis for box girders.....	20
3.2.1 Elastic longitudinal bending .....	20
3.2.1.1 Hypotheses.....	21
3.2.1.2 Bending equation .....	21
3.2.2 Transverse distribution - „Shear lag effect“ .....	22
3.2.2.1 Effective width .....	23
3.3 Torsional – distortional analysis of box girders.....	25
3.3.1 Girder response under eccentric loading.....	25





3.3.2	Uniform torsion.....	27
3.3.2.1	Hypotheses.....	27
3.3.2.2	Basic equations and relations .....	28
3.3.3	Non-uniform torsion .....	29
3.3.3.1	Hypotheses.....	29
3.3.3.2	Compatibility equations .....	30
3.3.3.3	Shear center .....	31
3.3.3.4	Equilibrium equation.....	32
3.3.3.5	Homogenization rules during torsion accompanied by warping and distortion in a composite girder .....	34
3.3.4	Distortion.....	34
3.3.4.1	Hypotheses.....	35
3.3.4.2	Longitudinal bending of the girder.....	36
3.3.4.3	Deformations at the cross-sectional level.....	39
3.3.4.4	Equilibrium equation.....	42
3.3.5	Load acting eccentrically in the webs of the girder.....	42
3.4	Solution of the equilibrium equation .....	44
3.4.1	Elastic bending .....	44
3.4.2	Warping torsion.....	45
3.4.3	Distortion.....	48
3.4.4	Distortion in composite box cross-section.....	51
3.4.4.1	Relation between $\theta_u$ and $\theta_l$ .....	53
3.4.4.2	Analysis of the distortional influences .....	54
3.4.4.3	Distortion energy analysis.....	55
3.4.4.4	External influences.....	56
3.4.4.5	Basic distortion differential equation .....	56
4.	First-order analysis of numerical examples.....	59
5.	Analysis and comparison of the results.....	61
6.	Conclusions.....	64
7.	Literature .....	66
	Appendices .....	68
	Appendix 1 , Software output .....	68



## LIST OF SYMBOLS

$\cos$	Cosine
$\cosh$	Hyperbolic cosine
$\sin$	Sine
$\sinh$	Hyperbolic sine
$\tanh$	Hyperbolic tangent
$d[ \ ]$	Infinitesimal portion
$\frac{d^n}{dx^n} [ \ ]$	$n^{th}$ derivative of a function with respect to the variable $x$
$\int_K [ \ ] dk$	Integral of $K$ with respect to the variable $k$
$\int_0^s [ \ ] ds$	Integral around the mid-line
$\int_0^{s,cell} [ \ ] ds$	Integral around the cell mid-line
$\oint [ \ ] ds$	Closed integral around the cell mid-line
$[ \ ]_{,k}$ or $\frac{\partial [ \ ]}{\partial k}$	Partial derivative with respect to $k$
$\frac{d[ \ ]}{dk}$	Derivative with respect to $k$
$( \ )_b, ( \ )_{b,SL}, ( \ )_w, ( \ )_d$	In terms of bending according to Euler-Bernoulli theory for beams subjected to bending, bending resulting from the so-called shear lag effect, torsion accompanied by warping and distortion
$( \ )^L, ( \ )^T$	Longitudinal bending of the beam as well as transverse deformation of the cross-section (distortion)



$\Sigma$	Sum
$[ \ ]^M, [ \ ]^F$	Membrane and deformable girder components
$[ \ ]^t$	Transpose
$\delta[ \ ]$	Imaginary infinitesimal variation

## LATIN LETTERS

$A$	Cross-sectional area; or a generic point along the midline of the cross section
$A_f$	Cross-sectional area of the flange
$A_r$	
$A_w$	Web area
$A_0$	Area delimiting the midline from the closed contour walls
$\bar{A}, \bar{B}, \bar{C}, \bar{D}$	Auxiliary functions that define the solution to the distortion problem
$F_A, F_B$	The vertical forces at points A and B defined in the Beam on Elastic Foundation analogy
$F_i$	Shear forces at surfaces in mutual contact
$G$	Shear modulus; or center of mass
$G_c, G_s$	Shear modulus for concrete and steel
$G_k$	Characteristic value for constant loads
$H_1, H_2, H_3, H_4$	Horizontal forces in an equivalent system



$I_x, I_y, I_z$	Moments of inertia with respect to $x, y, z$ axes
$I_{yz}$	Product of inertia with respect to $y$ и $z$ axes
$I_b, I_t, I_w$	Moments of inertia of top and bottom flange and web, viewed at cross-sectional level
$\bar{I}_b, \bar{I}_t, \bar{I}_w$	Transverse moments of inertia of top and bottom flange and web, per unit length
$I_c$	Secondary, central moments of inertia
$I_{w,e}$	Equivalent moment of inertia of the web, defined for solving the distortion problem
$I_\omega$	Warping constant
$J$	“Saint-Venant” torsion constant
$K$	The Global Stiffness Matrix
$L$	Girder span
$L_d$	Characteristic length of distortional strain
$M$	Generated bending moment
$M_A, M_B$	Bending moments at points A and B
$M_{oA}, M_{oB}$	Partial bending moments at points A and B defined on the infinite beam (Beam on Elastic Foundation analogy)
$M_t$	Applied concentrated torsional moment
$M_b, M_t, M_w$	Bending moments occurring at the top, bottom flange and web when considering distortion



$M_y$	The bending moments around the $y$ axis (if it refers to a moment at a precisely defined point, then instead of this deflection index, the one corresponding to the position of the moment's action is used)
$N$	Number of deformed states
$N_b, N_t, N_w$	Axial force acting at top and bottom flange level as well as at web level while resolving distortion
$N_w$	Number of deformed states during warping
$P$	An auxiliary point for the positioning of the shear center
$Q$	Concentrated load
$Q_k$	Concentrated load applied to the case under consideration
$R_b, R_t, R_w$	Radius of curvature for longitudinal bending of the bottom and top flanges and the web in the distortion problem
$R_A, R_B$	Vertical forces at points A and B
$R_{oA}, R_{oB}$	Partial forces applied at points A and B in the case of an infinite beam (Beam on Elastic Foundation analogy)
$R_z$	Radius of curvature around the $z$ axis
$S$	Midline domain
$S_d$	Diagonal force causing cross-sectional distortion
$S_{\omega y}, S_{\omega z}$	Sectoral product of inertia with respect to the $y$ and $z$ axes



$T$	Torsional moment; or concentrated torsional moment
$T_w$	Component of torsion-induced warping
$T_{SV}$	"Saint-Venant" torsional component
$U$	Displacement vector
$U_x, U_y, U_z$	Components of the displacement vector with respect to the $x, y$ and $z$ axes
$V$	Generating shear force
$W_{int}, W_{ext}$	Internal and external condition
$a_0$	Place of application of concentrated load along the beam
$a_0^z$	An additional length that defines the position of the concentrated load, seen along the beam. A length defined to solve the warping torsion problem.
$a_1, a_2, a_3$	Lengths that define the position of the distributed load along the beam
$a_4, a_5$	Auxiliary lengths defined for solving the bending problem according to the Euler-Bernoulli beam theory
$b$	Total width of the top flange
$b_b$	Total width of the bottom flange
$b_e$	Effective width of the generating flange
$b_{e,1}, b_{e,2}, b_{e,3}$	
$b_t$	Width of top flange defined in flange-web "contact" zone
$b_w$	Web width



$c_1, c_2, c_3$	Constants resulting from the solution of the distortion problem
$d; \mathbf{d}$	Distance between the centers of gravity of the top and bottom flanges and the "degrees of freedom" vector
$e$	Vertical eccentricity of the load relative to the flange-web "node".
$e_y, e_z$	Auxiliary coordinates for defining the shear center
$f$	Generic load vector
$f_i$	
$f_x, f_y, f_z$	Components of the generic load vector with respect to the $x, y$ и $z$ axes
$g$	Length of the diagonal of the cross-section
$k$	Transverse stiffness of the frame defined for the distortion problem
$k_1, k_2$	Dimensionless parameters defined to form the equilibrium equation for distortion
$l$	Span size
$l_i$	Length of considered element
$m_A$	Moment applied at the point A
$m_{anti}, m_{sym}$	Antisymmetric and symmetric component of the external bending moment
$m_i, n_i$	Displacement components at node $i$ along web centerline and vertical directions due to cross-sectional deformation
$\overline{m}_i$	Transverse bending moment at point $i$ due to diagonal loading



$m_{b,d}^L, m_{t,d}^L, m_{w,d}^L$	Longitudinal bending moments caused by the distortional loading of the plate in the bottom, top flange and web, considering each isolated from the others
$m_t$	Uniformly-distributed torsional loading
$n$	Homogenization coefficient, steel-concrete
$p$	Generated vertical load
$p_{anti}, p_{sym}$	Symmetric and antisymmetric component of the external load
$p_A$	Generated force at point A
$p_{b,PureT}, p_{t,PureT}, p_{w,PureT}$	The forces of the torsional subsystem in the bottom, top flange and the web, when considering pure torsion
$p_{b,d}, p_{t,d}, p_{w,d}$	The forces of the distortional subsystem in the bottom, top flange and the web
$p_{b,d}^T, p_{t,d}^T, p_{w,d}^T$	The forces of the distortional subsystem in the bottom, top web and rib, causing longitudinal bending
$p_d$	Generated distortional surface load
$p_d^L, p_d^T$	Components of the forces of the distortional subsystem that cause longitudinal bending
$q$	Uniformly distributed load applied; or shear occurring in the cross-section walls as a result of torsion followed by warping
$q_k$	Characteristic value of uniformly distributed load in Load Model 1





$q_w$	Shear occurring in the cross-section walls as a result of torsion followed by warping
$q_{SV}$	"Saint-Venant"-shear
$r$	Tangential radius between the shear center and the midline of the "walls" of the cross-section
$r_b, r_t$	Dimensionless ratios defined for the distortion problem
$r_p$	Tangential radius between point P and the midline of the "walls" of the cross-section
$s$	The coordinate is measured along the midline of the "walls" of the cross-section
$t$	Thickness of the generating plate
$t_b, t_t, t_w$	Thickness of the bottom, top flange and web
$t_t^s$	Equivalent homogenized thickness of the top flange
$\overline{u}_k, \overline{v}_k, \overline{z}_k$	Displacement with respect to the $x, y$ и $z$ axes
$\overline{u}_s$	Displacement component for K-mode

## GREEK LETTERS

---

$\alpha$	Stiffness ratio defined for the bending problem with shear lag
$\alpha_b, \alpha_t, \beta$	Dimensionless ratios defined for the distortion problem
$\gamma$	Shear stress induced by warping torsion



$\gamma_C, \gamma_S$	Density of steel. Shear dilatation induced by warping torsion
$\gamma_{SV}$	Shear stress according to Saint-Venant torsion
$\gamma_{xy}, \gamma_{yz}, \gamma_{xz}$	Components of shear stress in the $xy, yz$ and $zx$ planes
$\delta$	Diagonal cross-section deformation
$\delta_i$	Component of the diagonal cross-section deformation at node $i$
$\epsilon$	Strain vector
$\epsilon_w$	Normal strain during warping
$\epsilon_{xx}, \epsilon_{yy}, \epsilon_{zz}$	Normal components of strain along $x, y$ and $z$ axes
$\zeta$	Characteristic length defined for the warping torsion problem
$\theta$	Angle of rotation
$\lambda$	A parameter used in defining the solution to the distortion problem
$\mu$	Shear parameter followed by warping
$\nu$	Poisson's ratio
$\nu_C, \nu_S$	Poisson's ratio for concrete and steel
$\xi_I, \xi_{II}$	Auxiliary functions used in defining the solution to the distortion problem
$\sigma_b$	Stress due to normal bending as defined by Euler-Bernoulli beam theory



$\sigma_{b,SL}$	Stress due to normal bending, according to the occurrence of the so-called "shear lag" effect
$\sigma_{b,SL}^b, \sigma_{b,SL}^t$	Stress due to normal bending, while accounting for the „shear lag“ effect within the top and bottom flange
$\sigma_{b,SL}^{bMAX}, \sigma_{b,SL}^{tMAX}$	Maximum stress due to normal bending, while accounting for the „shear lag“ effect within the top and bottom flange
$\sigma_{i,d}$	Distortional normal warping stress
$\sigma_w$	Torsional normal warping stress
$\sigma_b^C, \sigma_b^S$	Stress induced by normal bending at the level of the homogenized top flange in homogeneous and heterogeneous configuration
$\sigma_{b,SL}^C, \sigma_{b,SL}^S$	Stress due to normal bending, while accounting for the „shear lag“ effect at the level of the homogenized top flange in homogeneous and heterogeneous configuration
$\sigma_d^C, \sigma_d^S$	Distortional normal warping stress at the level of the homogenized top flange in homogeneous and heterogeneous configuration
$\sigma_w^C, \sigma_w^S$	Torsional normal warping stress at the level of the homogenized top flange in homogeneous and heterogeneous configuration
$\sigma_{xx}, \sigma_{yy}, \sigma_{zz}$	Normal stress along the $x, y, z$ axis
$\tau_{xy}$	Shear stress in $xy$ plane



$\tau_{yz}$	Shear stress in yz plane
$\tau_w$	Shear stress under the action of torsional warping
$\tau_{SV}$	Shear stress under the action of uniform torsion
$\phi$	Angle of rotation of the cross-section around the shear center
$\varphi$	
$\chi$	A function of the torsional warping amplitude
$\omega_S, \omega_P$	Sectorial coordinates for the quasi-closed cross-section with respect to the shear center S and the point P
$\tilde{\omega}_S, \tilde{\omega}_P$	Equivalent sectorial coordinates for the quasi-closed cross-section with respect to the shear center S and the point P
$\Gamma$	Displacements of the intersection points between the midlines of the bottom, top flange and web respectively undergoing distortion
$\Delta_b, \Delta_t, \Delta_w$	Displacements of the intersection points between the midlines of the bottom, top flange and web respectively undergoing distortion



## LIST OF FIGURES

Figure 1 Load division for analysis of all phenomena in a box girder .....	18
Figure 2 Typical cross-section of a composite box girder and b) equivalent homogenized cross-section.....	20
Figure 3 Generated cross-sectional view of a box girder under symmetrical loading along the upper edge of the webs.....	21
Figure 4 Deformed state of the girder subjected to bending and static equilibrium of a girder segment under a vertical load.....	22
Figure 5 Longitudinal bending stresses with and without the influence of transverse distribution .....	23
Figure 6 Effective cross-section for box girder bridge, effective widths contributing to the cross-section response.....	24
Figure 7 Load decomposition into symmetric and asymmetric component.....	25
Figure 7.1 Decomposition of the asymmetric component of the load into uniform torsion, warping torsion and distortion.....	26
Figure 8 Decomposition of the asymmetric component of the load pure torsion and distortion .....	26
Figure 9 Deformation-displacement of the cross-section as a result of the rotation.....	28
Figure 10 Sectorial-coordinates, a diagram showing the warping function .....	30
Figure 11 Tangential radius for reference points .....	31
Figure 12 Equilibrium of an infinitesimal segment subjected to warping torsion.....	32
Figure 13 Equilibrium state of an infinitesimal segment of the girder subjected to torsion .....	34
Figure 14 Displacement compatibility under distortion .....	35
Figure 15 Displacement compatibility under distortion .....	36
Figure 16 Distortion warping stresses.....	39
Figure 17 Equivalent diagonal system of forces and corresponding stress distribution .....	40
Figure 18 Deformations and displacement of the distortion frame .....	41
Figure 19 Equivalent vertical load .....	43
Figure 20 Decomposition of the equivalent load into pure torsion and distortion .....	43
Figure 21 Support and loading conditions .....	44
Figure 22 Analogy-Beam on elastic foundation .....	48
Figure 23 Load decomposition of the part causing pure torsion and distortion .....	51
Figure 24 Cross-section of the composite box girder .....	51
Figure 25 Defining the distortion angle.....	52
Figure 26 a) Distortional forces H and V b) The corresponding bending moment diagram.....	53
Figure 27 Diagram of the bending moments under the action of the distortional imaginary moment M .....	53
Figure 28 Warping function as a result of distortion .....	54
Figure 29 Distribution of stresses and deformations in the box girder cross-section.....	59
Figure 30 Response of the considered composite box girder cross-section under asymmetrical loading.....	60
Figure 31 Response of the considered steel box girder cross-section under asymmetric loading.....	61
Figure 32 Diagram of stresses and manifested rotations in the key nodes of the considered composite box girder cross-section under asymmetric loading .....	62
Figure 33 Diagram of stresses and manifested rotations in the key nodes of the considered steel box girder cross-section under asymmetric loading - pure steel and composite node.....	63
Figure 34 Input parameters, load and network formation for the mathematical model .....	68



Figure 35 Girder response to the asymmetrical loading-longitudinal deflection, manifested strains and deformations at the cross-sectional level within its own plane ..... 69

Figure 36 Diagram of stresses and manifested rotations in the key nodes of the considered steel box girder cross-section under asymmetric loading - pure steel and composite node ..... 70

Figure 37 Diagram of stresses and manifested rotations and strains in the key nodes of the considered steel box girder cross-section under asymmetric loading - pure steel and composite node ..... 71

Figure 38 Diagram of shear stresses in the key nodes of the considered steel box girder cross-section under asymmetric loading - pure steel and composite node..... 72

Figure 39 Diagram of the strain change, stresses and rotations in the node-steel flange/steel web along the length of the span of the considered steel box girder cross-section under asymmetric loading..... 73

Figure 40 Diagram of the strain change, stresses and rotations in a node-concrete flange/steel web along the length of the span of the considered steel box girder cross-section under asymmetric loading..... 74

## LIST OF TABLES

Table 1 Equilibrium equations for elastic bending, warping torsion and distortion..... 44

Table 2 Solution of the equilibrium equation for longitudinal bending..... 45

Table 3 Solution of the equilibrium equation for warping torsion(adopted from Maisel & Roll (1974))..... 47

Table 4 Solution of the equilibrium equation for distortion (adapted from Pedro (1995)) ..... 50

Table 5 Equations for calculating the redistribution of internal influences at the cross-sectional level under symmetrical loading..... 57

Table 6 Equations for calculating the redistribution of internal influences at the cross-sectional level under asymmetrical loading..... 58

Table 7 Cross-sectional properties needed to solve the basic differential equations ..... 59

Table 8 Comparison of obtained values for the distortion angle and stress redistribution..... 60

Table 9: Comparison of the relevant-distortion angle and distortion stresses in a composite and steel cross-section, at the cross-sectional level ..... 62



## 1. INTRODUCTION

---

### 1.1 SCIENTIFIC JUSTIFICATION OF THE TOPIC

From an engineering perspective, bridges have consistently held a unique and vital significance for builders. This significance arises initially from the practical necessity of bridging geographical obstacles. Furthermore, it emerges from the intricacies involved in comprehending the structural response of bridges to external forces and perhaps, partly from the sense of magnificence attributed to these structures due to their imposing physiognomy. Nevertheless, it is primarily the first two rationales that underscore the gravity and import of bridge engineering endeavors. Over time, historical records reveal concerted efforts to advance the state of bridge construction in response to these compelling motivations.

Hence, the use of box-shaped main girders in bridge construction has enjoyed enduring popularity, primarily attributable to their suitability, arising from the notable torsional and flexural stiffness they offer. Bridges featuring a box cross-section have found widespread application, owing to the favorable relationship between their stiffness characteristics and their self-weight (Schlaich & Scheef, 1982; Chen & Yen, 1980). However, the persistent trend toward downsizing these cross-sections, especially for specific construction methods, inevitably results in structures that are increasingly flexible. This heightened flexibility, in turn, elevates the risk of significant deformations induced by torsion, distortion, and warping.

The analysis of these structures in the longitudinal direction can be effectively accomplished through the application of linear models where the loading pattern follows the influent lines. By employing such models, we can derive a distribution of internal forces and deformations, which, when combined with the specified boundary conditions, serve as the basis for constructing the cross-sectional analysis model.

In single-cell box girders subjected to uniform symmetrical loading, the longitudinal stresses can be defined by the effects of longitudinal bending and possibly, at wide spans, the effects of transverse forces. Under asymmetrical loading, planar buckling of the cross-section and deformation generate longitudinal deformations, leading to the development of longitudinal warping stresses. These effects can be very significant in the design of complex box girders, especially in cases of large bending stiffness (width–height) on the plate of the cross-section, as well as in cases of diaphragms that are either flexible or positioned at a substantial distance along the span.

The choice between a concrete prestressed cross-section, a pure steel cross-section, or a composite cross-section of the box girder significantly impacts the distribution of stresses and deformations at the cross-sectional level. However, research on the distortion response in composite box girders is relatively scarce due to the inherent complexity of the problem. Inspired by this complexity and guided by the saying, "Everything you've ever wanted is on the other side of fear, and all you have to do is cross the bridge," we have adopted a practical approach to investigate the distortion response of composite box girders. Since the girder is composite in nature, it is essential to account for the differing stiffness characteristics between the top concrete flange and the bottom steel flange, as this unquestionably influences the final deformation. To comprehensively capture the cross-sectional response of the girder, we introduce the concept of two distinct distortion angles.



We employ two distinct methods to analyze the behavior of box girders at the cross-sectional level:

Beam on Elastic Foundation (BEF) analogy

Finite Element Method

The first approach, despite its simplifications and the inherent complexity of the phenomenon, holds particular relevance and clarity, especially during the preliminary design phase. In comparison to other methods like the Finite Element Method, which necessitates a large volume of input data and thus introduces the potential for errors, this approach can offer more straightforward and informative results. The classical approach relies on several established theories. These theories include the Euler-Bernoulli beam theory, the torsion theory advocated by Benscoter (1954), and the "curve plates" theory based on the Beam on Elastic Foundation analogy, initially introduced by Wright, Abdel-Samed, and Robinson (1968) as a means of defining distortion in box girders. Additionally, this classical approach features a simplified method for determining the nonlinear stress distribution resulting from transverse redistribution during bending.

The second approach involves the analysis of models constructed using shell finite elements within the software package "ABAQUS." Analyzing and designing bridge structures with box main girders, as previously mentioned, is a complex endeavor. This complexity arises from the three-dimensional response of the girder itself, encompassing torsion, distortion, and bending in both the longitudinal and transverse directions. However, thanks to the advancement of modern analysis tools like the finite element method, we can now perform comprehensive box girder analyses using discretization techniques. This enables us to simultaneously consider the structural response in both longitudinal and transverse directions, as well as their mutual interactions. Consequently, these tools empower us to scrutinize the behavior of the box girder at the level of a characteristic cross-section, affording a detailed and holistic understanding of its performance.

The outcomes of the conducted analysis will provide an accurate depiction of the actual behavior exhibited by reinforced concrete prestressed box cross-sections within the cross-sectional plane, encompassing both symmetrical and asymmetrical loading scenarios. The focus is on assessing the response of the characteristic cross-section, which allows us to discern and understand the reactions of the box girder, perceived through the occurring stresses and strains. The key parameters under scrutiny pertain to the response of the girder during various conditions, including bending, warping, torsion, and distortion.

The importance of this research lies in the introduction of a novel and pragmatic approach for examining the distortional behavior of composite box girders. It offers a means to comprehend the stress distribution within these girders while considering the distinct influence of the varying stiffness characteristics introduced by the concrete slab. This method delivers valuable insights into how composite box girders respond to distortion, enhancing our ability to predict the behavior of single-cell box girders that exhibit at least one axis of symmetry.

## 1.2 AIM OF THE RESEARCH

As it is already known, the composite structures lead to the exhaustion of the maximum of the bearing capacity of the steel - its tensile strength and the bearing capacity of the concrete under pressure. The very choice of box girders for bridge structures underscores their exceptional load bearing capacity





and torsional stiffness, making them a preferred choice for spanning large distances. When subjected to symmetrical loads, box girders typically exhibit longitudinal stresses that can be accurately represented by the effects of longitudinal bending. Additionally, the shear lag effect becomes significant when the cross-section features a wide flange. However, when asymmetric loading comes into play, box girders, as thin-walled beams, undergo deformation within their own plane—commonly referred to as distortion. This deformation includes warping and out-of-plane deformations. These effects introduce additional stresses, arising from distortion itself, in conjunction with transverse bending stresses and the so-called "Saint-Venant" shear stresses. The presence of normal stresses arising from warping and bending stresses at the cross-sectional level due to distortion can indeed reach significant levels if not adequately addressed. This underscores the vital importance of comprehensively analyzing the behavior of box girders under the influence of asymmetric loading. Asymmetric loading induces complex phenomena such as elastic bending, torsion, and distortion. While several studies have explored distortion in box girders and proposed various methodologies, research specifically addressing composite box girders under asymmetric loading remains relatively limited. The inherent complexity of this problem contributes to this scarcity of studies. It's worth noting that some of the research conducted in this area has borrowed principles from the analysis of pure steel box girders, often without fully considering the distinct differences in flexural stiffness between the top concrete flange and the remaining steel section. This difference unquestionably influences distortional stiffness and resistance. Hence, there exists a clear need for the development of a simplified approach that can effectively define the resulting deformation and stress distribution within composite box girders when subjected to distortion induced by asymmetric loading. Such an approach would significantly contribute to our understanding of these complex structural behaviors.

The analysis and design of box girders can be tracked back to the theory of curved beams developed by Saint-Venant (1843), followed by the theory of thin-walled beams advocated by Vlasov (1961), while Kristek (1970) contributed by studying deformable girders and proposing an analytical solution. The analytical solution is essentially divided into two stages. The cross-section is first assumed to be solved as a rigid cross-section. Subsequently, the internal forces resulting from the support conditions are applied to the beam and analyzed again. The final result is a superposition of the two previous steps. Chapman et al. (1971) defined a finite element analysis of steel and concrete box girders to investigate the impact of diaphragms on stress distribution due to warping and distortion. The "BEF" analogy as employed by Wright et al. (1968) also defined the behavior of box girders when subjected to distortion itself.

Distortional warping is a crucial aspect of axial displacement caused by warping when a cross-section is allowed to deform freely. This deformation occurs in response to asymmetric and distortional loading, unless certain supports or diaphragms are strategically placed to constrain it. The extent of distortion largely depends on the transverse flexibility of the cross-section and the distribution of transverse bending moments throughout the box girder's cross-section, stemming from its behavior as a frame system. Both axial distortional warping and transverse elastic deformation are indicated.

The primary distinction between a pure steel or concrete box girder cross-section and a composite one lies in the material of the composite box girder where the top flange is made of concrete while the bottom flange is made of steel. This leads to variations in deformable stiffness due to different material responses. The deformability of the top concrete flange significantly differs from what would be observed in a purely steel flange. Consequently, the distinct stiffness characteristics directly influence



the cross-section's deformability, resulting in a unique distribution of distortional stresses across the box cross-section.

The objective of this thesis is to provide insights into the various approaches employed for the analysis of box girder cross-sections, with a particular emphasis on their mathematical formulations. Specifically, the research aims to offer a comprehensive understanding of the results obtained in terms of total longitudinal normal stresses and the influence of bending, torsion, distortion, and shear lag. A specific focus of this study centers on the analysis of composite box girders, which are known for their intricate response to torsional and distortional stresses. However, assessing this complex behavior poses considerable challenges. Through a critical examination and evaluation of existing methodologies, the research endeavors to pinpoint key engineering considerations. These considerations include the significance of torsion and distortion effects and the crucial role played by the geometric characteristics of the cross-section.

### 1.3 RESEARCH METHODOLOGY

In light of the distinct stiffness characteristics between the top concrete and bottom steel flanges, different rotation angles are assigned to the nodal points considered in the analysis. The response of the composite box girder to distortion is defined through two alternative methods: The first method relies on a set of differential equations derived from "energy methods," which are grounded in the theory of thin-walled beams. To solve these differential equations, relevant geometric characteristics are defined, including the distortion constant of warping  $I_{Dw}$ , and the distortion stiffness of the frame  $K_{Dw}$ , tailored to the composite cross-section. The cross-sectional deformation and stress distribution resulting from distortional loading are determined by solving these differential equations using the "BEF" analogy. The second approach involves the use of the finite element method, implemented in the "ABAQUS" software package. This method allows for a numerical analysis of the composite box girder's behavior analyzed as a simple beam.

### 1.4 BRIEF CONTENT OF THE PAPER

The Master's Thesis is structured into six chapters, with the current chapter serving as the introduction. The subsequent chapters are as follows:

Chapter 2 – This chapter provides an overview of various analytical methods employed to assess the transverse load capacity of composite box girder cross-section in bridge structures. It encompasses a review of prominent methods utilized in the analysis of box girder bridges, including the "BEF" analogy and methodologies employing shell finite elements.

Chapter 3 – Methods of analysis of bridge structures with box girders. This chapter delves into the theoretical formulations pertaining to bending, warping torsion, distortion. Furthermore, it presents a simplified technique for accounting for the shear lag effect. The chapter also introduces a computational analysis approach utilizing shell finite elements.

Поглавје 4 – First-order analyses of numerical examples. In this section, an in-depth analysis of a specific composite box girder and a simple beam system is conducted. The analysis employs both analytical methods and mathematical models utilizing finite elements.



Поглавје 5 – Analysis and comparative evaluation of findings. This chapter is dedicated to comparing the outcomes derived from the two distinct approaches outlined in the previous section. The comparative assessment serves to validate the accuracy of the proposed analytical method. Additionally, we carry out an analysis of a pure steel box girder using mathematical models with finite elements, aiming to discern differences in the response between a composite box girder and a pure steel box girder.

Chapter 6 – Conclusions and Future Directions. This concluding chapter summarizes the key findings and conclusions resulting from the research and analytical endeavors. It also provides insights into potential avenues for future research.

Chapter 7 – Literature. This section lists the references and literature sources employed in the preparation of this Master's Thesis.



## 2. METHODS OF ANALYSIS FOR BOX GIRDERS BRIDGES

### 2.1 GENERAL OVERVIEW OF THE PROBLEM

Historically, a significant amount of research has focused on predicting the behavior of diverse types of box girder bridges within the elastic range. However, only a limited number of studies have undertaken experimental investigations aimed at assessing the accuracy of existing design methodologies. The unique characteristics of box girder bridges, coupled with the intricate deformation and stress patterns that arise due to varying boundary conditions and load scenarios, pose challenges for designers. Approximate and conservative methods for static and dynamic analyses further compound these challenges. The literature review conducted is structured as follows:

- Box girders under construction
- Experimental studies on elastic response of box girders
- Limit state of load capacity of box girders
- Dynamic response of box girders
- Distribution and redistribution of loads and stresses in box girders, defined load distribution codes

#### 2.1.1. Box girders under construction

During the construction phase of bridges, particularly those with variable loads, a significant degree of distortion or warping-torsion may occur. This is primarily attributed to the flexibility of the bottom flange and webs during torsional loading. In bridges with straight configurations, the cross members and diaphragms play a secondary role in upholding the structural integrity of the bridge. However, in the case of horizontally curved bridges, a distinctive interaction between the webs and the bottom flange occurs, leading to cross members and diaphragms assuming the role of primary load-bearing elements. This shift in their function is particularly pronounced under torsional and bending loads. It's important to note that there has been a limited number of both experimental and analytical studies conducted to date that investigate the behavior of curved bridges during the construction phase.

Historically, several prominent bridges, including the Yarra Bridge in Australia, the Rhine River Bridge in Koblenz, the Fourth Danube Bridge in Vienna, and the Milford Haven Bridge in Wales, have experienced damage or failure during their construction phases. These unfortunate incidents prompted a reevaluation of the fundamental principles underpinning the design of box girder bridges. In 1976, a significant development occurred when Macdonald and colleagues conducted elastic experimental tests on two models of single-cell steel girders. These tests involved subjecting the girders to both centric and eccentric loading. The models were equipped with lateral bracings, and the number of cross bracings was systematically varied. Notably, the open cross-section models with top lateral bracings were analyzed as if they were equivalent closed box cross-sections, incorporating a steel plate on top. This analytical approach was inspired by a concept introduced by Dabrowski in 1968. Remarkably, the experimental findings closely aligned with the analytical results, signifying the reliability of this analytical method. In 1978, United States Steel (USS) reported several challenges encountered during the construction of steel box girder bridges. These challenges encompassed issues



such as the excessive rotation of girders before and during the placement of concrete slabs. In 1985, Branko and Green undertook a comprehensive experimental analysis involving a series of scale models, representing a system of simple beams, single-cell box-girder bridges, and interconnected box-girder bridges. The primary aim of their analysis was to investigate the impact of structural loading, bracing configurations, overall stability, and deformation on torsional open and quasi-closed box-girder bridges. The results of their experimental work were meticulously compared with analytical studies that incorporated both torsional bending analysis of open and quasi-closed cross-sections and the finite strip method. In 1989, Schelling and colleagues conducted an analytical study aimed at examining the response of a curved multi-I-beam system when subjected to self-weight loading and the weight of a concrete slab before curing. Their study involved the creation of a three-dimensional model of a spatial frame. The noteworthy outcome of their investigation included the derivation of general permanent load distribution factors. These factors could be applied to a range of commonly used structural configurations to prevent overstressing during the construction phase when temporary support structures are not required. In 1996, Davidson and associates employed the finite element method to conduct a study focused on warping stresses encountered in horizontally curved steel I-girder bridges. However, their study primarily concentrated on analyzing the influence of cross members in minimizing warping stresses developed in the steel flanges immediately after the concreting of the slab.

### 2.1.2. Experimental studies on elastic response of box girders

The primary objectives underlying the aforementioned experimental analyses were primarily centered around the validation and verification of the precision and reliability of computer programs and existing methodologies employed for studying the structural behavior of box girder bridges. It's important to note that, to date, field tests on box girder bridges have been relatively scarce, with most of these tests primarily focused on observing elastic behavior, thus presenting a limited scope in terms of comprehensive experimental assessments.

In 1975, Kissane and Beal conducted a test on a horizontally curved concrete-steel composite bridge situated on the Avoca-Bath section of the Southern Tier Expressway, spanning over the Genesee Expressway in Steuben County, New York. This bridge was characterized by two continuous spans. A year later, Yoo et al. carried out a similar test, focusing on a three-span bridge that also exhibited continuous curvature. This bridge was a composite box-girder structure and was located at the interchange of I-695 and I-83 near Baltimore. In 1975, Evans and Rifai engaged in experimental work centered around box girder bridges. Their research involved the investigation of eighteen single-cell models, all part of a simple beam system with varying degrees of curvature. These models were subjected to testing up to the elastic behavior limit, aiming to validate results obtained through the finite element method. The majority of these models were constructed using steel plates, while a portion were crafted from sand/araldite material. Rigid end diaphragms were exclusively placed at the ends of these models. Additionally, Aslam and Godden conducted an experimental analysis employing a series of small-scale aluminum models representing straight, inclined, and curved four-cell box girder bridges. These models were subjected to elastic testing, with and without the presence of a radial diaphragm at the midspan, by applying a single-point load at various positions along the span. In 1979, Brennan and Mandel conducted an investigation focused on the elastic behavior of small horizontally curved models of I-girders and multicolumn composite girders. The objective of this analysis was to collect data for potential use in future studies and comparisons. Utilizing this data and employing



methods such as the folded plate method, the finite strip method, and the finite element method, Skordelis summarized the findings from five representative bridge models to validate the accuracy of elastic solutions. Skordelis, along with colleagues, expanded on this work by conducting an analysis of three large-scale bridges. These bridges included rectilinear, slanted, and curved designs, comprising a two-lane reinforced concrete bridge and a four-cell box girder. These structures were continuous above the central support-column. The analysis involved subjecting these models to both constant and variable loads, assessing their behavior at working stress levels as well as the point of load failure. Additionally, in 1982, Buckle and Hood investigated a curved, continuous, single two-span laboratory model. This model was subjected to loading at various locations along its mid-span cross-section. The model was constructed using filled epoxy resin segments and incorporated diaphragms above the supports. It was prestressed with an enveloped parabolic profile.

In 1972, Haynes and Bonakdarpour conducted an elastic test on a small-scale model of a three-column curved box girder bridge made of Plexiglas. Their analysis aimed to assess the feasibility of applying deformation theory based on Vlasov's theory of thin-walled beams. It's important to note that this analysis did not consider distortional deformation or warping effects. In 1976, Pham and Turkstra investigated two single-cell Plexiglas models with substantial curvature. Their research focused on studying the impact of intermediate diaphragms and evaluating the suitability of three-dimensional finite element modeling for single-cell curved girders. In 1987, Xi-Jin and De-Rong conducted an elastic analysis using a Perspex model of a continuous curved, two-cell box-girder bridge. The objective of their study was to validate the accuracy of the finite-strip method in predicting the behavior of curved multi-cell bridges. In 1988, Siddiqui and Ng analyzed two Plexiglas, single-cell bridge models in the elastic range. This analysis aimed to investigate the influence of transverse diaphragms on the behavior of the box section under both centric and eccentric loading conditions. In 1990, Mirza and colleagues performed static and dynamic tests on two 1/7 scale model bridges. These bridges were simply supported, prestressed concrete structures, with the first model featuring one cell and the second having two cells. The primary objective of their work was to generate experimental data regarding the linear and nonlinear responses of box girder concrete bridges under various levels of damage, including concrete cracking. Lastly, in 1992, Ng and associates conducted an experimental study on a 1/24 linear scale model of the Searsville Road Bridge, spanning the Queensway east of Ottawa. This model was made of a four-cell, curved girder made of concrete and aluminum. The model was continuous over the central support and underwent elastic testing under various loading conditions, including the application of an OHBD truck.

### 2.1.3. Limit state of load capacity of box girders

Among the numerous experimental and theoretical studies conducted on box girder bridges discussed thus far, only a limited few have delved into nonlinear behavior, as well as the local bending and distortion of individual steel plates in both straight and curved bridge designs. In 1973, Abdel-Sayed conducted an investigation into the critical load limit and pre-bending of webs in curved girders subjected to combined loading, involving shear and normal stress. In 1979, Haynes and Humphreys undertook a series of experiments involving box girder models pushed to the point of failure. These models were subjected to a combination of increased torsional and bending forces and comprised top steel flanges, steel webs, bottom steel flanges, and cross bracings. Only some of these models featured a concrete slab. The results of this analysis served multiple purposes, including the validation of classical torsional theory within the elastic range and the development of a non-dimensional equation



designed to accelerate the determination of load factors for curved steel box girders. In 1984, Seible and Skordelis developed a numerical method and a computer program aimed at tracking the nonlinear behavior of multi-cell reinforced concrete box girder bridges when subjected to increased static loads. This analysis considered various nonlinear aspects related to the behavior of concrete as a material. These included the initiation of concrete cracking, yielding of reinforcement, the formation of plastic joints due to shear and concrete bending and crushing moments. To carry out this analysis efficiently, a three-dimensional grid was utilized to minimize computational requirements. The results obtained through this computational technique demonstrated a strong correlation with the outcomes of a physical test conducted on a two-span, four-cell reinforced concrete box girder. This experimental test was performed to failure by Skordelis and his colleagues. In 1985, researchers Perry et al. and Pinckney et al. conducted an investigation involving a scale model of a two-cell prestressed concrete bridge. This model represented a four-lane roadway that bifurcated into three-lane and two-lane spans. The bridge was constructed with typical one- and two-cell box girder design and featured cantilevers. Notably, the bridge had a significant curvature at its base and was continuous over the central supports. Additionally, it was torsionally stiffened over the three outer supports. A similar study was carried out by Owens et al.

In 1986 and 1988, researchers Choudhury and Choudhury, along with Scordelis, integrated the models developed by Bazant El Nimeiri and Zhang-Lyons. This integration resulted in the creation of a single-cell, curved, non-prismatic, thin-walled box element. Additionally, in 1988, Marie et al. introduced a box girder model with a non-deformable cross-section, comprising concrete panels and steel layers. This model aimed to replicate the behavior of a curved prestressed box girder. In 1989, Razaqpur and Nofal developed a finite element computer program capable of predicting the material nonlinear behavior to the point of failure in structures made of plain concrete, reinforced concrete, prestressed concrete, steel, and composite structures. Mirza et al. conducted tests to the point of failure on one-cell and two-cell prestressed concrete girder models. The results of these experiments were subsequently analyzed using the proposed nonlinear method. In 1989, Lopez and Aparicio introduced a mathematical model for the nonlinear analysis of reinforced concrete structures. To illustrate the practical application of their model, they utilized a prestressed concrete bridge with a double trapezoidal cell foundation curvature located at the Santamarca intersection of the La Paz highway in Madrid, Spain. This bridge featured a continuous design with five spans, each having a radius of 103.5 meters and a total length of 155.56 meters. In 1993, Ng et al. developed a similar finite element program tailored for monitoring the nonlinear response of reinforced concrete structures exclusively. As a comparison for their analysis, they utilized a two-span, four-cell reinforced concrete girder bridge that had been previously investigated by Skordelis et al.

In 1994, Soliman and ElMekaway employed a nonlinear finite element analysis to explore the impact of the bottom flange near the mid-support region on the deformation behavior of reinforced concrete girder bridges. Building upon this research, in the same year, Soliman and Ghali extended the theoretical investigation utilizing nonlinear finite element techniques. Their study delved into assessing how intermediate diaphragms and end diaphragms influenced the behavior of single-cell box-girder bridges across varying spans, including small, medium, and long spans. Subsequently, in 1995, Yabuki et al. introduced a numerical method designed to predict the effects of local bending and distortion phenomena on the nonlinear behavior and load-bearing capacity of thin-walled welded steel girders. These girders featured curvature at their base and were reinforced with intermediate diaphragms. The study's theoretical predictions, derived from the proposed method, were compared



with experimental test results conducted on two large curved steel box girders, each with a different number of internal diaphragms. Despite the extensive literature review, data from experimental analyses conducted to the point of complete failure of composite box girders remain scarce.

#### 2.1.4. Dynamic response of box girders

Over the last three decades, notable advancements in materials have emerged, introducing high-strength materials like high-strength steel. These innovations have facilitated the adoption of thinner structural elements in bridge construction. While these materials enable the creation of longer bridge spans, they also present challenges related to dynamic deflections and vibrations, which can result from factors such as heavy truck loads, wind forces, or seismic activity. These dynamic responses can pose inconveniences for both motorists and pedestrians using these bridges. In response, ongoing research efforts have been dedicated to conducting analytical and experimental studies aimed at comprehending and mitigating the dynamic response of box girder bridges.

In 1967 and 1972, researchers Culver and Shore, as well as Chaudhuri, employed closed-form solution of the equation of motion to investigate the impact of transverse shear deformation and rotational inertia on the natural frequencies of horizontally circularly curved girders. Their study was based on the differential equation of motion for a freely vibrating horizontally circular-curved girder. Similarly, in 1968, Tan and Shore used differential equations to model the out-of-plane vibrational motion of a girder within a horizontal circular-curved simple beam girder system. They adopted an appropriate idealization of the bridge, treating it as a thin, prismatic, curved girder subjected to a constant-magnitude moving force. In 1966 and 1970, Komatsu and Nakai employed the fundamental equation of motion, along with Vlasov's theory of thin-walled elements, to conduct various studies on the free and forced vibrations of horizontally curved one or two-cell box girder. They validated their theoretical analyses using experimental data obtained from tests on existing simple beam and continuous beam bridges in Japan. Furthermore, in 1972, Cheung and Cheung discussed the application of the finite-strip method in determining the natural frequencies and vibration modes of both straight and curved bridges.

In 1972 and 1973, Taba and Pham utilized the finite element method to apply dynamic loads in order to determine the behavior of bridges in their curved sections. They also performed an experimental analysis of two curved, plexiglass, two-cell box girder models that confirmed the reliability of the proposed analysis methods. In 1975, Rabizadeh and Shore introduced a finite element method for the dynamic analysis of curved multi-span bridges. Their work laid the foundation for the impact factor later adopted by the American Association of State Highway and Transportation Officials (AASHTO) in their Guide Specification of 1980. In their research, Rabizadeh and Shore employed two sets of concentrated forces to simulate a moving vehicle, with component forces acting radially and transversely. This simulated vehicle moved at a constant angular velocity along the circular path of the bridge. In 1981, Haynes and Lee presented the experimental results obtained from a vehicle-induced dynamic field test on a two-span continuous, curved, composite bridge located in Seoul, Korea.





In 1984, Billing compiled the findings of dynamic testing conducted in 1980 on 27 bridges featuring various configurations and span lengths. The outcomes of this research laid the groundwork for the dynamic load allowance (DLA) adopted by the Canadian Standards Association (CAN/CSA S6-88) and the Ontario Highway Bridge Design Code (OHBD 1983, Second Edition). The DLA was determined through bending theory and was contingent on the first frequency of the bridge. However, this dynamic load allowance/frequency relationship was subsequently revised in the third edition of the OHBD code in 1992, as well as in the CHBD code. The updated DLA was designed to be a constant value, dependent on the number of axes. In 1997, Akoussah et al. raised questions regarding this new revision. Using three-dimensional finite element modeling, they explored the interaction between vehicles and bridges, focusing on the dynamic reinforcement factor of reinforced concrete bridges. Their study encompassed simple beam systems with spans ranging from 20 to 32 meters. The bridge code of the American Association of State Highway and Transportation Officials, AASHTO 1996, has traditionally applied an impact factor depending solely on the span of the bridge.

In 1985, based on the shape function, Chang et al. utilized a method developed by Rayleigh-Ritz to predict the seismic response of continuous bridge systems consisting of one, two, three, and four spans. During 1985 and 1986, Mirza et al. and Cheung and Mirza conducted comprehensive research that encompassed both theoretical and experimental aspects, focusing on the impact of stiffening systems on the dominant frequency of composite bridges. The theoretical component of their work relied on the finite element method, while the experimental segment involved the construction of a composite model representing a double-cell box girder bridge. This model was continuous over both spans and featured varying heights for the central support. Their study specifically examined the fundamental frequency of the bridge. In 1987, Inbanatan and Wieland conducted an analytical investigation into the dynamic response of a box girder bridge, simple beam system, to a moving vehicle over a rough roadway surface. Their findings indicated that heavy vehicles traveling at high speeds over uneven road surfaces can induce stresses in the bridge structure that exceed the recommended limits specified by bridge codes. In 1988, Abdel-Salam and Haynes presented the results of a comprehensive study focused on the seismic response of continuous,, multi-cell, composite box girder bridges with curved configurations. They utilized the El Centro earthquake motion acceleration record and its corresponding response spectrum as dynamic input for their analysis. The bridge was modeled using three-dimensional space frame elements, with special elements incorporated to account for the curved geometry and boundary conditions of the structure. Their research highlighted the significant impact of higher vibrations on the seismic response of this type of bridge.

In 1988, 1990 and 1992, researchers such as Galdos, Galdos et al., and Schelling et al. conducted studies on the dynamic response of horizontally curved box girders with varying spans using plane web finite element analysis. In their investigations, they represented moving vehicles using two constant, forces without a mass, traveling at a consistent angular velocity along the same curve as the bridge. These studies played a pivotal role in the development of the current impact factors that are employed by AASHTO (Guide Specifications for Horizontally Curved Highway Bridges, 1993) for curved bridges. In 1990, Mirza et al. conducted free vibration tests on two models of prestressed girders, both part of a simple beam system. The first model was a single-cell girder bridge, while the second model featured a two-cell configuration. The primary focus of this study was to analyze the fundamental vibration frequency and damping ratios of these bridge models at various levels of cracking damage. These dynamic characteristics could subsequently be used to estimate the extent of damage resulting from bridge cracking. In 1991, Cheung and Magnout utilized the finite element method to investigate the



influence of diaphragms, cross members, and bridge behavior on the dynamic response of a 45 m span bridge. In 1990 and 1992, Kashif and Humar and Kashif developed a finite element technique to analyze the dynamic response of box-girder bridges, a simple beam system, taking into account the interaction between the vehicle and the bridge.

In 1993, Richardson et al. presented the results of seismic loading simulation tests. During these tests, substantial horizontal loads were rapidly applied and released, inducing vibrations in the bridge. The observed vibration modes were used to validate the analytical model of the bridge's dynamic response. Validation primarily relied on the fundamental vibration mode, which predominantly involved horizontal vibrations.

In 1995, Huang et al. conducted a study on the dynamic response of curved I-girder bridges under the influence of truck loading. Their research introduced a method to account for the dynamic response of a thin-walled box-girder bridge when subjected to live load. The girder was discretized into multiple thin-walled beam elements. Their analysis considered the occurrence of torsion accompanied by warping and distortion. The study incorporated four different road surface roughness classes, characterized as very good, good, average, and bad roads, using power spectral density functions. The analytical results indicated that the dynamic response was significantly influenced by higher vibration modes. In 1996, Wang et al. investigated the free vibration characteristics and dynamic response of a continuous, thin-walled box girder bridge subjected to multi-vehicle loading. Their findings demonstrated that continuous and cantilever bridges with only one lane at mid-span exhibited greater susceptibility to vibration compared to those with mid-span suspension. In 1997, Senthilvasan et al. explored the relationship between the live load and the response of a bridge with base curvature. Their investigation utilized both the finite strip analysis method and the horizontally curved folded-plate model to analyze the structural behavior of such bridges.

### 2.1.5. Distribution and redistribution of loads and stresses in box girders, defined load distribution codes

Composite box girder bridge structures offer advantages over composite steel-concrete plate I-girders due to their superior torsional stiffness, making them more efficient and cost-effective. Additionally, composite box girders exhibit enhanced load-bearing capacity during deformations at the cross-sectional level. The following summary provides an overview of research conducted on load distribution and deformation characteristics in various types of composite bridges.

The impact of cross bracing on the stresses induced by warping and bending in curved I-beams was initially investigated by Yoo and Littrell in 1985, employing a comprehensive three-dimensional finite element model. Subsequently, in 1986, Brockenbrough also utilized finite element modeling to determine load distribution factors, taking into account warping effects, for curved composite I-girder bridges. These factors were examined in relation to span length, radius of curvature, and the spacing between girders and cross bracing. In 1967 and 1968, researchers like Johnston and Mattock, as well as Fontaine and Mattock, delved into the lateral load distribution in single-span, composite, multi-cell box-girder bridges that lacked transverse diaphragms. They employed a computer program to analyze these structures, accounting for the "folded plate" effect. Additionally, experimental tests were conducted to validate the analysis and assess the accuracy of the computer program. Two bridges were constructed for this experimental analysis. The first bridge was a two-lane structure with a 25-meter span, comprising three box girders as the primary girders. The second bridge was a scaled-down model,



one-fifth the size, featuring two lanes and a 31-meter span, constructed with two box girders. Both bridges underwent testing with concentric and eccentric truck loading, following AASHTO standards. The outcomes of this research were used to develop an equation that described the bending moment distribution factor under live load action for each girder, considering roadway width and the number of girders. These findings served as the foundation for the lateral redistribution of bending stresses, a method currently employed by AASHTO in 1996 and included in the initial two editions of the Ontario Highway Bridge Design Code (OHBDC) in 1979 and 1983. However, this equation did not consider the beneficial impact of cross-bracing between box girders and was limited to bridges where the number of spines matched the number of lanes. AASHTO LRFD in 2000 introduced an alternative equation for ultimate limit state load distribution to determine bending moments and shear forces in each box girder of the multi-cell bridge cross-section under live load.

In 1985 and 1992, Bacht and Jaeger proposed load distribution factors for bending moment and shear effects, which served as the foundation for the dynamic load distribution under live loads in the third edition of the OHBDC in 1992, specifically for multi-spine bridges. Their research was centered on multi-spine bridges with a minimum of three spines, featuring zero transverse bending stiffness and load transfer between different spines through transverse shear mechanisms. In 1994, Normandin and Massicot established distribution patterns for multi-spine bridges with varying characteristics and geometries by leveraging the results obtained from refined finite element analysis. Their study considered parameters such as the type of live load, the use of external bracing, and the existence of internal diaphragms. Their findings emphasized the crucial role of internal diaphragms within the box girders, significantly reducing cross-sectional deflection under various loads. Furthermore, their research revealed that in fully loaded bridges, external bracing between girders did not substantially impact the distribution characteristics of bending and shear moments. However, it's important to note that this method is applicable to bridges where the number of spines matches the number of lanes.

In 1978, Haynes introduced a modification factor aimed at broadening the applicability of the moment distribution equation, initially proposed by Fountain and Mattock, for horizontally curved, composite, multi-cell box girder bridges. The proposed modification factor is a function of the radius of curvature only in the case where cross bracings are incorporated within the girder itself. In 1980, Mukherjee and Trikha employed the finite strip method and established a collection of coefficients encompassing moment action, shear, transverse moment, and vertical displacement for two-cell, curved, reinforced concrete girder bridges. These coefficients were designed to facilitate the practical design process for such bridges. However, it's important to note that their applicability was limited to concrete bridges featuring two lanes, span lengths ranging from 20 to 40 meters, and radius of curvature falling within the range of 45 to 150 meters.

The AASHTO (Guide Specification for Horizontally Curved Highway Bridges, 1993) also provides guidelines for curved composite I-girder and box-girder bridges. These specifications are founded on the research conducted by Heins and Jin in 1984, which examined the live load distribution in composite I-girders for both simple beam and continuous beam systems. Their research employed a space frame idealization that considered the interaction of diaphragms (cross bracing in the radial direction) and lower lateral support. The specifications include design equations for use in conjunction with a plane web solution. For curved I-girders and box girders, AASHTO (Guide Specification for Horizontally Curved Highway Bridges, 1993) mandates that moments and shear forces used to define the behavior of individual elements should be derived from a rational analysis of the entire structure,



accounting for the complete load distribution. Moreover, if this rational analysis treats the system as a planar structure rather than a space frame, and includes the influence of bottom lateral bracing, the code modifies the resulting maximum stresses from live load using the Hines-Gean equation. This adjustment takes into account additional warping stresses in addition to normal bending stresses.

In 1981, Davies and Bohn introduced a curvature correction factor for load distribution in concrete and prestressed concrete multi-cell box girders. They recommended that for the outermost girder (furthest from the center of the curve), the bridge load should be directly distributed without any modifications. However, for all other girders, they proposed using a correction factor that considers the ratio of the distance from the center of the curve to the girder to the radius of curvature. It's important to note that this method did not account for the positive impact of transverse diaphragms. In 1988, Nutt et al. proposed a set of equations to calculate moment distribution in a rectilinear reinforced concrete and prestressed multi-cell box girder. These equations were based on various parameters, including the number of lanes, cell width, span length, and number of cells. In 1989, Ho et al. utilized the finite strip method to analyze a two-cell girder, simple beam system, and plate bridges without intermediate diaphragms. They derived empirical equations to determine the ratio of the maximum longitudinal bending moment to the equivalent beam moment. These equations were developed for bridges with different lane configurations and span lengths, 40 m in the case of two lanes, 50 m in the case of three lanes and 67 m in the case of four lanes. However, these empirical equations were specifically designed for two-cell straight bridges made of either concrete or steel. In 1995, Cheung and Fu employed the finite strip method to establish equations describing the relative behavior of curved and straight box girders. These equations were formulated as functions of various parameters, including span length, number of lanes, girder spacing, and radius of curvature. However, it's important to note that this study did not take into account the influence of the number of girders and the distribution of permanent loads. Additionally, it did not consider the beneficial effects of diaphragms located within the box girder itself or the effects of bracing between the girders.

Upon the suggestions for specific load distribution factors from California engineers dating back to 1959, AASHTO made refinements to the specified load distribution factors for bending moments in straight reinforced concrete bridges in 1996. These refined factors stipulated  $S/8$  for one-lane traffic and  $S/7$  for two or more lanes, with 'S' representing the cell width. However, these factors lack any insight into the structural behavior of the bridge or the factors influencing its response. In 1991, Zokaye and colleagues conducted research that contributed to the development of the moment and shear load distribution factors currently utilized in the AASHTO LRFD guidelines from 1994, specifically for straight concrete multi-cell bridges. Furthermore, in 1996, Brighton conducted a study aimed at determining the live load distribution factor for a new type of precast, concrete, two-cell box girders, which was proposed for use in a precast system designed for the rapid construction of short-span bridges.

The Canadian Bridge Design Code currently lacks specifications and design guidance for horizontally curved bridges, including box-girder bridges. However, these are highly effective due to their superior torsional stiffness compared to other composite I-main girder cross-sections. They offer improved load distribution characteristics and reduced permanent load effects. The American Association of State Highway and Transportation Officials (AASHTO) guidelines from 1996 propose that a curved bridge can be designed as a straight bridge when the central angle is 12 degrees. Furthermore, they suggest that for horizontally curved bridges, the curvature's effect can be disregarded in structural design



calculations as long as the ratio  $L/R$  is less than 1.0. Here,  $L$  represents the length of the curved span,  $b$  is half the width of the bridge, and  $R$  is the radius of curvature. However, these constraints have raised questions, particularly in terms of moment and shear considerations for curved composite bridge structures. As a result, there is a need for further research to gain a better understanding of moment and shear distribution in both composite concrete-steel straight and curved box girders, as well as multicell configurations.

Box girders are currently one of the most commonly used main girder types in bridge structures, (Schlaich & Scheef, 1982). They typically consist of a top and bottom flange, along with two or more webs, forming a closed box-like configuration. This configuration can be either single-cell or multi-cell. One of the primary focuses of analysis and development in this context is understanding how box girders respond to asymmetric loading, especially when dealing with composite cross-sections. The closed cross-section design of box girders provides them with high torsional stiffness, making them advantageous in scenarios where torsional stiffness is crucial, such as in inclined or curved bridges. Additionally, these superstructures offer significant longitudinal stiffness relative to the permanent weight. This characteristic enables them to span large distances, making box girders a viable and economically justified solution from both aesthetic and structural standpoints. (Schlaich & Scheef, 1982, Pedro, 1995).

The behavior of box girders often entails substantial plane deformations within the cross-section, which necessitates the use of methods that simultaneously include both longitudinal and transverse behavior. Several approaches are used to achieve this goal:

- Classical approach(classical formulation)
- Finite Element Method (solid finite element)



## 2.2 ANALYTICAL APPROACH

The determination of the longitudinal stress state in box girders can be achieved using classical formulations for bending, torsion, and distortion. This approach involves decomposing the complex problem associated with "folded plate action" into its constituent components, namely bending, torsion, and distortion. It is particularly applicable to girders that meet certain criteria, including having a length-to-height ratio ( $l/d$ ) of 4 or greater, a span size that is 1.5 times the width ( $b$ ) of the girder, where the local zones of influence resulting from the direct impact of external forces are considered separately (Schlaich & Scheef, 1982).

In cases where loads are symmetrically applied to the cross-section of the girder, the transverse and longitudinal analysis can be carried out separately. The phenomenon of girder warping becomes prominent in such scenarios. Additionally, the impact of shear stresses on the wide flanges, often referred to as the shear lag effect, may or may not be taken into account.

On the other hand, when an asymmetric load is applied, the analysis of transverse and longitudinal behavior becomes interconnected. Eccentric forces lead to deformation within the plane of the cross-section, resulting in distortion, as well as longitudinal bending of the plates, leading to the generation of longitudinal stresses. This phenomenon is commonly referred to as distortional warping.

Eccentric loads also introduce torsional effects. In locations where there is a variation in the torsional moment, the uneven torsion contributes to the development of longitudinal stresses. This phenomenon is particularly significant in cross-sections located near supports that resist warping, such as cross-sections close to the concentrated eccentric load.

Distortion and torsional warping can lead to an increase in longitudinal stresses, and whether or not these effects are considered significant depends on the specific case being analyzed.

According to the analysis conducted by Pedro (1995) and Schlaich & Scheef (1982), the analysis of box girders with thin-walled webs subjected to a load, as depicted in Figure x1, involves a systematic breakdown of the load into the following steps:

- Longitudinal analysis of the girder, treating it as having a rigid cross-section. This analysis considers the vertical and torsional loading resulting from direct integration along the transverse direction.
- Cross-sectional analysis:
  - The top flange is assumed to be fixed into the webs, as shown in Figure x11. In this analysis, the vertical load is replaced by equivalent forces and moments applied to the webs. For permanent loads and distributed live loads, the corresponding forces and moments are considered uniformly distributed in the longitudinal direction. However, for concentrated live loads, they are transferred through the top flange in a way that results in a non-linear longitudinal distribution of transverse flexural moments. This distribution can be determined using influence surfaces and shell/finite strip analysis. As a simplification, it is assumed that the vertical loading is equivalent to the action of a concentrated load and moment applied at the nearest point of the **web plate**. If this



approach is considered too conservative, it is possible to make certain simplifications to the models for in-plane load degradation, as determined by a specific study.

- The analysis involves a segment with a length  $d_x = 1$ , treated as a frame subjected to the action of eccentric loads  $(m_A, p_A), (m_B, p_B)$  – Figure 1
- Division of applied loads (concentrated and distributed) into symmetrical and asymmetrical parts

$$p_{sym} = \frac{p_A + p_B}{2} ; \quad p_{anti} = \frac{p_A - p_B}{2} \quad (1)$$

$$m_{sym} = \frac{m_A + m_B}{2} ; \quad m_{anti} = \frac{p_A + p_B}{2} \quad (2)$$

- Calculation of the bending moment in the transverse direction. For symmetrical loading, the distribution of bending moments in the transverse direction is considered by adding the results to those obtained from step 2.1.) The effect of longitudinal bending responsible for the girder's flexure has already been considered in step 1).
- Substitution of the asymmetric load on the torsional and distortional subsystem. In the case of shear stresses, which are defined using St. Venant's uniform torsion theory, non-uniform torsion leads to longitudinal stresses in the girder. These torsional warping stresses can be determined using Bescoter's torsion theory, which takes into account torsion bi-shear (Bescoter 1954)
- Finally, the effects of the distortion subsystems must be considered in the analysis. The results obtained from analyzing a single frame separately from the rest of the structure are not entirely accurate because part of the load is transmitted longitudinally and transferred as such to the adjacent frames. Therefore, there is a direct relationship between the transverse deformation of the girder and the longitudinal bending of the plates, a relationship established through compatibility and equilibrium. This provides an opportunity to develop a theoretical model of a beam on elastic foundations, which allows the replacement of the effect of girder distortion along the span. This theory was originally proposed by Wright, Abdel-Samed, & Robinson (1968). Analyzing the web as a beam on elastic foundations enables the simulation of bending moments, which are added to those calculated in steps 1) and 2.2.2), and longitudinal stresses, which are added to those caused by bending and torsional buckling.



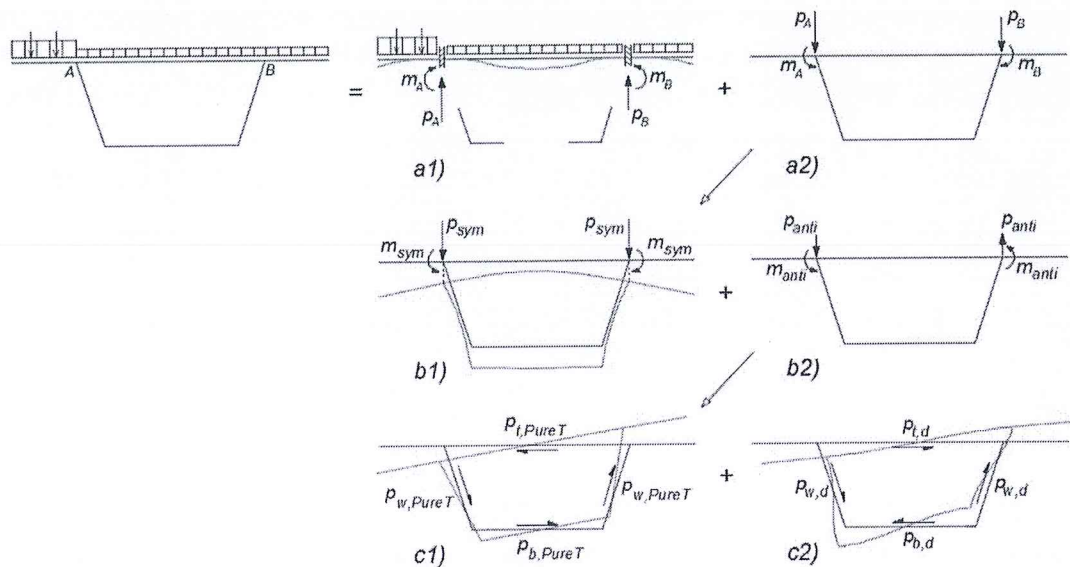


Figure 1 Load division for analysis of all phenomena in a box girder

## 2.3 FINITE ELEMENT METHOD

The analysis of a girder's response to asymmetric loading, which results from cross-section deformation, is conducted using both analytical methods and mathematical modeling through the finite element method. This analysis is carried out using software capable of three-dimensional modeling and analysis, with "ABAQUS" being a notable software application for this purpose that defines a new template for advanced nonlinear and detailed analysis. ABAQUS is a specialized software used for modeling and analyzing mechanical components and assemblies. It facilitates both the pre-processing phase of modeling and the visualization of results from finite element analysis. It is particularly well-suited for detailed analysis of girders with complex geometry. It offers efficient modeling of complex models that rely on the method of solid and shell-finite elements, instead of using simplified 1D elements. A key feature of ABAQUS is its ability to perform detailed analysis at the local cross-sectional level. This means that it can focus on specific elements of interest within the girder, such as top and bottom node distortion angles, normal stresses due to cross-section distortion, transverse bending moments, transverse stresses, longitudinal bending, and warping. ABAQUS not only calculates these parameters but also visualizes the results graphically. An appropriate modeling procedure is outlined below:

### Part 1) Input parameters:

The analysis process involves establishing various inputs regarding geometry, constitutive parameters, loading (concentrated loads, line loads, surface loads and permanent load specifications), support conditions and adequate placement of internal diaphragms if any. The material and strength characteristics of both steel and concrete are given. All loads are assumed vertical and are defined by their magnitude and their relevant coordinates in a global  $XYZ$  reference system.

### Part 2) Defining the model:

This phase of the analysis involves considerations related to longitudinal discretization and the choice of deformation modes. Each element's walls are defined by the coordinates of their endpoint nodes ( $X, Y, Z$ ). The loads are then distributed based on their position relative to these finite elements.





Additionally, it is possible to specify which deformation modes should be considered in the analysis and define the characteristics of the finite element network.

Part 3) Solving the equilibrium equations:

During this stage, it resolves the system of linear equilibrium equations and obtains the approximate longitudinal and transverse nodal amplitudes for each deformation mode.

Part 4) Calculation of longitudinal and transverse stresses:

The software calculates and records the stresses at the initial and final nodes of each element for various deformation and loading modes. This data provides a comprehensive understanding of the structure's response, including deformation, strains, stresses, rotations at specific points, reactions, and longitudinal deflections of the modeled girder. This information allows for the determination of distortion angles at critical nodes (node-concrete/steel and node-steel/steel), as well as the assessment of strains and subsequent stress distribution at the cross-sectional level. These calculations are crucial for recognizing the substantial influence of the rigid yet deformable characteristics of the cross-sectional frame, which significantly impact stress redistribution, both within the cross-section and longitudinally, leading to longitudinal warping and girder deformations.



### 3. ANALYTICAL APPROACH

#### 3.1 ANALYTICAL APPROACH-INTRODUCTION

This chapter provides a detailed explanation of analysis methods rooted in classical formulations for bending, torsion, and distortion. Despite the simplifications and inherent complexity of the physical processes involved, this approach can be more suitable and straightforward during the preliminary design phase when compared to finite element or surface element methods. Utilizing finite element and surface element approaches entails handling vast amounts of data, which can introduce a greater potential for errors (Schlaich & Scheef, 1982).

The chapter commences with an examination of longitudinal analysis, specifically focusing on the behavior of the box girder when subjected to bending. Simultaneously, shear lag effects are considered by applying defined effective widths. Subsequently, the chapter delves into the combined longitudinal and transverse behavior of the box girder when exposed to eccentric loading, incorporating the influences of torsion and distortion.

This approach is primarily applicable to homogeneous box girders. However, since the girders in question are prestressed, reinforced concrete box girders, they inherently possess heterogeneity due to the presence of reinforcement in both the transverse and longitudinal directions. To simplify the problem, a common approach is to replace the heterogeneous cross-section with an equivalent homogeneous one (as illustrated in Figure 2). This homogenization process is contingent on the structural characteristics themselves. It assumes that the girder is devoid of cracks and reinforcement. While this assumption holds true for prestressed concrete girders, caution is warranted in cases involving composite elements, where cracking may occur in the slab above the supports. Composite box girders are also susceptible to shearing at the concrete-steel contact.

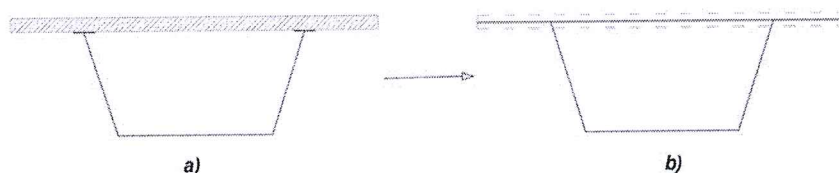


Figure 2 Typical cross-section of a composite box girder and b) equivalent homogenized cross-section

#### 3.2 BENDING ANALYSIS FOR BOX GIRDERS

##### 3.2.1 Elastic longitudinal bending

The loads applied to the box girder induce longitudinal stresses primarily caused by longitudinal bending. The ratio of the dimensions of the cross-section in relation to the span length permits analysis and treatment of the girder as a slender prismatic element capable of undergoing elastic bending. This behavior can be determined using the Euler-Bernoulli theory.

Under certain simplifying hypotheses, it becomes feasible to derive the differential equation governing linear elastic bending. These outcomes are suitable for homogeneous box girders as mentioned in section 3.2.1.3.



### 3.2.1.1 Hypotheses

- The hypotheses made during the analysis of the box girder are as follows:
- The girder is prismatic in shape;
- The material is homogeneous and follows Hooke's law for elasticity, characterized as isotropic;
- Plane cross-sections of the girder remain plane and perpendicular to its axis, following Bernoulli's hypothesis;
- Cross-sections are free to deform within their own plane, i.e.  $\sigma_{yy} = \sigma_{zz} = \tau_{yz} = 0$  – Navier's Hypothesis.

### 3.2.1.2 Bending equation

If we examine a box girder subjected to a symmetrical load, as depicted in Figure 3.

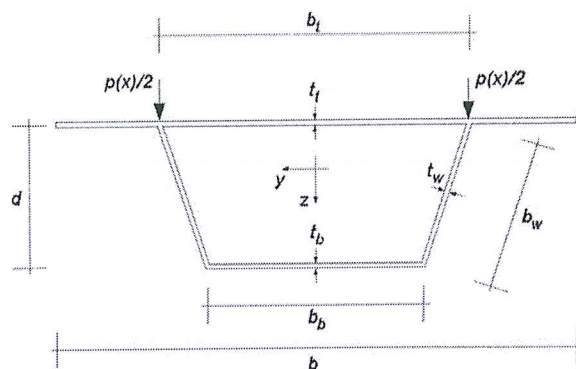


Figure 3 Generated cross-sectional view of a box girder under symmetrical loading along the upper edge of the webs

According to Bernoulli's hypothesis, for a structure with infinite length, the longitudinal deformation at any point within the cross-section can be expressed by the equation:

$$\varepsilon_{xx} = \frac{z}{R_z} \quad (3)$$

Here  $z$  represents the vertical coordinate measured from the center of gravity, and  $R_z$  is the radius of curvature, positive, as depicted in Figure 4.

According to Hooke's law and utilizing Navier's hypotheses, along with Young's Modulus  $E_z$ , the longitudinal stresses resulting from bending are expressed as:

$$\sigma_b = \varepsilon_{xx} \cdot E = \frac{E}{R_z} \cdot z \quad (4)$$

Considering that the vertical load does not induce any axial force  $N$ , it can be deduced that the cross-section in the region where strain is zero, known as the neutral axis, passes through the center of gravity. Therefore:

$$N = \int_A \sigma_b dA = \int_A \frac{E}{R_z} \cdot z dA = \frac{E}{R_z} \int_A z dA = 0 \quad (5)$$

Given that the longitudinal stresses need to be balanced only by the bending moment caused by the external load:



$$M_y = \int_A \sigma_b z dA = \int_A \frac{E}{R_z} \cdot z^2 = \frac{EI_y}{R_z} \quad (6)$$

where  $I_y$  represents the secondary moment of inertia around the  $y$  – axis and is obtained through the equation:

$$I_y = \int_A z^2 dA \quad (7)$$

Combining the first and last equations, the balance between the bending moment and the longitudinal stresses at any point of the cross-section is defined as:

$$\sigma_b = \frac{M_z}{I_y} \cdot z \quad (8)$$

If the deformed state of the girder is considered as shown in Figure 4 from the differential equation and assuming that the displacements are small, it can be taken that:

$$\frac{1}{R_z} = -\frac{v_{xx}}{[1+v_x^2]^{\frac{3}{2}}} \approx -v_{xx} = \frac{M_y}{EI_y}, \quad (9)$$

where  $v$  represents the displacement of the center of gravity seen along the vertical axis  $z$  and  $v_x$  and  $v_{xx}$  are the first and second derivatives along the axial axis respectively.

If we establish the static equilibrium, of an infinitesimal segment of a girder exposed to a general vertical load  $p_x$ , (Figure 4) it follows that:

$$p(x) = -\frac{dV}{dx}; \quad v(x) = \frac{dM}{dx} \quad (10)$$

The simplified Euler–Bernoulli equation for bending, obtained through the last two equations, is as follows:

$$\frac{d^4v}{dx^4} EI_y = p(x) \quad (11)$$

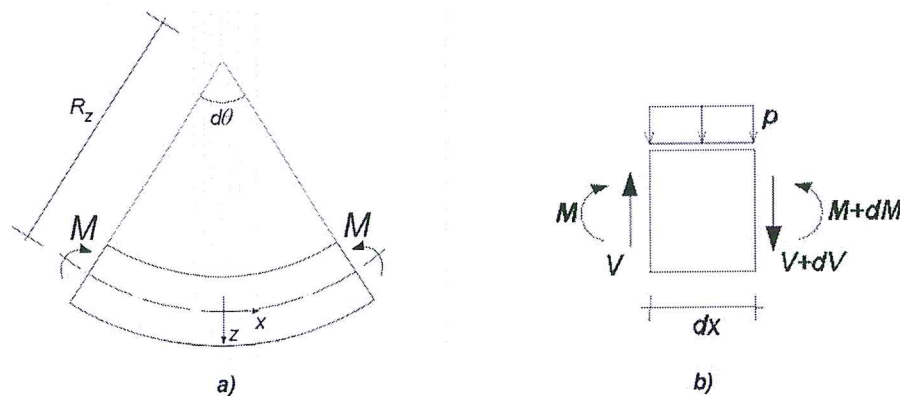


Figure 4 Deformed state of the girder subjected to bending and static equilibrium of a girder segment under a vertical load

### 3.2.2 Transverse distribution - „Shear lag effect“

The theory of elastic bending is correct for pure bending, as long as the shear forces are equal to zero. However, in the general case shear stresses exist and when present they are responsible for the deformation of the cross-section in its own plane, including warping. Plane cross-sections are no longer



plane, so Bernoulli's plane-section hypothesis and theory accordingly no longer hold, although they provide a good basis for an initial approximation.

When shear deformations are taken into account in the analysis of a girder, it leads to a change in the longitudinal stress distribution within the wide flanges of the girder compared to the previously established stress distribution according to the Euler-Bernoulli theory. This change is attributed to the phenomenon known as the shear lag effect. As illustrated in the figure below, the stresses increase in the regions near the nodes where the web and flanges meet, and they decrease as you move away from these nodes. The ratio between the maximum stress and the average stress within the cross-section of the box girder has been identified as an important factor in the elastic analysis of the cross-section. This effect is particularly pronounced near concentrated loads and when the flange width-span ratio is high (Chen & Yen, 1980).

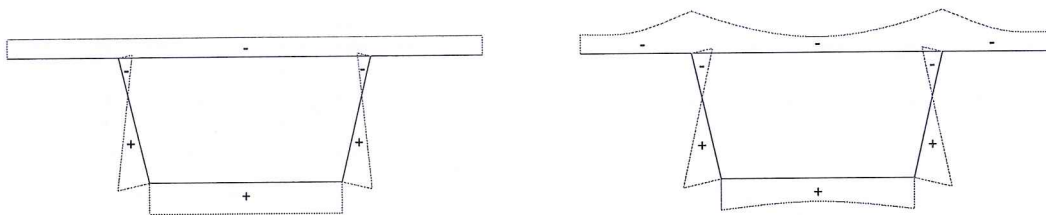


Figure 5 Longitudinal bending stresses with and without the influence of transverse distribution

The traditional approach for incorporating the shear lag effect involves calculating the cross-sectional properties while using reduced effective widths for the wide flanges. Various methods can be employed to define these parameters, but the one outlined in (B.S.I., 2004), which is based on stress distribution, is commonly utilized. In this approach, the effective width is determined in such a way that it can accommodate a force equivalent to what the flange itself can bear, all while assuming that the longitudinal stresses remain constant and equal to the maximum longitudinal stresses resulting from the non-linear stress distribution. Once these maximum values are defined, an analytical approach can be employed to determine the stresses throughout the entire cross-section.

The calculation of the effective width is a more practical approach when compared to determining analytical methods for defining the normal stress distribution. Analytical methods often involve complex equations and multiple approximations, which restrict their applicability to specific, typical cases.

### 3.2.2.1 Effective width

The calculation of longitudinal stresses across the span of a box girder while considering the shear lag effect can be accomplished by analyzing an equivalent cross-section with flanges of reduced width. This reduced width corresponds to the effective width, defined as:

$$\frac{b_c}{b} = \frac{\sigma_b}{\sigma_{b,sl}^{max}} = \eta \quad (12)$$

Here  $\eta$  represents the effective width coefficient, which is the ratio between the mean and maximum longitudinal stress, respectively.

The effective width factor is primarily influenced by the following factors:



- Segment width/length ratio  $(b_c; b_b; b - b_t)/(2l)$
- Type of load (concentrated or distributed)
- Support conditions
- Stiffness coefficient defined as:

$$\alpha = \frac{A_r}{A_f} \quad (13)$$

Where  $A_r$  is the transverse surface area of the longitudinal bracings, and  $A_f$

is the corresponding flange area, both measured along the width  $(\frac{b_c}{2}; \frac{b_b}{2}; \frac{b-b_t}{2})$ .

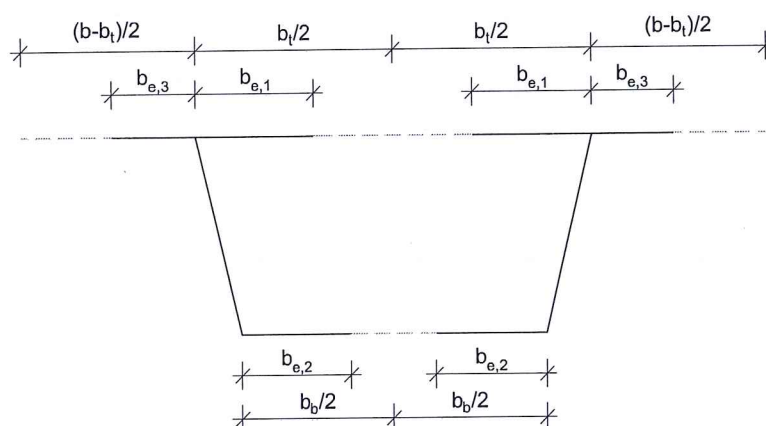


Figure 6 Effective cross-section for box girder bridge, effective widths contributing to the cross-section response

Considering the parameters mentioned earlier, a series of coefficients for effective width is provided, explained below. Although these coefficients are primarily intended for uniformly distributed loads along the entire span, the code specifies that they can also be used for concentrated loads from vehicles or railway vehicles. For cantilever extensions beyond the web, an appropriate coefficient  $k$  is used:  $k = [1 - 0.15 (b - b_t)/(2l)]$ .

Effective width coefficients for intermediate values can be obtained through linear interpolation. The same can be done for intermediate positions in the span.

With the fully defined effective width of the cross-section, the maximum longitudinal stress in the top and bottom flanges, particularly at the joint with the web, can be determined using the results of the standard Euler-Bernoulli theory:

$$\sigma_{b,SL}^{t,max} = \sigma_b^t \frac{b}{2(b_{e,1} + b_{e,3})} \quad (14)$$

$$\sigma_{b,SL}^{b,max} = \sigma_b^b \frac{b_b}{2b_{e,2}} \quad (15)$$

Finally, the non-linear stress distribution over the entire cross-section can be calculated using the equations provided in B.S. 5400 Part 3 (2004), where  $y$  is the distance to the web-flange joint (Figure 6):

$$\sigma_{b,SL}^t = \sigma_{b,SL}^{t,max} \left[ \left( \frac{b_t - 2y}{b_t} \right)^4 + 0.25(5\eta - 1) \left( 1 - \left( \frac{b_t - 2y}{b_t} \right)^4 \right) \right] \quad (16)$$



$$\sigma_{b,SL}^t = \sigma_{b,SL}^{t,max} \left[ \left( \frac{(b-b_t)-2y}{(b-b_t)} \right)^4 + 0.25(5\eta - 1) \left( 1 - \left( \frac{(b-b_t)-2y}{(b-b_t)} \right)^4 \right) \right] \quad (17)$$

$$\sigma_{b,SL}^b = \sigma_{b,SL}^{b,max} \left[ \left( \frac{b_b-2y}{b_b} \right)^4 + 0.25(5\eta - 1) \left( 1 - \left( \frac{b_b-2y}{b_b} \right)^4 \right) \right] \quad (18)$$

### 3.3 TORSIONAL-DISTORTIONAL ANALYSIS OF BOX GIRDERS

The action of live loads on bridge structures can often result in asymmetric loading relative to the bridge's axis. This asymmetry leads to not only pure bending but also torsional or distortion effects. Torsion or distortion behavior in elements with closed cross-sections, like box girders, can be divided into three separate effects (Kollbrunner&Basler, 1969):

- Uniform torsion or Saint – Venant torsion
- Non-uniform torsion or warping
- Distortion

The first two mechanisms involve the external influence being considered through twisting and warping. Saint-Venant torsion is characterized by a constant circulatory shear force in each cross-section, while warping is associated with the development of stresses caused by **bi-moment u bi-shear stresses** (Koll Brunner & Basler, 1969). The total torsional moment is the sum of uniform and non-uniform torsion. In cases where both phenomena exist and neither predominates, the cross-section is said to undergo mixed torsion.

When analyzing the two previous effects, it is assumed that the cross-sections maintain their planar shape. However, if this assumption is not valid, it becomes necessary to consider the effects of cross-sectional distortion, as these effects can be significant.

Therefore, the interaction of all three effects will be discussed under the influence of asymmetric loading. Ultimately, analytical equations will be derived to calculate longitudinal and transverse normal stresses. The focus is on a single-cell box girder that is symmetrical about the vertical axis and exhibits clear behavior in this context.

#### 3.3.1 Girder response under eccentric loading

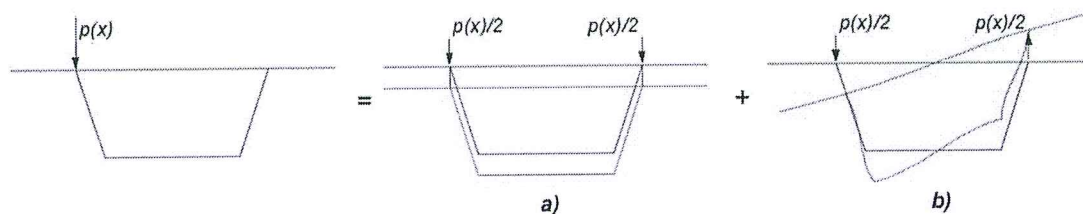


Figure 7 Load decomposition into symmetric and asymmetric component

The load can be categorized into symmetric and asymmetric components, as depicted in Figure 7. The symmetric component induces longitudinal bending across the entire cross-section, resulting in vertical displacement as a rigid body. Conversely, the box girder's response to the asymmetric portion

of the load can be described as the interaction of three subsystems related to uniform torsion, non-uniform torsion, and distortion.

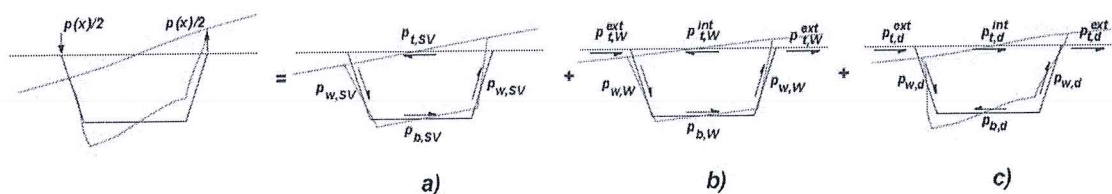


Figure 7.1 Decomposition of the asymmetric component of the load into uniform torsion, warping torsion and distortion

The next step is to determine the force system for each of the individual subsystems. The force systems for the first two can be established using Benscoter's theory (Benscoter, 1954) for torsional warping, which accounts for bi-shear deformation as a contributing factor.

Distortion forces on the other hand can only be determined through the disposition of the torsion in the initial load. Considering the longitudinal variation of torsional forces (while only considering torsional warping) adds complexity. However, since warping stresses caused by torsion are typically small, it's reasonable to neglect them when calculating distortional forces (Fan & Helwig, 2002). Therefore, torsion forces can be determined using Saint-Venant torsion theory (as described in sections 3.3.2 and 3.3.3).

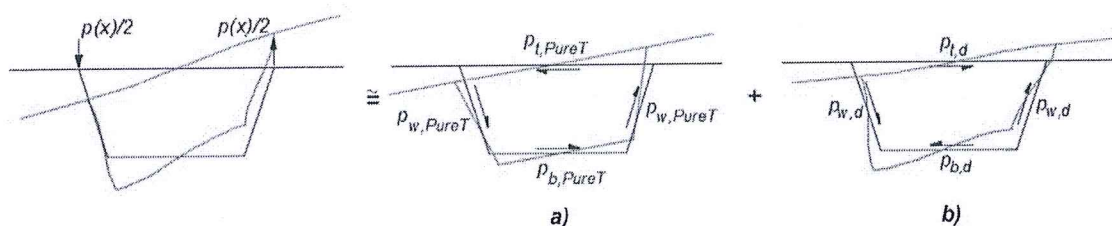


Figure 8 Decomposition of the asymmetric component of the load pure torsion and distortion

These approximate torsional forces, commonly referred to as pure torsional load, are obtained by integrating shear stresses calculated using Bredt's formula (along plate cross-sectional areas):

$$p_{w,pureT} = \left( \frac{b_t \cdot b_w}{(b_t + b_b) \cdot d} \right) \left( \frac{p(x)}{2} \right) \quad (19)$$

$$p_{t,pureT} = \left( \frac{b_t}{b_w} \right) p_{w,pureT}, \quad p_{b,pureT} = \left( \frac{b_b}{b_w} \right) p_{w,pureT}. \quad (20)$$

The components constituting the distortion system can be determined by ensuring that the force system is in self-equilibrium, and the sum of the vertical components must be equal to  $\frac{p(x)}{2}$  according to:5





$$p_{w,d} = \left( \frac{b_b \cdot b_w}{(b_t + b_b) \cdot d} \right) \left( \frac{p(x)}{2} \right) \quad (21)$$

Next, the horizontal forces can be calculated by considering the resultant moments and forces. Calculating the moments at the top and bottom nodes gives:

$$p_{t,d} = \left( \frac{b_b}{b_w} \right) p_{w,d}, \quad p_{b,d} = \left( \frac{b_t}{b_w} \right) p_{w,d}. \quad (22)$$

Now that the torsional and distortional loads have been defined, they can be considered individually as uniform torsion, torsional warping, and distortion. For simplicity, the „ $x$ “ is omitted, but it should be noted that parameters such as  $q, u, T$  and others vary along the longitudinal direction.

### 3.3.2 Uniform torsion

Uniform torsion can be simply described as a twisting reaction that results in circular shear within the cross-section. It involves shear stresses that are linear to the geometry. In the case of closed cross-sections, such as box girders, the torsional stiffness is primarily represented by a uniform torsional flow circulating around the closed cross-section. Shear stresses that are linear to the geometry can often be neglected in this context.

Assuming that the cross-section is rigid as it rotates about its shear center of rotation, it will remain plane only if the strains at the midpoints of the plates are proportional to their normal distance to the shear center Vlasov (1961). For constant shear flow, this is only possible if the thickness grows at the same rate as the normal distance to the shear center. These conditions are not relevant for most situations, meaning that cross-sections will generally undergo warping.

In Saint-Venant's torsion theory, the displacement caused by warping can be expressed as a function of twist  $\phi, x$ , which is treated as a constant (the comma indicates a differentiation). This understanding will be of practical importance in the chapters that delve into torsional warping, as it is closely linked to the behavior of the cross-section beyond its plane.

#### 3.3.2.1 Hypotheses

When discussing the behavior of box girders according to Saint-Venant torsion theory, four key assumptions are typically considered:

- The shape of the cross-section remains unchanged within its own plane, meaning it remains undeformed in that plane while rotating around the shear center and undergoing warping perpendicular to that plane;
- Stresses within the girder are directly proportional to strains, following Hooke's law;
- The box girder is prismatic, which means its constituent elements may vary in thickness within the cross-section, but not along the length of the girder itself;



- The cross-section of the box girder is thin-walled. This implies that the variation of shear stresses across the thickness of the elements and the resulting secondary displacements due to warping are small and can be safely neglected;

### 3.3.2.2 Basic equations and relations

In the context of thin-walled closed cross-sections, the torsional system generates a constant shear flow that circulates around the closed perimeter. This shear flow is quantified using Bredt's formula:

$$q_{sv} = \frac{T_{sv}}{2 \cdot A_0} = \frac{T_{sv}}{(b_b + b_t) \cdot d} \quad (22)$$

Here  $A_0$  represents the area enclosed by the central line of the walls composing the cross-section.

The true shear strain in the mid-surface is related to the tangential and axial displacements  $v$  and  $u$ , as shown in Figure 8. This relationship can be expressed as:

$$\gamma_{sv} = \frac{q_{sv}}{G \cdot t} = \frac{\delta u}{\delta s} + \frac{\delta v}{\delta x} \quad (23)$$

For small angles, the rotation of rigid bodies is related to the tangential displacements of the central line as follows:

$$\frac{\delta v}{\delta x} = r \phi_{,x} \quad (24)$$

Where  $r$  represents the normal distance between the shear center and the considered closed wall segment and  $\phi_{,x}$  is constant as already stated. By replacing 88 and 99 we get:

$$du = \left( \frac{q_{sv}}{G \cdot t} - r \phi_{,x} \right) \cdot ds \quad (25)$$

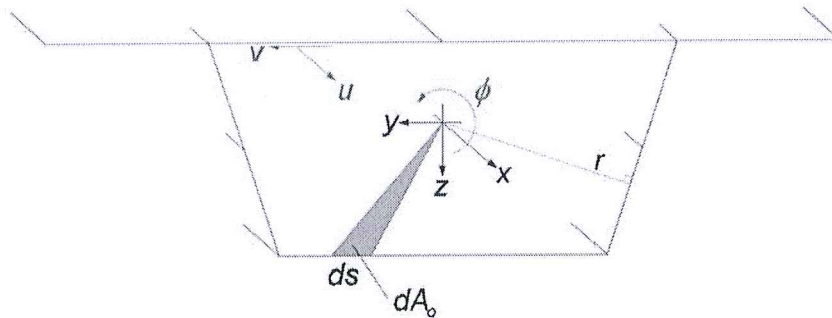


Figure 9 Deformation-displacement of the cross-section as a result of the rotation

The warping function at any point of the cross-section can be determined by integrating  $du$  along the central line of the entire cross-section, starting from some arbitrary point:

$$u(s) = u_0 + \int_0^{s, cell} \frac{q_{sv}}{G \cdot t} ds - \phi_{,x} \int_0^s r ds \quad (26)$$

Noting that  $u$  is not a function of  $x$  given the hypotheses employed. In this relation  $u_0$  denotes the warping-induced displacement at the initial point and the first integration is applied only to the cell

walls, not to the cantilever parts of the top flange. If  $u_s$  integrated around the closed perimeter and set to zero, to ensure the continuity of the displacements caused by warping, we get:

$$\oint \frac{q_{sv}}{G \cdot t} ds = 2 \cdot A_0 \cdot \phi_{,x} \quad (27)$$

Here  $2 \cdot A_0 = \int_0^s r ds$  as a result of geometric analysis (Calgaro, J. A. Virlogeux, 1988).

By substituting the Saint-Venant shear flow,  $q_{sv}$ , according to 5, we get:

$$\phi_{,x} = \frac{T_{sv}}{G \cdot J} \quad (28)$$

$$J = \frac{4 \cdot A_0^2}{\oint \frac{ds}{t}} \quad (29)$$

$J$  is the Saint-Venant torsional constant for single-cell box girders. If  $u_0 = -\phi_{,x} \cdot C_0$ , then we can understand that:

$$u_s = -\phi_{,x} \cdot \left( w_s(s) - \frac{2 \cdot A_0}{\oint \frac{ds}{t}} \cdot \int_0^s \frac{ds}{t} + C_0 \right) \quad (30)$$

Here  $w_s(s)$  is the so-called "sectorial coordinate" and is calculated through the integration of the previously defined tangential radii around the central line, viewed relative to the shear center and starting at an arbitrary point of the closed perimeter:

$$w_s(s) = \int_0^s r ds \quad (31)$$

Since the second expression between the brackets is also a function of integration along the midline, an equivalent sectorial coordinate  $\widetilde{w}_s$  can be defined:

$$\widetilde{w}_s(s) = w_s(s) - \frac{2 \cdot A_0}{\oint \frac{ds}{t}} \cdot \int_0^s \frac{ds}{t} \quad (32)$$

By defining a new quantity  $\widetilde{u}_s(s)$ , defined as a stabilized warping function, it is possible to reach a compatible relation, taking the warping displacements and rate of twist  $\phi_{,x}$  for Saint-Venant torsion. The value of the constant  $C_0$  will be determined in the subsequent chapter.

$$\widetilde{u}_s(s) = \widetilde{w}_s(s) + C_0 \quad (33)$$

$$u_s(s) = -\phi_{,x} \cdot \widetilde{u}_s(s) \quad (34)$$

### 3.3.3 Non-uniform torsion

If the warping is not constant along  $x$ , the normal strains and stresses increase. The basis of warping-induced displacements is such that these warping torsional stresses vary along the perimeter of the cross-section and along the length of the girder itself, thus some of the shear stresses are balanced by the torsional moment.

#### 3.3.3.1 Hypotheses

The development of a formulation to include and define non-uniform torsion is based on the same assumptions as those for uniform torsion, according to the following conditions:



The longitudinal normal stresses can be calculated without considering the Poisson effect;

The normal displacements (flexures) resulting from the warping  $u_s(x, s)$  are obtained through:

$$u_s(x, s) = -\widetilde{u}_s(s) \cdot \frac{d\chi}{dx} \quad (35)$$

Here  $\chi = \chi(x)$  is a function that should be determined, and its derivative is used analogously to the derivative of the rotation angle described in (3.37)  $\widetilde{u}_s(s)$  represents a stabilized value of the warping function.

### 3.3.3.2 Compatibility equations

As mentioned earlier, uniform torsion formulations establish a correlation between Saint-Venant torsional shear and warping-induced deformations of the cross-section. When warping-induced deformation varies along  $x$ , a set of warping torsional stresses  $\sigma_w$ , and corresponding shear stresses  $\tau_w$  are generated. These are added to the stresses associated with uniform torsion  $\tau_{s,v}$ . The key difference between these newly introduced stresses and those considered in Saint-Venant's theory is that the deformations of the closed cross-section are no longer exact because  $\phi_{,x}$  is no longer constant. To account for this, a new auxiliary function  $\chi(x)$  is defined, which depends on the total shear flow  $q = q_{sv} + q_w$ . This leads to the adoption of hypothesis 2, assuming that warping-induced deformations should result from 3.38.

With warping deformations already defined, the normal strains and stresses can be derived from the standard compatibility and constitutive equations for linear elements:

$$\varepsilon_w(x, s) = \frac{du}{dx} = -\widetilde{u}_s(s) \frac{d^2\chi}{dx^2} \quad (36)$$

$$\sigma_w(x, s) = -E \cdot \widetilde{u}_s(s) \frac{d^2\chi}{dx^2} \quad (37)$$

Before writing the equilibrium equation, we first need to fully define the warping function  $\widetilde{u}_s(s)$ . For this to happen, the position of the shear center and the value of the constant  $C_0$  relating to the cross-section under consideration must first be determined. The cross-sectional diagrams relating to the coordinates  $w_s(s)$  and the warping function  $\widetilde{u}_s(s)$  are schematically shown in Figure 9, where  $S$  represents the shear center. They are usually obtained starting with integration from point 0, also presented in Figure 9.

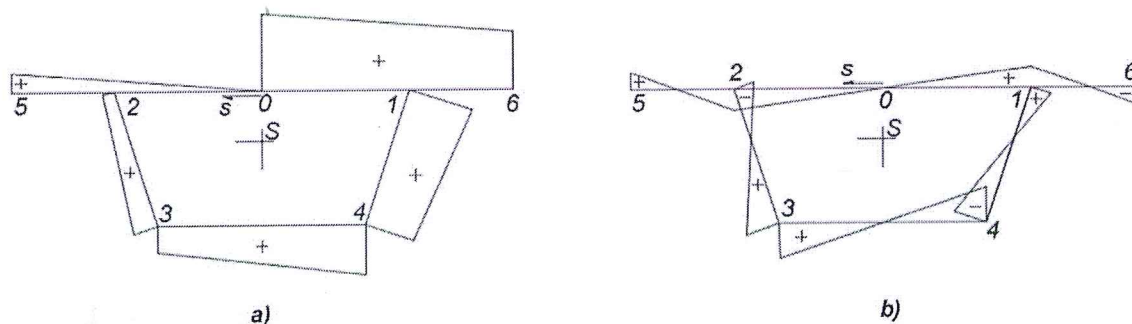


Figure 10 Sectorial-coordinates, a diagram showing the warping function

### 3.3.3.3 Shear center

In a thin-walled cross-section as the one presented in Figure 10, S is the shear center, G is the center of mass, A is a generic point along the mid-line, P is defined as the initial point from which the characteristics of the cross-section can be calculated.

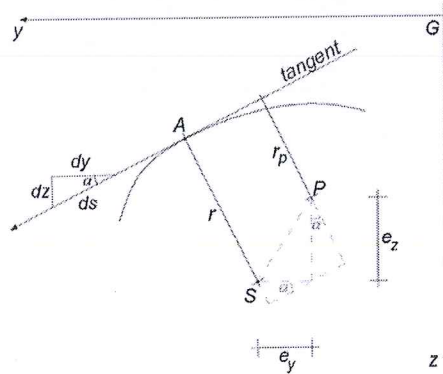


Figure 11 Tangential radius for reference points

The relation between the tangential radius  $r$  and  $r_p$  is expressed using geometric characteristics and can be defined as:

$$r = r_p + e_z \cdot \frac{dy}{ds} - e_y \cdot \frac{dz}{ds} \quad (37)$$

When integrating between the arbitrary starting point of the **mid-line** and point A, and using the equation (3.34), the following expression is obtained:

$$\int_S (r - r_p) ds = \int_S e_z dy - \int_S e_y dz \Leftrightarrow w_s = w + (e_z)y - (e_y)z + C_0 \quad (38)$$

By utilizing (3.35), a relationship can be established between equivalent sectorial coordinates calculated relative to the shear center  $\bar{w}_s$  and to the initially defined point P  $\bar{w}_p$ :

$$\bar{w}_s = \bar{w}_p + (e_z) \cdot y - (e_y) \cdot z + C_0 \quad (39)$$

For an element subjected solely to an external moment of rotation, the equations express:

$$\int_A \sigma_w dA = 0 \quad (39)$$

$$\int_A \sigma_w y dA = 0 \quad (40)$$

$$\int_A \sigma_w z dA = 0 \quad (41)$$

With (3.40) and (3.36), the preceding system of equations can be written as:

$$\int_A \bar{w}_p dA + C_0 \cdot A = 0 \quad (42)$$

$$\int_A \bar{w}_p y dA - e_y \cdot I_y - e_z \cdot I_{yz} = 0 \quad (43)$$

$$\int_A \bar{w}_p z dA + e_y \cdot I_{yz} + e_z \cdot I_z = 0 \quad (44)$$

The system of equations can be solved via  $C_0$  and the location coordinates for the shear center:

$$C_0 = -\frac{1}{A} \cdot \int_A \tilde{w}_p dA \quad (45)$$

$$e_y = \frac{I_z \cdot S_{wz} - I_{yz} \cdot S_{wy}}{I_y \cdot I_z - I_{yz}^2} \quad (46)$$

$$e_z = -\frac{I_y \cdot S_{wy} - I_{yz} \cdot S_{wz}}{I_y \cdot I_z - I_{yz}^2} \quad (47)$$

Here  $S_{wy}$  и  $S_{wz}$  are inertial quantities of the cross-section defined as

$$S_{wy} = \int_A \tilde{w}_p y dA \quad (48)$$

$$S_{wz} = \int_A \tilde{w}_p z dA \quad (49)$$

### 3.3.3.4 Equilibrium equation

The normal stresses caused by warping according to equation (37). Applying the equation to an infinitesimal wall element – Figure 12 – the following is obtained:

$$\frac{d\sigma_w}{dx} \cdot t + \frac{dq_w}{ds} = 0 \quad (50)$$

By substituting (3.40) into (3.49) and subsequent integration along the central line of the cross-section we can define the equation for the secondary warping shear flow  $q_w$  which is in self-equilibrium.

$$E \cdot \tilde{u}(s) \cdot \frac{d^3 \chi}{d \cdot x^3} \cdot \int_0^s \tilde{u}(s) \cdot t ds \quad (51)$$

$$q_w(s) = E \cdot \frac{d^3 \chi}{d \cdot x^3} \cdot \int_0^s \tilde{u}(s) \cdot t ds \quad (52)$$

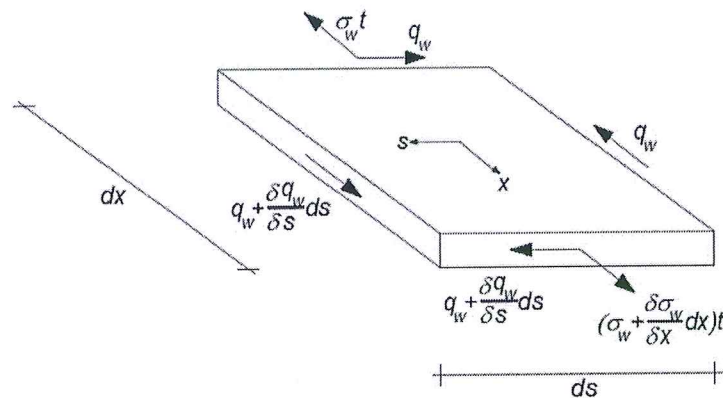


Figure 12 Equilibrium of an infinitesimal segment subjected to warping torsion

With the already defined warping shear flow, the warping torsion  $T_w$  can be obtained through integration, as follows:

$$T_w = \int_s q_w r ds = -EI_w \cdot \frac{d^3 \chi}{d \cdot x^3} \quad (53)$$

Here  $I_w$  is the warping constant, defined as



$$I_w = \int_s (\tilde{u}(s))^2 t ds \quad (54)$$

The torsional moment is balanced through the sum of the contribution of both uniform and non-uniform torsion, given in (28) and (53):

$$T = T_{sv} + T_w = GJ \cdot \frac{d\phi}{dx} - EI_w \cdot \frac{d^3 \chi}{dx^3} \quad (55)$$

On the other hand, the torsional moment can be expressed as a function of the total shear flow, which can be determined by using (23) and (24) according to (Calgaro, J. A. Virlogeux, 1988):

$$q = G \cdot t \cdot \left( \frac{\delta u}{\delta s} + \frac{d\phi}{dx} \right) \quad (56)$$

$$T = \int_s q r ds = G \cdot I_c \cdot \frac{d\phi}{dx} - G \cdot (I_c - J) \cdot \frac{d\chi}{dx} \quad (57)$$

Here  $I_c$  is the shear central second moment of inertia

$$I_c = \int_s r^2 t ds \quad (58)$$

Eliminating  $\frac{d\phi}{dx}$  from (55) and (57), a differential equation is obtained, which is related to the warping function  $\chi$  and the torsional moment:

$$-EI_w \frac{d^3 \chi}{dx^3} - \mu GJ \frac{d\chi}{dx} = \mu T \quad (59)$$

Here  $\mu$  is the shear-induced warping parameter presented as

$$\mu = 1 - \frac{J}{I_c} \quad (60)$$

This is a parameter for the curvature of the cross section, and that in terms of torsion. For very thin walls, unity is performed, considering the effect of "shear warping" to have little influence. This effect can also be described as torsion bi-shear. This is related to the shape of the warping function  $\tilde{u}$  (Figure 10), where the two webs bend with the same magnitude, but in the opposite direction. With the same analogy it is possible to define a new quantity B, defined as the bi-moment or warping moment, by which the longitudinal stresses can be calculated through the "bending moment" equation:

$$\sigma_w(x, s) = \tilde{u}(x, s) \frac{B}{I_w} \quad (61)$$

$$B = -EI_w \frac{d^2 \chi}{dx^2} \quad (62)$$

Solving the differential equation  $-EI_w \frac{d^3 \chi}{dx^3} - \mu GJ \frac{d\chi}{dx} = \mu T$  with respect to  $\frac{d\chi}{dx}$  and introducing another derivative we can define the bi-moment B as defined in  $B = -EI_w \frac{d^2 \chi}{dx^2}$ , followed by the calculation of stresses caused by torsional warping according to

$$\sigma_w(x, s) = \tilde{u}(x, s) \frac{B}{I_w} \quad (63)$$

On the other hand, it is possible to derive more generating differential equilibrium equations, which will correlate with the warping function  $\chi$  and will generate a value for the torsional load  $m_T$ . This can be achieved first by solving the static equation of an infinitesimal segment of the girder (Figure 13):



$$-T + m_T dx + \left(T + \frac{dT}{dx} dx\right) = 0 \quad (64)$$

which simplifies to:

$$-\frac{dT}{dx} = m_T \quad (65)$$

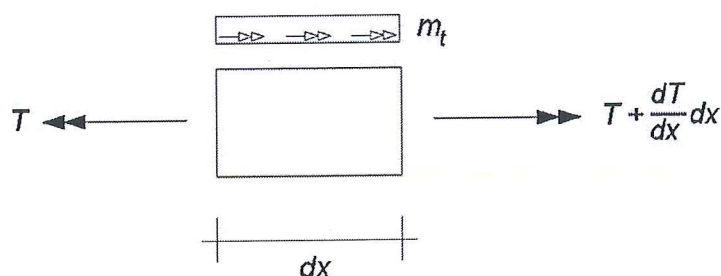


Figure 13 Equilibrium state of an infinitesimal segment of the girder subjected to torsion

By introducing a derivative in  $-EI_w \frac{d^3 \chi}{dx^3} - \mu GJ \frac{d\chi}{dx} = \mu T$  and using the equation developed in  $-\frac{dT}{dx} = m_T$  the general equilibrium equation is obtained:

$$\frac{EI_w}{\mu} \left(\frac{d^4 \chi}{dx^4}\right) + GJ \left(\frac{d^2 \chi}{dx^2}\right) = m_T(x) \quad (66)$$

An interesting observation is the fact that the function  $\chi(x)$  would be taken equal to  $\phi(x)$ , i.e., if **bi-shear** is neglected, the same equilibrium equation will be obtained, where the parameter defining the warping shear is not taken into consideration. The simplified equation corresponds to the so-called Karman-Christensen theory of torsion:

$$EI_w \left(\frac{d^4 \chi}{dx^4}\right) + GJ \left(\frac{d^2 \phi}{dx^2}\right) = m_T(x) \quad (67)$$

### 3.3.3.5 Homogenization rules during torsion accompanied by warping and distortion in a composite girder

Warping torsion in composite box girders has been analyzed by Chen & Yen (1980). The definition of the distribution of shear and stresses is carried out through an appropriate substitutive thickness of the concrete plate-flange as follows:

$$\gamma = \frac{q}{G_c(t_t)_w} = \frac{q}{G_s(t_t)_{SV+W}} \leftrightarrow \left(\frac{t_t'}{t_t}\right)_{SV+W} = \frac{G_s}{G_c} \approx \frac{E_s}{E_c} = n \quad (68)$$

$$\sigma_w^c = \frac{\sigma_w^s}{n} = \tilde{u}(x, s) \frac{B}{nl_w} \quad (69)$$

### 3.3.4 Distortion

When a box girder experiences distortion, it undergoes deformations within its own cross-sectional plane. The compatibility in the deformations of the web-flange node contributes for the walls that form the cross-section, to submit and deform in the direction of their mid-lines, which means that if it is assumed that the membrane shear strains are equal to zero, warping occurs. So every response of





the frame is between the response of those "freely deformable" and "stiff" cross-sections, where the degree of stiffness increases simultaneously in both transverse and longitudinal directions. According to Schlaich & Scheef (1982) if the load is changed to a small extent in the longitudinal direction and if the deformation in the transverse direction is not prevented, then the cross-section behaves closer to the free distortion frames. On the other hand under concentrated load action or for areas near transverse bracings, the fully rigid frame approach is closer to reality (Schlaich & Scheef, 1982).

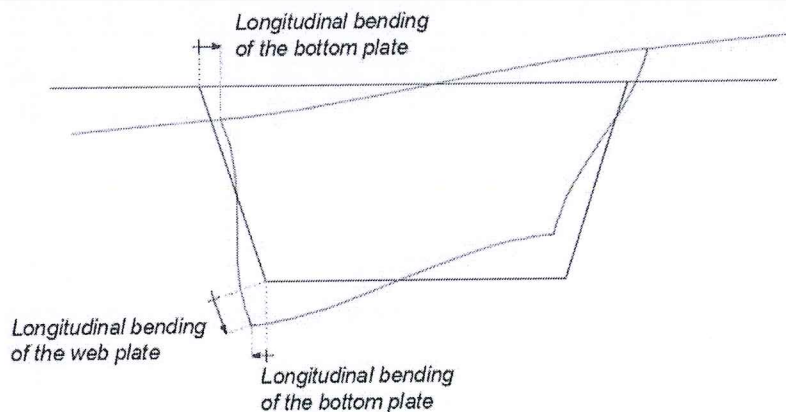


Figure 14 Displacement compatibility under distortion

The redefinition of the distortion load  $p_d$  acting on the box girder means simultaneous balancing through two composite mechanisms:

- Longitudinal bending of the flanges, correlated with the load  $p_d^L$
- Deformation occurring in the transverse direction of the cross-section itself, correlated with the load  $p_d^T$
- The sum of these two distinct deformations results in the total force, expressed as:

$$p_d = p_d^L + p_d^T \quad (70)$$

- Considering that the distortion system is in a state of self-equilibrium, we can infer the following equations:

$$p_{w,d}^L = p_{w,d} - p_{w,d}^T$$

$$p_{t,d}^L = p_{t,d} - p_{t,d}^T = -\left(\frac{b_b}{b_w}\right)(p_{w,d} - p_{w,d}^T) \quad (71)$$

$$p_{b,d}^L = p_{b,d} - p_{a,l}^T = -\left(\frac{b_t}{b_w}\right)(p_{w,d} - p_{w,d}^T)$$

### 3.3.4.1 Hypotheses

When considering the distortion of box girders, the analysis is based on the following key assumptions (Schlaich & Scheef, 1982):

- The dimensions of the flanges, when viewed longitudinally, are significantly larger compared to their width  $\left(\frac{l}{b}\right) > 4$ ;
- The girder is thin-walled in nature;



- The girder exhibits symmetry in the transverse direction relative to the vertical axis;
- The entire bridge structure is symmetrical, implying that the girder maintains a consistent width throughout its length;
- The thickness of both the web and the flanges remains constant in the transverse direction, and the effect of haunches is neglected;
- The end supports are assumed to be rigid with respect to transverse deformations, owing to their adequate rigidity and the prevention of torsional rotations;
- Longitudinal connections primarily transmit shear stresses in the longitudinal direction, due to the influence of a torsional load;

### 3.3.4.2 Longitudinal bending of the girder

First, a segment of the girder is considered, subjected to a distortional load  $p_d^L$  as illustrated in Figure 3.16.

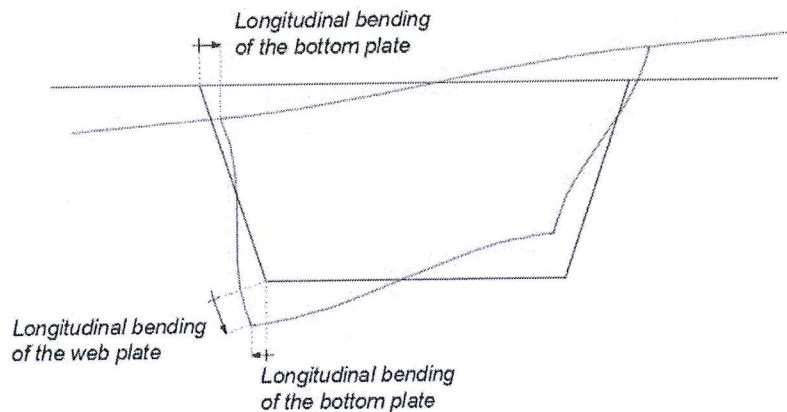


Figure 15 Displacement compatibility under distortion

The loading and the cross-section are asymmetrical i.e. symmetrical about the y-axis respectively, leading to an asymmetrical "box response" (for example  $F_1 = F_2$  и  $F_3 = F_4$ ).

The connection of the plates at the interfaces include equivalent shear flows  $f_2(x)$  and  $f_3(x)$ , whose resultants along the longitudinal direction are  $F_2(x)$  and  $F_3(x)$  :

$$F_2(x) = \int_x f_2(x) dx \quad (72)$$

$$F_3(x) = \int_x f_3(x) dx \quad (72)$$

The equilibrium equations for each plate, taking symmetry into account, lead to the determination of internal forces and moments that are equal to the distortional load and shear forces. Specifically,  $m_{t,d}^L$ ,  $m_{w,d}^L$  и  $m_{b,d}^L$  represent the bending moments resulting from  $p_{t,d}^L$ ,  $p_{w,d}^L$  и  $p_{b,d}^L$  respectively. The following equations describe this relationship:

- Top flange

$$N_t = 0 \quad (73)$$



$$M_t = F_2 b_t - m_{t,d}^L \quad (73)$$

▪ Web

$$N_w = F_3 - F_2 \quad (73)$$

$$M_w = -(F_2 + F_3) \frac{b_w}{2} + m_{w,d}^L \quad (73)$$

▪ Bottom flange

$$N_b = 0 \quad (73)$$

$$M_b = F_3 b_3 - m_{b,d}^L \quad (73)$$

The stresses in the cross-section are obtained as a function of the internal moments and forces and the characteristics of the cross-section respectively,

▪ Top flange

$$\sigma_{2d} = -\frac{M_t b_t}{2I_t} \quad (74)$$

▪ Web

$$\sigma_{2d} = -\frac{N_w}{A_w} - \frac{M_w b_w}{2I_w} \quad (74)$$

$$\sigma_{3d} = -\frac{N_w}{A_w} - \frac{M_w b_w}{2I} \quad (74)$$

▪ Bottom flange

$$\sigma_{3d} = \frac{M_b b_b}{2I_b} \quad (74)$$

In these calculations, the following moments of inertia and surface areas are utilized:

$$I_t = \frac{b^3 t_t}{12}, I_w = \frac{b_w^3 t_w}{12}, I_b = \frac{b_b^3 t_b}{12}; A_w = b_w t_w \quad (75)$$

By substituting 3.70 into 3.71 we obtain:

▪ Top flange

$$\sigma_{2d} = -\frac{[F_2 b_t - m_{t,d}^L] b_t}{2I_t} \quad (76)$$

▪ Web

$$\sigma_{2d} = -\frac{[F_3 - F_2]}{A_w} - \frac{[-(F_2 + F_3) \frac{b_w}{2} + m_{w,d}^L] b_t}{2I_t} \quad (76)$$

$$\sigma_{3d} = -\frac{[F_3 - F_2]}{A_w} - \frac{[-(F_2 + F_3) \frac{b_w}{2} + m_{w,d}^L] b_t}{2I_t} \quad (76)$$

▪ Bottom flange

$$\sigma_{3d} = \frac{[F_3 b_3 - m_{b,d}^L] b_b}{2I_b} \quad (76)$$



Since there is longitudinal bending in the girder, taking into account the relationship between the distortional load from (71), the following can be observed:

$$\frac{d^2 m_{t,d}^L}{dx^2} = p_{t,d}^L = -\left(\frac{b_b}{b_w}\right) p_{w,d}^L = \left(\frac{b_b}{b_w}\right) \frac{d^2 m_{w,d}^L}{dx^2} \quad (77)$$

$$\frac{d^2 m_{b,d}^L}{dx^2} = p_{b,d}^L = -\left(\frac{b_t}{b_w}\right) p_{w,d}^L = \left(\frac{b_t}{b_w}\right) \frac{d^2 m_{w,d}^L}{dx^2} \quad (77)$$

Assuming that the boundary conditions are the same for the top and bottom flange as well as for the web, which is often the case, the relationship between the distortional load and moments is the same:

$$m_{t,d}^L = -\left(\frac{b_b}{b_w}\right) m_{w,d}^L, m_{b,d}^L = \left(\frac{b_t}{b_w}\right) m_{w,d}^L \quad (78)$$

Hence the stresses can be expressed as a function of  $F_2$ ,  $F_3$ ,  $m_{w,d}^L$ :

- Top flange

$$\sigma_{2d} = -\frac{[F_2 b_t + \left(\frac{b_b}{b_w}\right) m_{w,d}^L] b_t}{2I_t} \quad (79)$$

- Web

$$\sigma_{2d} = -\frac{[F_3 - F_2]}{A_w} - \frac{[-(F_2 + F_3) \frac{b_w}{2} + m_{w,d}^L] b_w}{2I_w} \quad (79)$$

$$\sigma_{3d} = -\frac{[F_3 - F_2]}{A_w} - \frac{[-(F_2 + F_3) \frac{b_w}{2} + m_{w,d}^L] b_w}{2I_w} \quad (79)$$

- Bottom flange

$$\sigma_{3d} = \frac{[F_3 b_b - \left(\frac{b_t}{b_w}\right) m_{w,d}^L] b_b}{2I_b} \quad (79)$$

By equating the stresses for the different flanges (plates) from 3.76 and by defining certain geometric dependencies, we can extract the following equations:

$$F_2 \left(\frac{3}{\alpha_t} + 2\right) + F_3 = 3 \left(1 - \frac{\beta}{\alpha_t}\right) \frac{m_{w,d}^L}{b_w} \quad (80)$$

$$F_2 + F_3 \left(\frac{3}{\alpha_b} + 2\right) = 3 \left(1 - \frac{1}{\beta \alpha_t}\right) \frac{m_{w,d}^L}{b_w} \quad (80)$$

Where

$$\alpha_t = \frac{12I_t}{b_t^2 A_w}; \alpha_b = \frac{12I_b}{b_b^2 A_w}; \beta = \frac{b_b}{b_t} \quad (81)$$

The system of equations can be solved with respect to  $F_2$  and  $F_3$ :

$$F_2 = \frac{\alpha_t(\alpha_b \beta + 3\beta + 1) - (2\alpha_b + 3)\beta^2 m_{w,d}^L}{\beta[(\alpha_t + 2) + (\alpha_b + 2) - 1]} \frac{m_{w,d}^L}{b_w} \quad (82)$$

$$F_3 = \frac{\alpha_b(\alpha_b \beta + 3\beta + \beta^2) - (2\alpha_t + 3) m_{w,d}^L}{\beta[(\alpha_t + 2) + (\alpha_b + 2) - 1]} \frac{m_{w,d}^L}{b_w} \quad (82)$$

By substituting the shear resultants in 3.76 for the stresses in the top and bottom points of the web, a relationship is established with the moment in the web itself, as follows:

$$\sigma_{2d} = \frac{(1+\beta)(1+\alpha_b \beta + 2\beta)}{\beta[(\alpha_t + 2) + (\alpha_b + 2) - 1]} \frac{m_{w,d}^L b_w}{2I_w} \quad (83)$$

$$\sigma_{3d} = \frac{(1+\beta)(2+\alpha_t + \beta)}{\beta[(\alpha_t + 2) + (\alpha_b + 2) - 1]} \frac{m_{w,d}^L b_w}{2I_w} \quad (83)$$



The position of the neutral axis can now be defined by considering the linear stress distribution in the web which is consistent with the hypothesis set for the longitudinal bending of the plates.  $y_t$  и  $y_b$  are defined as the distance measured along the length of the web to the top and bottom edges respectively:

$$y_t = \frac{|\sigma_2|}{|\sigma_2|+|\sigma_3|} = \frac{(1+\beta)(1+\alpha_b\beta+2\beta)}{\alpha_t+\alpha_b\beta+3(1+\beta)} b_w \quad (84)$$

$$y_b = b_w - y_t \quad (85)$$

An equivalent secondary moment of inertia for the web  $I_{w,e}$ , can also be defined, whereby the stresses resulting from the bending of the flanges in the cross-section expressed by the individual web-plate analysis subjected to  $p_{w,d}^L$ . Considering a local web referential:

$$\sigma_{2d} = \frac{m_{w,d}^L y_t}{2I_{w,e}}; \sigma_{3d} = \frac{m_{w,d}^L y_b}{2I_{w,e}} \quad (86)$$

Where:

$$I_{w,e} = \frac{2\beta[(\alpha_t+2)+(\alpha_b+2)-1]}{(1+\beta)(\alpha_t+\alpha_b\beta+3(1+\beta))} I_w \quad (87)$$

The cross-sectional stress diagram is fully defined as being asymmetrical and linear. The web subjected to  $p_{w,d}^L$  can be considered as a beam element, for which the deformation in the plane itself  $\Delta_w$  is expressed through the equalization with an equation similar to that of 3.2.1.2:

$$p_{w,d}^L = \frac{d^4 \Delta_w}{dx^4} E I_{w,e} \quad (88)$$

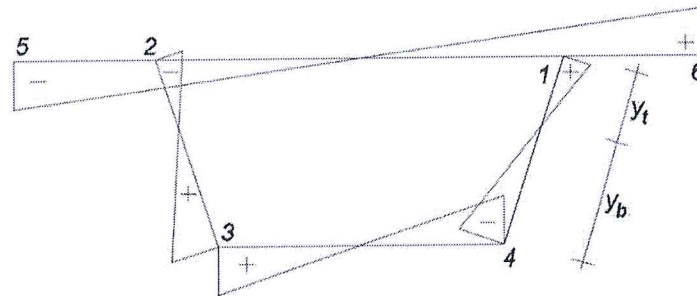


Figure 16 Distortion warping stresses

### 3.3.4.3 Deformations at the cross-sectional level

The cross-section is analyzed as an individual frame subject to the distortion subsystem  $p_d^L$ . This subsystem is equivalent to the system of asymmetric diagonal forces applied at the nodes (Figure 17). This can be defined by specifying the length of the diagonal so that:

$$S_d = \frac{g}{b_w} p_{w,d}^T \quad (89)$$

$$g = \sqrt{\left(\frac{b_t+b_b}{2}\right)^2 + d^2} \quad (90)$$



Solving the statically indeterminate system leads to the definition of the asymmetric transverse distribution of the moments (Figure 3.18b):

$$\bar{m}_2 = -\bar{m}_1 = \frac{1+\beta(2+r_b)}{2+2\beta+2\beta^2+r_t+r_b\beta^2} \frac{b_b d}{g} \left( \frac{S_d}{2} \right) \quad (91)$$

$$\bar{m}_4 = -\bar{m}_3 = \frac{2+\beta+r_t}{2+2\beta+2\beta^2+r_t+r_b\beta^2} \frac{b_b d}{g} \left( \frac{S_d}{2} \right) \quad (91)$$

Where

$$r_t = \frac{b_t \bar{I}_w}{b_w \bar{I}_t}; r_b = \frac{b_b \bar{I}_w}{b_w \bar{I}_b} \quad (92)$$

From here, the moments of inertia in the transverse direction are derived, for a unit of length specifically

$$\bar{I}_t = \frac{t_t^3}{12(1-\nu^2)}; \bar{I}_w = \frac{t_w^3}{12(1-\nu^2)}; \bar{I}_b = \frac{t_b^3}{12(1-\nu^2)} \quad (93)$$

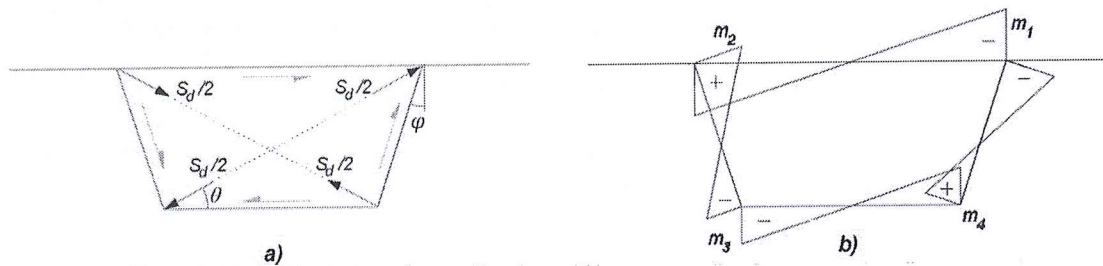


Figure 17 Equivalent diagonal system of forces and corresponding stress distribution

Applying the unit dummy load method, considering only the influence of transverse bending, and substituting (3.86) and (3.88), the diagonal displacements  $\delta$  are related to  $p_{w,d}^T$  as follows:

$$p_{w,d}^T i = \frac{12gE\bar{I}_w}{b_t b_b d^2} k_2 \delta \quad (94)$$

$$k_2 = \frac{2+2\beta+2\beta^2+r_t+r_b\beta^2}{\beta[(r_t+2)(r_b+2)-1]} \quad (95)$$

The relationship between the diagonal deformation of the cross-section and the transverse deformation of the flanges themselves is still written as unknown. To calculate it, the displacements  $\Delta_t, \Delta_w, \Delta_b, m_i$  and  $n_i$  are defined (Figure 3.19). The first three relate to web and flange displacements, while  $m_i$  and  $n_i$  are displacements normal to the flanges, i.e., the webs. These displacements can be defined by establishing geometric correlations:

$$m_1 = \left[ |\Delta_w| - |\Delta_t| \frac{b_t - b_b}{2b_w} \right] \frac{d}{b_w} \quad (96)$$

$$n_1 = \left[ |\Delta_t| - |\Delta_w| \frac{b_t - b_b}{2b_w} \right] \frac{d}{b_w} \quad (96)$$

$$m_3 = \left[ |\Delta_w| + |\Delta_b| \frac{b_t - b_b}{2b_w} \right] \frac{d}{b_w} \quad (96)$$

$$n_3 = \left[ |\Delta_b| + |\Delta_w| \frac{b_t - b_b}{2b_w} \right] \frac{d}{b_w} \quad (96)$$



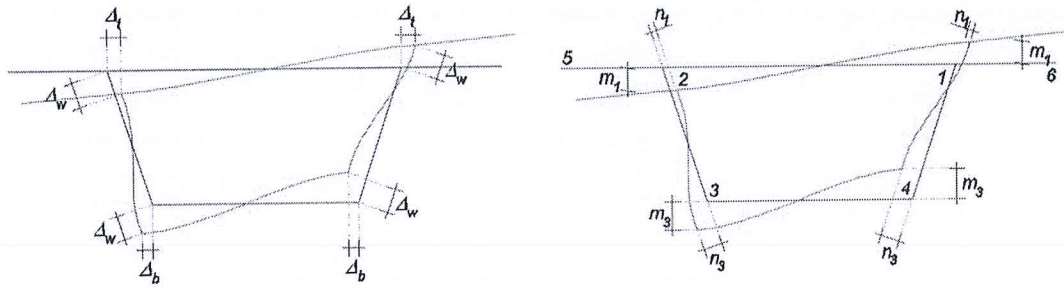


Figure 18 Deformations and displacement of the distortion frame

As depicted in Figure 3.17, the longitudinal stresses, which are equal at the ends of the flanges, indicate that the curve followed by the webs and the flanges is proportional. Assuming that the support conditions are the same for all plates, the curvature and displacement between different plates are related by the same absolute ratio. Taking into account (3.81) for the ratio, we obtain:

$$\frac{\sigma_{2,d}}{E} = \left(\frac{1}{R_t}\right) \frac{b_t}{2} = \left(\frac{1}{R_w}\right) y_t \leftrightarrow \frac{|\Delta_t|}{|\Delta_w|} = \frac{\left(\frac{1}{R_t}\right)}{\left(\frac{1}{R_w}\right)} = \frac{2y_t}{b_t} \quad (97)$$

$$\frac{\sigma_{3,d}}{E} = \left(\frac{1}{R_b}\right) \frac{b_b}{2} = \left(\frac{1}{R_w}\right) y_b \leftrightarrow \frac{|\Delta_b|}{|\Delta_w|} = \frac{\left(\frac{1}{R_b}\right)}{\left(\frac{1}{R_w}\right)} = \frac{2y_b}{b_t} \quad (97)$$

By using the previous equations in (3.93) we get:

$$m_1 = |\Delta_w| \left[ 1 - \frac{2y_t}{b_t} \frac{b_t - b_b}{2b_w} \right] \frac{d}{b_w} \quad (98)$$

$$n_1 = |\Delta_w| \left[ \frac{2y_t}{b_t} - \frac{b_t - b_b}{2b_w} \right] \frac{d}{b_w} \quad (98)$$

$$m_3 = |\Delta_w| \left[ 1 + \frac{2y_b}{b_b} \frac{b_t - b_b}{2b_w} \right] \frac{d}{b_w} \quad (98)$$

$$n_3 = |\Delta_w| \left[ \frac{2y_b}{b_b} - \frac{b_t - b_b}{2b_w} \right] \frac{d}{b_w} \quad (98)$$

Utilizing the geometric dependencies and correlations, the diagonal displacements can be expressed as a function of the normal displacements:

$$\delta_1 = \frac{n_1}{\cos \varphi} \cos \theta + \frac{m_1}{\cos \varphi} [\sin \theta \cos \varphi + \cos \theta \sin \varphi] \quad (99)$$

$$\delta_3 = \frac{n_3}{\cos \varphi} \cos \theta + \frac{m_3}{\cos \varphi} [\sin \theta \cos \varphi - \cos \theta \sin \varphi] \quad (99)$$

Here  $\theta$  and  $\varphi$  are the angles that the diagonals make with the horizontal flanges and the inclined webs. The trigonometric equations that are helpful include:

$$\sin \theta = \frac{d}{g}; \quad \cos \theta = \frac{b_t + b_b}{2g}; \quad \sin \varphi = \frac{b_t - b_b}{2b_w}; \quad \cos \varphi = \frac{d}{b_w} \quad (100)$$

The diagonal deformations are the result of the combination of displacements  $\delta_1$  and  $\delta_3$ . Combining the equations given in (3.96) and (3.95), we can define:

$$\delta = \delta_1 + \delta_3 = \frac{2b_w}{\beta g} k_1 \Delta_w \quad (101)$$



$$k_1 = \frac{[\alpha_t + \beta^2(\alpha_b + 2) + 2(\beta + 1)](1 + \beta)}{\alpha_t + \alpha_b\beta + 3(\beta + 1)} \quad (102)$$

Finally, it is possible to write an equation that relates the distortional load and the displacements in the plane of the girder, consistent with the global effect on the frame in the transverse direction:

$$p_{w,d}^T = k\Delta_w \quad (103)$$

$$k = \frac{24b_w}{b_b^2d^2}k_1k_2E\bar{I}_w \quad (104)$$

#### 3.3.4.4 Equilibrium equation

The effect of distortion on the box girder can be calculated through the displacements in the web  $\Delta_w$ , after which the equations for defining the displacements, stresses and internal forces and moments for the entire cross-section are used. From here, it is possible to carry out an individual analysis for the in-plane bending of the girder under the action of  $p_{w,d} = p_{w,d}^L + p_{w,d}^T$ , with the girder being elastically supported along its entire length, resembling a beam on an elastic foundation. Substituting (3.85) and (3.100) into (3.67) leads to:

$$p_{w,d} = \frac{d^4\Delta_w}{dx^4}EI_{w,e} + k\Delta_w \quad (105)$$

This bending equation is the same as the derivative in 3.2.1.2, but with its own specificity relating to elastic support. Thus, the stiffness of the cross-section is simulated in terms of transverse deformation. Once the deformation field of the web is defined along its axis, it becomes possible to calculate the longitudinal bending moment:

$$m_{w,d}^L - EI_{w,e} \frac{d^2\Delta_w}{dx^2} \quad (106)$$

The stresses arising from distortional warping can be determined using equation (3.83).

The forces and moments can then be divided into symmetrical and asymmetrical components, as illustrated in Figure 3.20.

The previous sections focused on analyzing the distortion effect in single-material girders. This analysis can be extended to composite cross-sections by transforming them into homogeneous cross-sections with equivalent thicknesses, typically referring to steel. However, as demonstrated earlier, distortion involves the simultaneous response of plates to longitudinal and transverse bending. Therefore, when considering distortion, it's essential to account for two separate equivalent thicknesses (Calgaro, J. A. Virlogeux, 1988):

- Longitudinal bending

$$\left(\frac{t_s}{t_t}\right)_d^L = n = \frac{E_s}{E_c} \quad (107)$$

- Longitudinal bending

$$\left(\frac{t_s}{t_t}\right)_d^T = \sqrt[3]{n} \quad (108)$$

#### 3.3.5 Load acting eccentrically in the webs of the girder





Up to this point, the equations have been based on the assumption that the box girder is subjected to loads equal to the vertical loads applied directly at the web-flange nodes. However, in practice, this is a rare scenario, and eccentric loading is more common.

Various combinations of vertical loading positioned at different locations along the length of the top flange are considered (Figure 3.21). The values of  $m_A, m_B, p_A, p_B$  can be calculated through static equivalent load analysis, as depicted in the drawing.

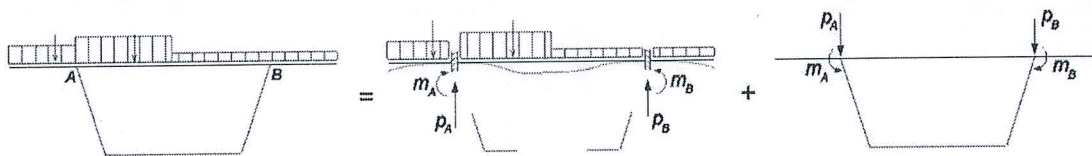


Figure 19 Equivalent vertical load

Forces and moments are divided into symmetrical and asymmetrical components as shown in Figure 20.

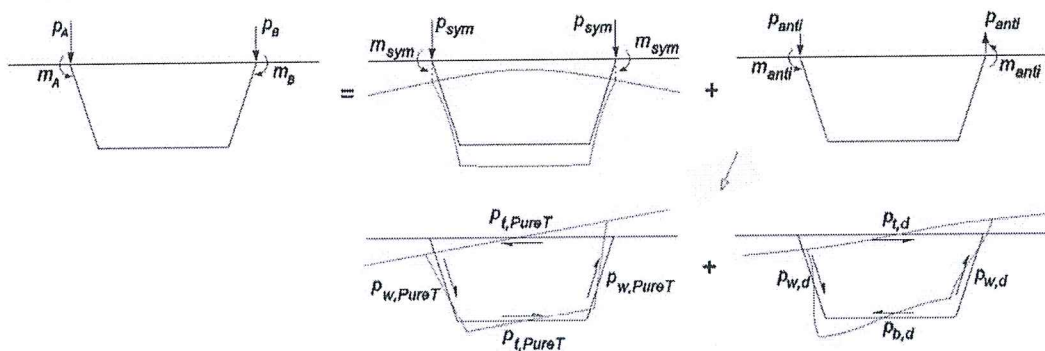


Figure 20 Decomposition of the equivalent load into pure torsion and distortion

The division of the asymmetrical components leads to pure torsion

$$p_{t,pureT} = \left(\frac{b_t}{b_w}\right) p_{w,pureT}, \quad p_{b,pureT} = \left(\frac{b_b}{b_w}\right) p_{w,pureT} \quad (107)$$

Where

$$p_{w,pureT} = \left(\frac{b_w}{(b_t+b_b)d}\right) \left(\frac{(p_A-p_B)b_t}{2} + m_A - m_B\right) \quad (108)$$

and distortional load subsystem (Schlaich & Scheef, 1982),

$$p_{t,d} = \left(\frac{b_b}{b_w}\right) p_{w,d}, \quad p_{b,d} = \left(\frac{b_t}{b_w}\right) p_{w,d} \quad (109)$$

Where

$$p_{w,d} = \left(\frac{b_b b_w}{(b_t+b_b)d}\right) \left(\frac{(p_A-p_B)b_t}{2}\right) - \left(\frac{b_w}{b_d d}\right) \left(\frac{\beta}{1+\beta} + \frac{r_t-3\beta-2\beta r_b}{(r_t+2)(r_b+2)-1}\right) (m_A - m_B) \quad (110)$$

The calculation of the distortional load involves analyzing the girder as a beam on elastic foundations subjected to the distortional load, as presented in 3.60a. For the torsional analysis, the external load is defined as:



$$m_T = \left( \frac{(p_A - p_B)b_t}{2} + m_A - m_B \right) \quad (111)$$

### 3.4 SOLUTION OF THE EQUILIBRIUM EQUATION

The solution of the equilibrium equation for elastic bending, torsion, and distortion (Table 3.3) is the one that ensures equilibrium and compatibility for a given load and boundary conditions. The solutions will be presented for the analysis of cases involving the action of a concentrated force  $Q$  and a distributed load  $q$ . Based on the specified boundary conditions for each scenario, two types of boundary conditions are considered: a simple beam (3.22a) and a double fixed beam (Figure 21).

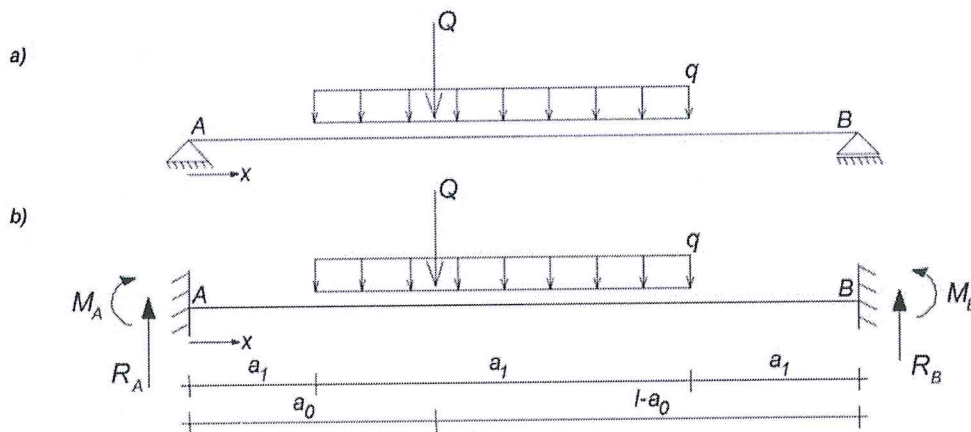


Figure 21 Support and loading conditions

Table 1 Equilibrium equations for elastic bending, warping torsion and distortion

Loading	Equations
Elastic bending	$\frac{d^4 w}{dx^4} EI_y = q(x)$
Torsion and warping	$\frac{EI_w}{\mu} \frac{d^4 \chi}{dx^4} + GJ \left( \frac{d^2 \chi}{dx^2} \right) = m_T(x)$
Distortion	$\frac{d^4 \Delta_w}{dx^4} I_{w,e} + k \Delta_w = q_{w,d}(x)$

#### 3.4.1 Elastic bending

The solution of the Euler-Bernoulli beam equation is provided here. Table 3.3 presents the results for the support reactions  $R_A$ ,  $R_B$ ,  $M_A$  and  $M_B$ , as well as the bending moment  $M(x)$  for two different scenarios of support conditions (Figure 20).

Table 2 Solution of the equilibrium equation for longitudinal bending

Simple beam		Double fixed beam	
Concentrated load	Uniformly distributed load	Concentrated load	Uniformly distributed load
$Q \frac{(l - a_0)}{l}$	$q \frac{a_2(2a_3 + a_2)}{2l}$	$Q \frac{(l - a_0)^2}{l^3} (l + 2a_0)$	$q \frac{a_2}{4l^3} [4a_3l^2 + 2a_2l^2 + 4a_4a_3^2]$
$Q - R_A$	$qa_2 - R_A$	$Q - R_A$	$qa_2 - R_A$
0	0	$-Qa_0 \frac{(l - a_0)^3}{l^2}$	$-q \frac{a_2}{12l^2} [12a_4a_3^2 + a_2^2(l - 3a_0)]$
0	0	$-Qa_0^2 \frac{(l - a_0)}{l^2}$	$-q \frac{a_2}{12l^2} [12a_4^2a_5 + a_2^2(l - 3a_0)]$
Concentrated load		Uniformly distributed load	
$M_A + R_A x$	$0 \leq x \leq a_0$	$M_A + R_A x$	$0 \leq x \leq a_1$
$M_B + R_B(l - x)$	$a_0 \leq x \leq l$	$M_B + R_A a_1 + [2R_A - q(x - a_0)](l - x)$	$a_1 \leq x \leq a_1 + a_2$
		$M_B + R_B(l - x)$	$a_1 + a_2 \leq x \leq l$

### 3.4.2 Warping torsion

The solution to the problem of torsion accompanied by warping in its general form is expressed as:

$$\frac{d\chi}{dx} = c_1 \cosh\left(\frac{x}{\zeta}\right) + c_2 \sinh\left(\frac{x}{\zeta}\right) + c_3 \frac{x}{\zeta} + c_4 \quad (112)$$

Here  $\chi$  is a function previously defined in (3.38) that allows for the variation of warping along the length of  $x$ ;  $c_1$ ,  $c_2$ ,  $c_3$  и  $c_4$  are constants of integration and  $\zeta$  is a characteristic length defined as:

$$\zeta = \sqrt{\frac{EI_\omega}{\mu GJ}} \quad (113)$$





Table 3 Solution of the equilibrium equation for warping torsione (adapted from Maisel & Roll (1974))

Support conditions	Simply supported girder	Fixed girder
Type of load	Concentrated load ( $M_T$ )	
Bi-moment $B$	$M_T \mu \zeta \frac{\sinh \frac{l-a_0}{\zeta} \sinh \frac{x}{\zeta}}{\sinh \frac{l-a_0}{\zeta}}$	$0 \leq x \leq a_0$ $m_T \mu \zeta^2 \left( C_1 \cosh \frac{x}{\zeta} + C_2 \sinh \frac{x}{\zeta} \right)$
	$M_T \mu \zeta \frac{\sinh \frac{a_0}{\zeta} \sinh \frac{l-x}{\zeta}}{\sinh \frac{a_0}{\zeta}}$	$a_0 \leq x \leq l$ $m_T \mu \zeta^2 \left( C_1 \cosh \frac{x}{\zeta} + C_2 \sinh \frac{x}{\zeta} - \sinh \frac{x-a_0}{\zeta} \right)$
Type of load	Uniformly distributed load ( $m_T$ )	
Bi-moment $B$	$m_T \mu \zeta^2 \left( 1 - \frac{\sinh \frac{l-x}{\zeta}}{\sinh \frac{l}{\zeta}} - \frac{\sinh \frac{x}{\zeta}}{\sinh \frac{l}{\zeta}} \right)$	$m_T \mu \zeta^2 \left( 1 - \frac{l}{\tanh \frac{l}{2\zeta}} - \frac{\sinh \frac{x}{\zeta} + \sinh \frac{l-x}{\zeta}}{\sinh \frac{l}{\zeta}} \right)$

$$C_1 = \frac{\left( \frac{l-a_0}{\mu \zeta} - \sinh \frac{l-a_0}{\zeta} \right) \left( 1 - \cosh \frac{l}{\zeta} \right) - \left( \frac{l}{\mu \zeta} - \sinh \frac{l}{\zeta} \right) \left( 1 - \cosh \frac{l-a_0}{\zeta} \right)}{2 - 2 \cosh \frac{l}{\zeta} + \mu \zeta \sinh \frac{l}{\zeta}}$$

$$C_2 = \frac{\left( \frac{l-a_0}{\mu \zeta} - \sinh \frac{l-a_0}{\zeta} \right) \sinh \frac{l}{\zeta} + \left( 1 - \cosh \frac{l}{\zeta} \right) \left( 1 - \cosh \frac{l-a_0}{\zeta} \right)}{2 - 2 \cosh \frac{l}{\zeta} + \mu \zeta \sinh \frac{l}{\zeta}}$$



### 3.4.3 Distortion

As already stated previously, the distortion response can be analyzed using the beam on elastic foundation analogy. The solution to this "equivalent" problem was partially explored by Hetenyi (1946), and his work laid the foundation for subsequent research that has yielded valuable results.

In the analysis, we consider a beam on elastic foundation subjected to either a concentrated or uniformly distributed load (Figure 3.23a). Additionally, we examine a beam exposed to the same load but with the distinction that it is infinitely long (Figure 3.23b).

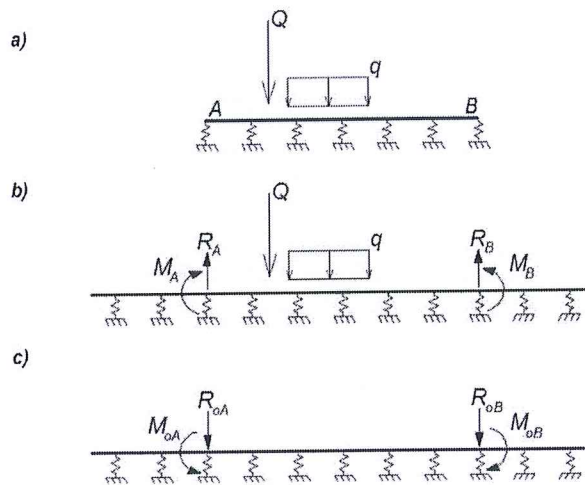


Figure 22 Analogy-Beam on elastic foundation

The first step involves analyzing the infinite beam. As a result of this analysis, bending, bending forces, rotations and displacements are developed at point A and B, points corresponding to the ends of the beam which has defined end points. To make the two systems correspond, forces and bending moments must be applied at the corresponding points A and B of the "infinite" beam on elastic foundation to satisfy the support conditions. Satisfying the support conditions in this case means that:

$$\sum F_A = \sum F_B = 0 \quad (117)$$

$$\sum M_A = \sum M_B = 0 \quad (118)$$

The solution for the beam of defined length involves superimposing the solution for the infinite beam subjected to the load, as shown in Figure 3.23b, and the corresponding forces and bending moments needed to satisfy the equilibrium conditions (3.12c). These forces and moments are obtained by solving the system of equations (3.112). This process results in the equations given in (3.113) and (3.114).

$$\Delta_{w,A} = \frac{\lambda}{2k} [R_{0A}\bar{A}(x) + R_{0B}\bar{A}(l-x) + Q\bar{A}(l-x-a_0)] + \frac{\lambda^2}{k} [M_{0A}\bar{B}(x) + M_{0B}\bar{B}(l-x)] + \frac{q}{2k} \{c_1[\bar{D}(a_1-x) - \bar{D}(a_1+a_2-x)] + c_2[2 - \bar{D}(x-a_1) - \bar{D}(a_1+a_2-x)] + c_3[\bar{D}(x-a_1 - a_2) - \bar{D}(x-a_1)]\} \quad (119)$$



$$M_{w,A} = \frac{1}{4\lambda} [R_{0A}\bar{C}(x) + R_{0B}\bar{C}(l-x) + Q\bar{C}(|x-a_0|)] + \frac{1}{2} [M_{0A}\bar{D}(x) + M_{0B}\bar{D}(l-x)] + \frac{q}{4\lambda^2} \{-c_1[\bar{B}(a_1-x) - \bar{B}(a_1+a_2-x)] + c_2[\bar{B}(x-a_1) + \bar{B}(a_1+a_2-x)] - c_3[\bar{B}(x-a_1-a_2) - \bar{B}(x-a_1)]\} \quad (120)$$

Where

$$c_1 = 1 \quad c_2 = c_3 = 0 \quad 0 \leq x \leq a_1 \quad (121)$$

$$c_2 = 1 \quad c_1 = c_3 = 0 \quad a_1 \leq x \leq a_1 + a_2 \quad (122)$$

$$c_3 = 1 \quad c_1 = c_2 = 0 \quad a_1 + a_2 \leq x \leq l \quad (123)$$

The functions  $\bar{A}(x)$ ,  $\bar{B}(x)$ ,  $\bar{C}(x)$  и  $\bar{D}(x)$  are defined according to:

$$\bar{A}(x) = e^{-\lambda x} (\cos \lambda x + \sin \lambda x) \quad (124)$$

$$\bar{B}(x) = e^{-\lambda x} \sin \lambda x \quad (125)$$

$$\bar{C} = e^{-\lambda x} (\cos \lambda x - \sin \lambda x) \quad (126)$$

$$\bar{D}(x) = e^{-\lambda x} \cos \lambda x \quad (127)$$

$$\lambda = \frac{1}{L_d} = \sqrt[4]{\frac{k}{4EI_{w,e}}} \quad (128)$$

The parameter  $L_d$  represents the characteristic distortion length (Schlaich & Scheef, 1982), which defines the longitudinal stiffness related to bending in the girder ( $EI_{w,e}$ ) relative to the stiffness in the transverse direction of the cross-section ( $k$ ).

Solving the system of equations defined in (3.112) is simplified by separating the base load into its symmetric and asymmetric components

$$M_A^{sym} = \frac{1}{2}(M_A + M_B) \quad R_A^{sym} = \frac{1}{2}(R_A + R_B) \quad (129)$$

$$M_A^{anti} = \frac{1}{2}(M_A - M_B) \quad R_A^{anti} = \frac{1}{2}(R_A - R_B) \quad (130)$$

Combining the symmetric and asymmetric sets of moments and forces, the following result is obtained:

$$M_{0A} = M_{0A}^{sym} + M_{0A}^{anti} \quad R_{0A} = R_{0A}^{sym} + R_{0A}^{anti} \quad (131)$$

$$M_{0B} = M_{0B}^{sym} + M_{0B}^{anti} \quad R_{0B} = R_{0B}^{sym} + R_{0B}^{anti} \quad (132)$$

The previous explanations were specific to the case of a beam on elastic foundation along the length of the span without end support points. For the case illustrated in Figure 3.22, the support conditions can be defined as:

- Simply supported beam

$$\Delta_{w,A} = \Delta_{w,B} = 0 \quad (133)$$

$$\sum M_A = \sum M_B = 0 \quad (134)$$

- Double fixed beam

$$\Delta_{w,A} = \Delta_{w,B} = 0 \quad (135)$$

$$\sum M_A = \sum M_B = 0 \quad (136)$$



Table 4 Solution of the equilibrium equation for distortion (adapted from Pedro (1995))

Support conditions	Simple beam		Double fixed beam	
	Concentrated load	Uniformly distributed load	Concentrated load	Uniformly distributed load
$R_A$	$y_A = \frac{Q\lambda}{2k} \bar{A}(a_0)$	$y_A = \frac{q}{2k} [\bar{D}(a_1) - \bar{D}(a_2 + a_3)]$	$y_A = \frac{Q\lambda}{2k} \bar{A}(a_0)$	$y_A = \frac{q}{2k} [\bar{D}(a_1) - \bar{D}(a_2 + a_3)]$
$R_B$	$y_B = \frac{Q\lambda}{2k} \bar{A}(1 - a_0)$	$y_B = \frac{q}{2k} [\bar{D}(a_3) - \bar{D}(a_2 + a_3)]$	$y_B = \frac{Q\lambda}{2k} \bar{A}(1 - a_0)$	$y_B = \frac{q}{2k} [\bar{D}(a_3) - \bar{D}(a_2 + a_3)]$
$M_A$	$M_A = \frac{Q}{4\lambda} \bar{C}(a_0)$	$M_A = -\frac{q}{4\lambda^2} [\bar{B}(a_1) - \bar{B}(a_2 + a_3)]$	$M_A = \frac{Q\lambda^2}{k} \bar{B}(a_0)$	$\theta_A = \frac{q}{2k} [\bar{A}(a_1) - \bar{A}(a_2 + a_3)]$
$M_B$	$M_B = \frac{Q}{4\lambda} \bar{C}(1 - a_0)$	$M_B = -\frac{q}{4\lambda^2} [\bar{B}(a_3) - \bar{B}(a_2 + a_3)]$	$\theta_B = \frac{Q\lambda^2}{k} \bar{B}(1 - a_0)$	$\theta_B = \frac{q}{2k} [\bar{A}(a_3) - \bar{A}(a_2 + a_3)]$
	$y_A^{sym} = \frac{1}{2}(y_A + y_B)$	$M_A^{sym} = \frac{1}{2}(M_A + M_B)$	$y_A^{sym} = \frac{1}{2}(y_A + y_B)$	$\theta_A^{sym} = \frac{1}{2}(\theta_A + \theta_B)$
	$y_A^{anti} = \frac{1}{2}(y_A - y_B)$	$M_A^{anti} = \frac{1}{2}(M_A - M_B)$	$y_A^{anti} = \frac{1}{2}(y_A - y_B)$	$\theta_A^{anti} = \frac{1}{2}(\theta_A - \theta_B)$
	$R_{0A}^{sym} = 4\lambda \xi_l [M_A^{sym} \bar{B}(0) - 2\lambda^2 EI_{w,e} y_A^{sym} [1 + \bar{D}(0)]]$		$R_{0A}^{sym} = 8\lambda^2 EI_{w,e} \xi_l [\theta_A^{sym} \bar{B}(0) - \lambda^2 y_A^{sym} [1 + \bar{C}(0)]]$	
	$M_{0A}^{sym} = -2\xi_l [M_A^{sym} [1 + \bar{A}(0)] - 2\lambda^2 EI_{w,e} y_A^{sym} [1 + \bar{C}(0)]]$		$M_{0A}^{sym} = -4\lambda EI_{w,e} \xi_l [\theta_A^{sym} [1 + \bar{A}(0)] - 2\lambda y_A^{sym} \bar{B}(0)]$	
	$R_{0A}^{anti} = -4\lambda \xi_l [M_A^{anti} \bar{B}(0) + 2\lambda^2 EI_{w,e} y_A^{anti} [1 - \bar{D}(0)]]$		$R_{0A}^{anti} = -8\lambda^2 EI_{w,e} \xi_l [\theta_A^{anti} \bar{B}(0) + \lambda^2 y_A^{anti} [1 + \bar{C}(0)]]$	
	$M_{0A}^{anti} = -2\xi_l [M_A^{anti} [1 - \bar{A}(0)] - 2\lambda^2 EI_{w,e} y_A^{anti} [1 - \bar{C}(0)]]$		$M_{0A}^{anti} = -4\lambda EI_{w,e} \xi_l [\theta_A^{anti} [1 - \bar{A}(0)] + 2\lambda y_A^{anti} \bar{B}(0)]$	
	$\xi_l = \frac{1}{2} \frac{e^{\lambda l}}{\cosh \lambda l + \cos \lambda l}$	$\xi_{fl} = \frac{1}{2} \frac{e^{\lambda l}}{\cosh \lambda l - \cos \lambda l}$	$\xi_l = \frac{1}{2} \frac{e^{\lambda l}}{\sinh \lambda l + \sin \lambda l}$	$\xi_{fl} = \frac{1}{2} \frac{e^{\lambda l}}{\sinh \lambda l - \sin \lambda l}$
	$R_{0A} = R_{0A}^{sym} + R_{0A}^{anti}$	$R_{0B} = R_{0B}^{sym} + R_{0B}^{anti}$	$M_{0A} = M_{0A}^{sym} + M_{0A}^{anti}$	$M_{0B} = M_{0B}^{sym} + M_{0B}^{anti}$





### 3.4.4 Distortion in composite box cross-section

As previously mentioned, the onset of distortion is triggered by the action of asymmetric loading. When a box girder with a symmetrical cross-section is loaded with a vertical load that has a certain eccentricity relative to the axis of the cross-section, the applied load can be divided into a flexural force  $p$  and a torsional force  $m = qe$ . The torsional force can be further divided into pure torsion and distortion components.

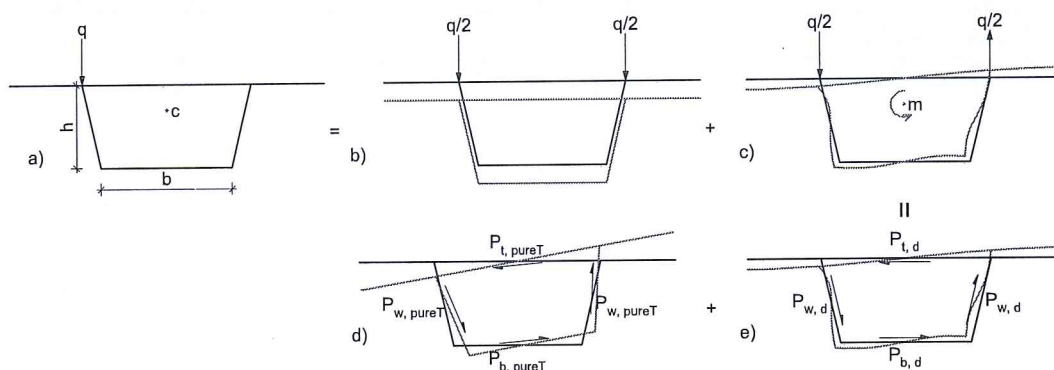


Figure 23 Load decomposition of the part causing pure torsion and distortion

The distortional behavior of box girders has been extensively studied and analyzed by various researchers, primarily focusing on either pure steel or pure concrete box girders. However, the influence of differing stiffness characteristics between the top concrete flange and the steel webs and bottom flange, which collectively form the cross-section of a composite box girder, has not been thoroughly investigated. The specific cross-sectional configuration under consideration is depicted in Figure 2.

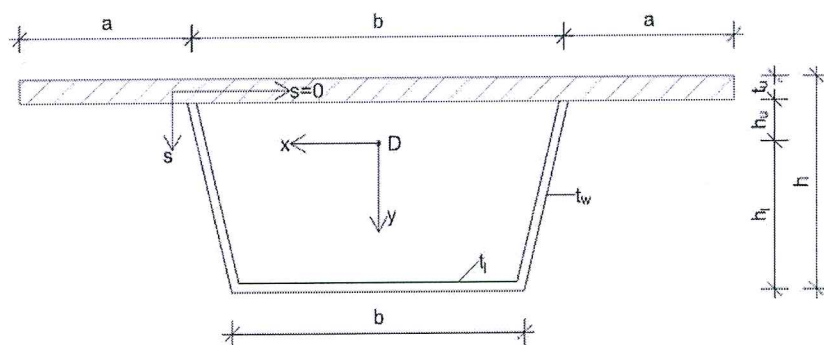


Figure 24 Cross-section of the composite box girder

$A$  - width of cantilever extension,  $A = 3500$  [mm]

$B, b$  - distance between the two webs,  $B = 7000$  [mm],  $b = 7000$  [mm]

$h$  - height of the steel cross-section,  $h = 3000$  [mm]

$h_u, h_l$  - distance from the distortion center to the top and bottom flange, respectively

$t_u$  - thickness of the concrete slab,  $t_u = 400$  [mm]



$t_w, t_l$  – thickness of the webs and bottom flange respectively

$A_u = t_u(2a + b)$  – area occupied by the concrete slab

$A_w = t_w h$  – area occupied by each of the webs respectively

$A_l = t_l b$  – area of the bottom steel flange

As depicted in Figure 2, the position of the coordinate system is located in the center of distortion.

The cross-section will be deformed in relation to the original shape and will manifest out-of-plane warping under the effect of the distortion load and the so-called distortion angles will be formed in the corners, at the joints between the webs and the top and bottom flange respectively. When steel or concrete box girders are analyzed, it is assumed that all four distortion angles that occur in the four corners are equal. But in composite box girders, the top concrete flange deforms at a different angle compared to the bottom steel flange as a result of their different deformable stiffness. Accordingly, the different angle of distortion cannot be neglected. It is defined through the following geometric characteristics:

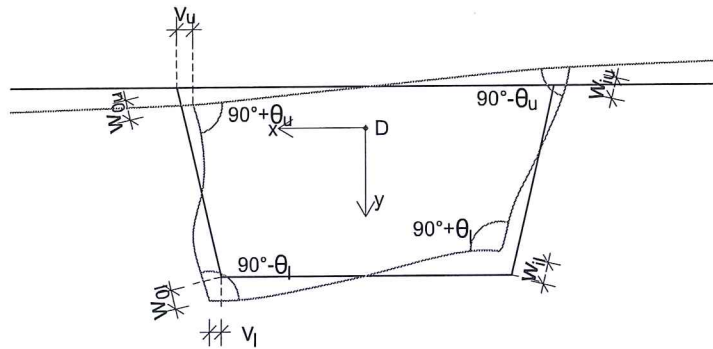


Figure 25 Defining the distortion angle

$$\theta_u = \frac{v_l - v_u}{h} + \frac{w_{lu} - w_{ou}}{b}, \theta_l = \frac{v_l - v_u}{h} + \frac{w_{ll} - w_{ol}}{b} \quad (137, 138)$$

$\theta_u$  is the distortion angle taken at the concrete top flange,  $\theta_l$  is the distortion angle taken at the bottom steel flange,  $v$  and  $w$  are displacements in the direction of the  $x$  and  $y$  axes whose coordinate origin is positioned at the center of distortion  $D$ . Analogous to the definition from the theory of distortional warping, the derivative of the angular distortion  $\theta' = d\theta/dz$  will take the displacements in the direction of the  $z$  coordinate axis. From here it can be derived:

$$u_u = w_D \theta'_u; u_l = w_D \theta'_l \quad (139, 140)$$

Where  $w_D$  is defined as the warping function resulting from the distortion itself. When the displacement  $u$ , is constrained, normal stresses and shear stresses are induced.





## 3.4.4.2 Analysis of the distortional influences

The distortional stress  $\sigma_{Dw}$  is described using Hooke's law:

$$\sigma_{Dw} = E\varepsilon = E \frac{\partial u}{\partial z} = E \frac{\partial^2 \theta}{\partial z^2} w_D \quad (151)$$

Assuming that the distortion does not cause axial forces  $N_z$  or bending moments  $M_y$  and  $M_x$  then the following equation must be satisfied:

$$N_z = \int_A \sigma_{Dw} dA = 0; M_x = \int_A \sigma_{Dw} y dA = 0; M_y = \int_A \sigma_{Dw} x dA = 0 \quad (152-1(2,3))$$

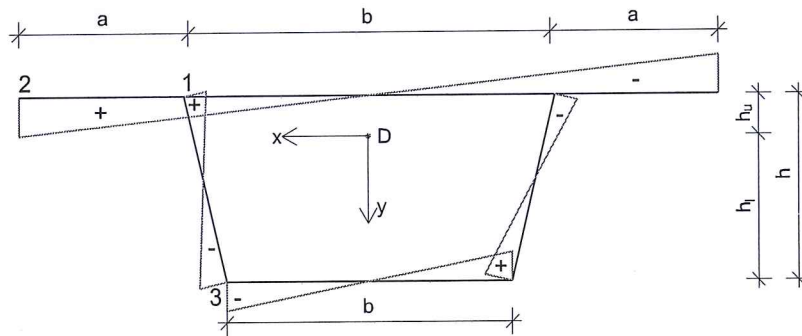


Figure 28 Warping function as a result of distortion

By substituting equation 13 into equation 14 the shape of the warping distortion function can be defined as shown in Figure 6. The cross-section is symmetric along the  $y$  axis even though the stress distribution is viewed along the  $y$  axis. Therefore equations (14-1) and (14-2) are automatically satisfied. The value of  $w_{Dw}$  in points 1, 2 and 3 can be simply defined by

$$w_{Dw,1} = \frac{bh}{4} \frac{1}{1+\beta}; w_{Dw,2} = \left(1 + \frac{2a}{b}\right) w_{Dw,1}; w_{Dw,3} = \beta w_{Dw,1} \quad (153-1(2,3))$$

Where  $\beta$  is defined as a coefficient that defines the ratio of the warping distortion function at node 3- $w_{Dw,3}$  and node 1- $w_{Dw,1}$  and  $\beta$  can be calculated from the equation (14-3) according to the following:

$$\int_A \sigma_{Dw} x dA = \int_{A_u} E_c \frac{\partial^2 \theta_u}{\partial z^2} w_{Dw} x dA_u + \int_{A_{w1}} E_s \frac{\partial^2 \theta_u}{\partial z^2} w_{Dw} x dA_{w1} + \int_{A_{w2}} E_s \frac{\partial^2 \theta_l}{\partial z^2} w_{Dw} x dA_{w2} + \int_{A_l} E_c \frac{\partial^2 \theta_l}{\partial z^2} w_{Dw} x dA_l$$

$$\beta = m \frac{\left(\frac{2a+b}{b}\right)^2 \frac{A_u + 3h_u t_w}{n_E}}{A_l + 3h_l t_w} \approx m \frac{\left(\frac{2a+b}{b}\right)^2 \frac{A_u + 3A_w}{n_E}}{A_l + 3A_w} \quad (154)$$

Furthermore, the strain energy  $U_\sigma$  due to distortional warping stress  $\sigma_{Dw}$  can be calculated as:

$$U_\sigma = \frac{E_c}{2} \int_{A_u} w_{Dw}^2 dA_u \int_0^l \left(\frac{\partial^2 \theta_u}{\partial z^2}\right)^2 dz + \frac{E_s}{2} \int_{A_{w1}} w_{Dw}^2 dA_{w1} \int_0^l \left(\frac{\partial^2 \theta_u}{\partial z^2}\right)^2 dz + \frac{E_s}{2} \int_{A_{w2}} w_{Dw}^2 dA_{w2} \int_0^l \left(\frac{\partial^2 \theta_l}{\partial z^2}\right)^2 dz + \frac{E_s}{2} \int_{A_l} w_{Dw}^2 dA_l \int_0^l \left(\frac{\partial^2 \theta_l}{\partial z^2}\right)^2 dz = \frac{E_s I_{Dw,1}}{2} \int_0^l \left(\frac{\partial^2 \theta_u}{\partial z^2}\right)^2 dz + \frac{E_s I_{Dw,2}}{2} \int_0^l \left(\frac{\partial^2 \theta_l}{\partial z^2}\right)^2 dz \quad (155)$$

$$\text{Where: } I_{Dw,1} = \frac{I_{Dw,u}}{n_E} + I_{Dw,w1}; I_{Dw,2} = I_{Dw,w2} + I_{Dw,1} \quad (156-1(2))$$



$$\text{For the top flange } I_{Dw,u} = \int_{A_u} w_{Dw}^2 dA_u = \frac{b^2 h^2}{48(1+\beta)^2} \left(\frac{2a+b}{b}\right)^2 A_u \quad (158)$$

$$\text{For the first steel web } I_{Dw,w1} = \int_{A_{w1}} w_{Dw}^2 dA_{w1} = \frac{b^2 h^2}{48(1+\beta)^2} 2h_u t_w \quad (159)$$

$$\text{For the other steel web } I_{Dw,w2} = \int_{A_{w2}} w_{Dw}^2 dA_{w2} = \frac{b^2 h^2}{48(1+\beta)^2} 2h_l t_w \quad (160)$$

$$\text{For the bottom flange } I_{Dw,l} = \int_{A_{w1}} w_{Dw}^2 dA_l = \frac{b^2 h^2}{48(1+\beta)^2} \beta^2 A_l \quad (161)$$

$I_{Dw}$  is defined as the distortional warping constant

### 3.4.4.3 Distortion energy analysis

Despite the distortional warping, the box girder components will deform in a direction perpendicular to their plane, i.e. the distortional transverse flexure, which is limited by the transverse frame stiffness of the box girder itself. When analyzing the frame function, the cantilever extensions at the top flange are neglected. A finite element  $dz$  is detached from the girder and subjected to analysis, with the top, bottom flange and webs isolated accordingly. Figure 7 shows the distribution of moments and shear forces in each isolated element. According to the symmetry in terms of distribution of forces, certain relations can be established

$$m_{AD} = m_{DA}; m_{BC} = m_{CB}; q_{yA} = q_{yD}; q_{xA} = q_{xB}; q_{yB} = q_{yC}; q_{xA} = q_{xD} \quad (162-1(2,3,4,5,6))$$

From the equilibrium conditions for the bending moments the equation (24) can be defined as:

$$m_{AD} + m_{AB} = 0; m_{BA} + m_{BC} = 0; q_{yA} = q_{yD} = \frac{-2m_{AD}}{b}; q_{yB} = q_{yC} = \frac{-2m_{BC}}{b}; q_{xA} = q_{xB} = q_{xC} = q_{xD} = \frac{(m_{AB} + m_{BA})}{h} \quad (163-1(2,3,4,5))$$

By combining the equations (162) and (163) the equation (164) is derived:

$$q_x = q_{xA} + q_{xD} = \frac{2(m_{AB} + m_{BA})}{h} = -\frac{2(m_{AD} + m_{BC})}{h}; q_y = q_{yA} + q_{yD} = -\frac{2(m_{AD} + m_{BC})}{b}; q_x = q_y \frac{b}{h} \quad (164-1(2,3))$$

The nodes of the frame are treated as rigid, essentially considering the box girder components as a "fixed girder." Based on the equations defining the deformations, the equation between the transverse moment and transverse flexural displacement can be expressed as follows:

$$m_{AD} = \frac{2EI_u}{b} \left(3\theta_A - 6\frac{\Delta w_u}{b}\right); m_{BC} = \frac{2EI_l}{b} \left(3\theta_B - 6\frac{\Delta w_l}{b}\right); m_{AB} = \frac{2EI_w}{b} \left(2\theta_A + \theta_B + 6\frac{\Delta v}{h}\right); m_{BA} = \frac{2EI_w}{b} \left(\theta_A + 2\theta_B + 6\frac{\Delta v}{h}\right) \quad (165-1(2,3,4))$$

Where  $\theta_A$  and  $\theta_B$  represent the angles of rotation at points  $A$  and  $B$  respectively, and therefore

$$\Delta v = \frac{\Delta v_u + \Delta v_l}{2} \quad (166)$$

By uniting the equations (165-1)-(165-3) into (163-1) and (163-2), the equation (166) is obtained:

$$\frac{2EI_u}{b} \left(3\theta_A - 6\frac{\Delta w_u}{b}\right) + \frac{2EI_w}{b} \left(2\theta_A + \theta_B + 6\frac{\Delta v}{h}\right) = 0, \frac{2EI_l}{b} \left(3\theta_B - 6\frac{\Delta w_l}{b}\right) + \frac{2EI_w}{b} \left(\theta_A + 2\theta_B + 6\frac{\Delta v}{h}\right) = 0 \quad (167-1(2))$$





Summing up the equations (17), (36) and (37), the total potential energy  $\Pi$  is given as:

$$\Pi = U_{\sigma} + U_{\tau} + V_m$$

$$\Pi = \frac{E_s I_{Dw,1}}{2} \int_0^l \left( \frac{d^2 \theta_u}{dz^2} \right)^2 dz + \frac{E_s I_{Dw,2}}{2} \int_0^l \left( \frac{d^2 \theta_l}{dz^2} \right)^2 dz + \frac{1}{2} \left( K_{Dw,u} \int_0^l \theta_u^2 dz + K_{Dw,l} \int_0^l \theta_l^2 dz \right) - \int_0^l \frac{m_T}{4} \theta_u dz - \int_0^l \frac{m_T}{4} \theta_l dz \quad (178)$$

In order to minimize the total potential energy  $\Pi$ , the variation potential energy  $\delta\Pi = 0$  is valid for any set of boundary conditions, the following equation must be satisfied:

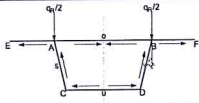
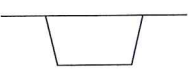
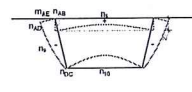
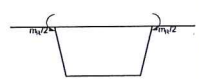
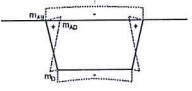
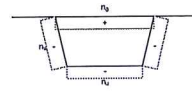
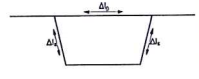
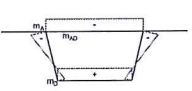
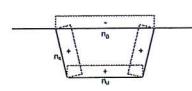
$$E_s I_{Dw,1} \frac{d^4 \theta_u}{dz^4} + K_{Dw,u} \theta_u = \frac{m_T}{4}; E_s I_{Dw,2} \frac{d^4 \theta_l}{dz^4} + K_{Dw,l} \theta_l = \frac{m_T}{4} \quad (179-1(2))$$

Here the distortion equations for a box girder are defined:

$$\frac{d^4 \theta_u}{dz^4} + 4\lambda_u^4 \theta_u = \frac{1}{E_s I_{Dw,1}} \frac{m_T}{4}, \quad \lambda_u = \sqrt[4]{\frac{K_{Dw,u}}{4E_s I_{Dw,1}}}; \frac{d^4 \theta_l}{dz^4} + 4\lambda_l^4 \theta_l = \frac{1}{E_s I_{Dw,2}} \frac{m_T}{4}, \quad \lambda_l = \sqrt[4]{\frac{K_{Dw,l}}{4E_s I_{Dw,2}}} \quad (180-1(2))$$

These differential equations are solved using the BEF analogy and by analyzing the equilibrium conditions.

Table 5 Equations for calculating the redistribution of internal influences at the cross-sectional level under symmetrical loading

Load	Transverse moments	Axial forces
	 $m = 0$	
	 $m_{AB} = \frac{1 + 2r_u}{k_3} \cdot \frac{m_R}{2}$ $m_{AD} = m_{AB} + \frac{m_R}{2}$ $m_D = \frac{r_0}{k_3} \cdot \frac{m_R}{2}$	 $n_0 = \frac{3r_0(1+r_u)}{k_3} \cdot \frac{m_R}{2}$ $n_s = n_u \cdot \sin \varphi$ $n_u = -n_0$ $n_u = -n_0$
	 $m_{AB} = \frac{3(1+r_u)}{k_3} \cdot \frac{E_c I_s}{d \cdot b_s} \cdot \Delta l_0$ $m_D = \frac{3(1+r_0)}{k_3} \cdot \frac{E_c I_s}{d \cdot b_s} \cdot \Delta l_0$	 $n_s = n_u \cdot \sin \varphi$ $n_u = \frac{3(2+r_0+r_u)}{k_3} \cdot \frac{E_c I_s \Delta l_0}{d^2 \cdot b_s}$ $n_u = -n_u$

$$k_3 = 1 + 2r_0 + 2r_u + 3r_0 r_u$$

$$n_{AB} = n_{AE} + \frac{q_R}{2} \tan \varphi,$$

$$n_{DC} = 0$$

$$n_5 = n_{AB} - \frac{q_R}{8I_x} t_0 b_0^2 z_s$$

$$n_{10} = \frac{q_R}{8I_x} t_u b_u^2 (d - z_s)$$

$$n_5 = n_{AD} + \frac{q_R}{I_x} \left( \frac{t_s b z_s^2}{2 \cos \varphi} + \frac{t_s z_s^3}{3 \cos^2 \varphi} \right)$$

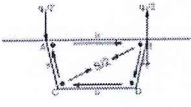

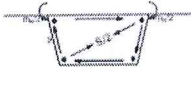






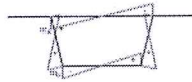
$$n_{AE} = \frac{q_R}{2I_x} t_0 b_K^2 z_s$$

$$k_4 = (r_0 + 2)(r_u + 2) - 1$$

$$k_5 = 2 + 2\beta + 2\beta^2 + r_0 + r_u \beta^2, \quad \cos \vartheta = \frac{4d^2 + b_0^2 - b_u^2}{4gb_s}$$



Table 6 Equations for calculating the redistribution of internal influences at the cross-sectional level under asymmetrical loading

Load	Transverse moments	Diagonal forces	Axial forces
	 $m = 0$	$S = \frac{\beta \cdot g \cdot q_R}{2(1 + \beta)d}$	$n_{AB} = -\frac{b_b \cdot q_R}{4(1 + \beta)d}$ $n_{AD} = -\frac{(2 + \beta)b_s \cdot q_R}{4(1 + \beta)d}$ $n_{DA} = -\frac{\beta \cdot b_s \cdot q_R}{4(1 + \beta)d}$
	 $m_{AB} = -\frac{3 + 2r_u}{k_4} \cdot \frac{m_R}{2}$ $m_{AD} = m_{AB} + 2$ $m_D = -\frac{r_D}{k_3} \cdot \frac{m_R}{2}$	$S = -\left(\frac{\beta}{1 + \beta} + \frac{r_D - 3\beta - 2\beta r_u}{k_4}\right) \cdot \frac{g \cdot m_R}{b_u d}$	$n_{AB} = \frac{m_R}{2d(1 + \beta)}$ $n_{AD} = \frac{S}{2} \cdot \cos \vartheta \cdot \frac{2m_{AB}}{b_b} \cos \varphi - n_{AB} \sin \varphi$ $n_{DA}$
	 $m_A = -\frac{\beta(1 + 2\beta + r_u \beta)}{4(1 + \beta)k_5} \cdot b_u \cdot q_R$ $m_D = -\frac{\beta(2 + \beta + r_D)}{4(1 + \beta)k_5} \cdot b_u \cdot q_R$		$n_{AB} = \frac{b_b q_R}{4(1 + \beta)d}$ $n_{AD} = n_{DA} - \frac{b_s \cdot q_R}{2(1 + \beta)d}$ $n_{DA} = \frac{2m_D}{b_u} \cos \varphi + n_{AB} \sin \varphi$
	 $m_{AB} = -\frac{m_R}{2(1 + \beta)} \cdot \frac{m_D}{\beta}$ $m_{AD} = m_{AB} + \frac{m_R}{2}$ $m_D = \frac{\beta[r_D - \beta(2 + \beta)]}{(1 + \beta)k_5} \cdot \frac{m_R}{\beta}$		$n_{AB} = \frac{m_R}{2d(1 + \beta)}$ $n_{AD} = n_{DA} - \frac{b_s \cdot m_R}{d(b_b + b_u)}$ $n_{DA} = -\frac{2m_D}{b_u} \cos \varphi$
	 $m_A = \frac{1 + \beta(2 + r_u)}{k_5} \cdot \frac{\zeta}{2} \cdot \frac{b_u d}{g}$ $m_D$		$n_{AB} = n_{DC} = 0$ $n_{AD} = n_{DA} = \frac{2m_A}{b_b} \cos \varphi - \frac{\zeta}{2} \cos \vartheta$





## 4. FIRST-ORDER ANALYSIS OF NUMERICAL EXAMPLES

The proposed approach is implemented in a practical example involving a detached segment of a composite box girder with a length of 30 meters. The analysis covers bending, torsion, and distortion effects. To simulate real-world conditions, an asymmetric uniform load of 27 kN/m is applied to comprehensively capture all cross-sectional responses, including deformations both within and out of its own plane. Appropriate boundary support conditions are applied to ensure an accurate representation of the box girder's behavior in this scenario.

The chosen example is initially analyzed using the proposed method, involving the solution of the differential equation based on the BEF analogy. Subsequently, the same analysis is conducted using a finite element model within the commercial software "SIMULIA-ABAQUS." The results obtained from both approaches are presented in separate tables.

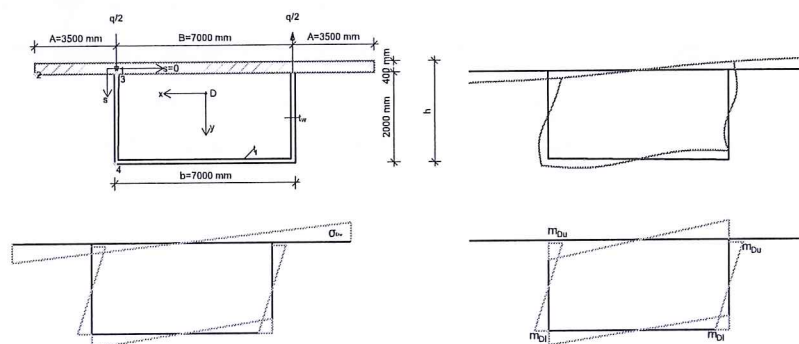


Figure 29 Distribution of stresses and deformations in the box girder cross-section

Table 7: Cross-sectional properties needed to solve the basic differential equations

Equation (40-1)	Equation (40-2)
$\beta = 14.69$	
Warping function in:	
Point 1	$\omega_{d1} = 0.379 [m^2]$
Point 2	$\omega_{d2} = 0.758 [m^2]$
Point 3	$\omega_{d3} = -5.571 [m^2]$
Distortion constant of warping For the top flange $I_{Dw,u} = 0.957 [m^6]$ For the web $I_{Dw,w1} = 0.001 [m^6]$	Distortion constant of warping For the bottom flange $I_{Dw,l} = 0.975 [m^6]$ For the web $I_{Dw,w2} = 0.837 [m^6]$
$E_s I_{Dw,w1} = 3.067 \cdot 10^{10} [Nm^4]$	$E_s I_{Dw,w2}$
Distortional stiffness of the frame $K_{Dwu} = 4.093 \cdot 10^5 [N]$	Distortional stiffness of the frame $K_{Dwl} = 1.152 \cdot 10^2 [N]$
$\lambda_u l = 2.479$	$\lambda_l l = 0.171$



Table 8: Comparison of obtained values for the distortion angle and stress redistribution

		Analytical method (A)	„FE“ 3D model (B)	A/B
Distortion angle	$\theta_u$	0.04714	0.04786	0.98
	$\theta_l$	0.00951	0.0096	0.99
Normal stresses due to distortion	$\sigma_{dw1}$	-0.22 MPa	-0.25 MPa	0.88
	$\sigma_{dw2}$	-0.43 MPa	-0.44 MPa	0.97
	$\sigma_{dw3}$	0.05 MPa	0.07 MPa	0.71
	$\sigma_{dw4}$	21.89 MPa	21.63 MPa	$\approx 1.00$
Transverse bending moments	$m_{dbu}$	16.15 MPa	13.74 MPa	$\approx 1.10$
	$m_{dbl}$	0.95 MPa	0.81 MPa	$\approx 1.10$
Transverse stresses	Max, горен	0.31 MPa	0.36 MPa	0.86
	Max, долен	6.11 MPa	5.65 MPa	$\approx 1.00$

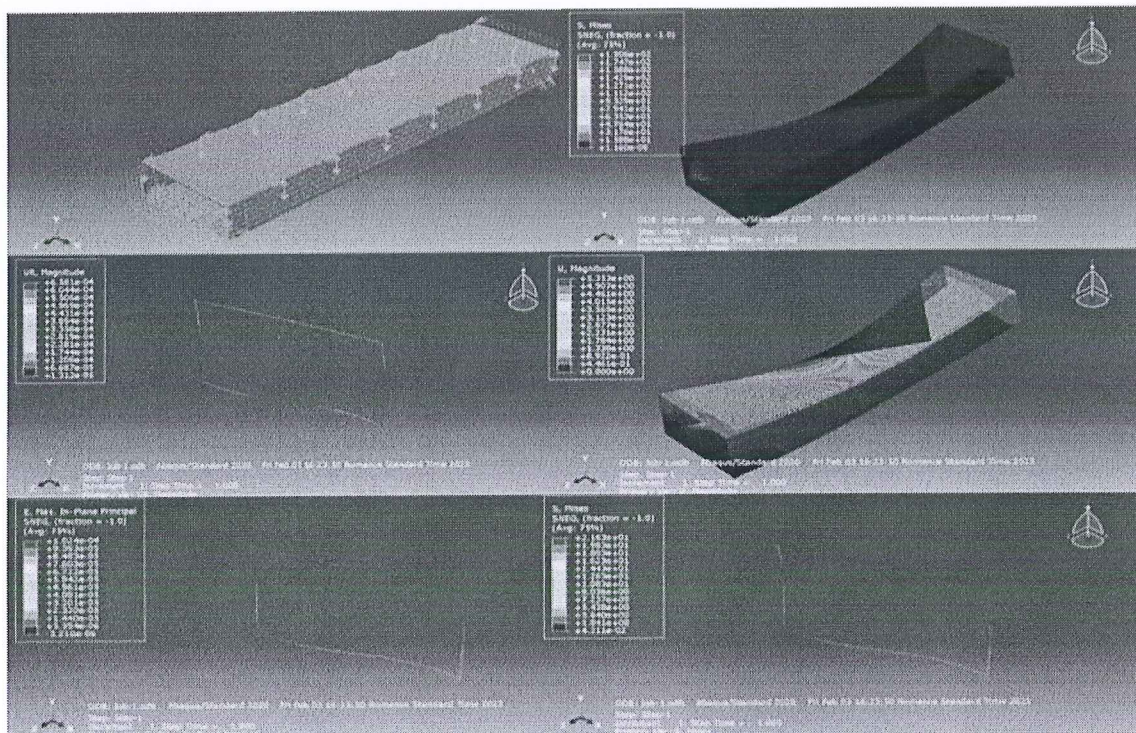


Figure 30 Response of the considered composite box girder cross-section under asymmetrical loading



## 5. ANALYSIS AND COMPARISON OF THE RESULTS

To conduct a comparative analysis focusing on deformability and distortion response within the girder's plane, an analysis was performed on a pure steel box girder which once again determines the influence of the stiffness characteristics of the cross-section on the overall distortion response. The cross-section will be deformed in relation to the original shape and will manifest out-of-plane warping under the effect of the distortion load and the so-called distortion angles will be formed in the corners, at the joints between the webs and the top and bottom flange respectively. During the analysis of steel or concrete box girders, it is typically assumed that all four distortion angles occurring at the four corners of the cross-section are equal. However, in composite box girders, the top concrete flange and the bottom steel flange deform at different angles due to their varying stiffness properties. This leads to two distinct distortion angles, each carrying different stress magnitudes. The shape that represents the distortion response provides insight into how differences in stiffness characteristics, arising from the composition of the box (composite vs. pure steel), impact the girder's behavior.

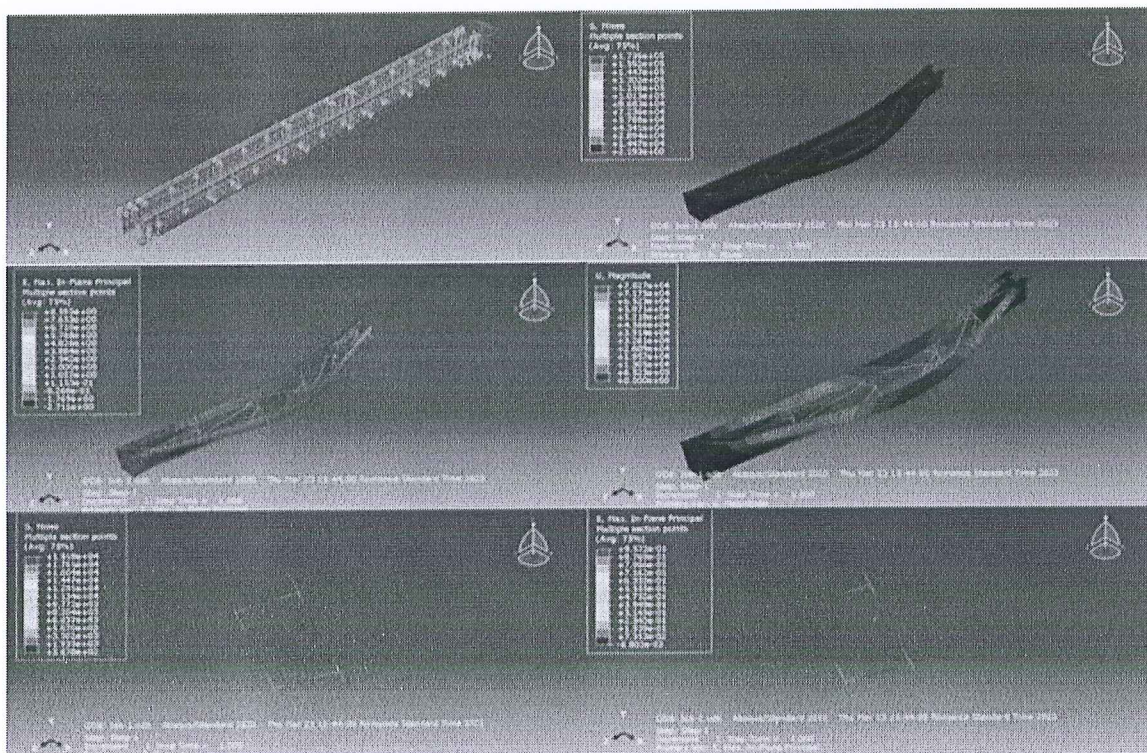


Figure 31 Response of the considered steel box girder cross-section under asymmetrical loading



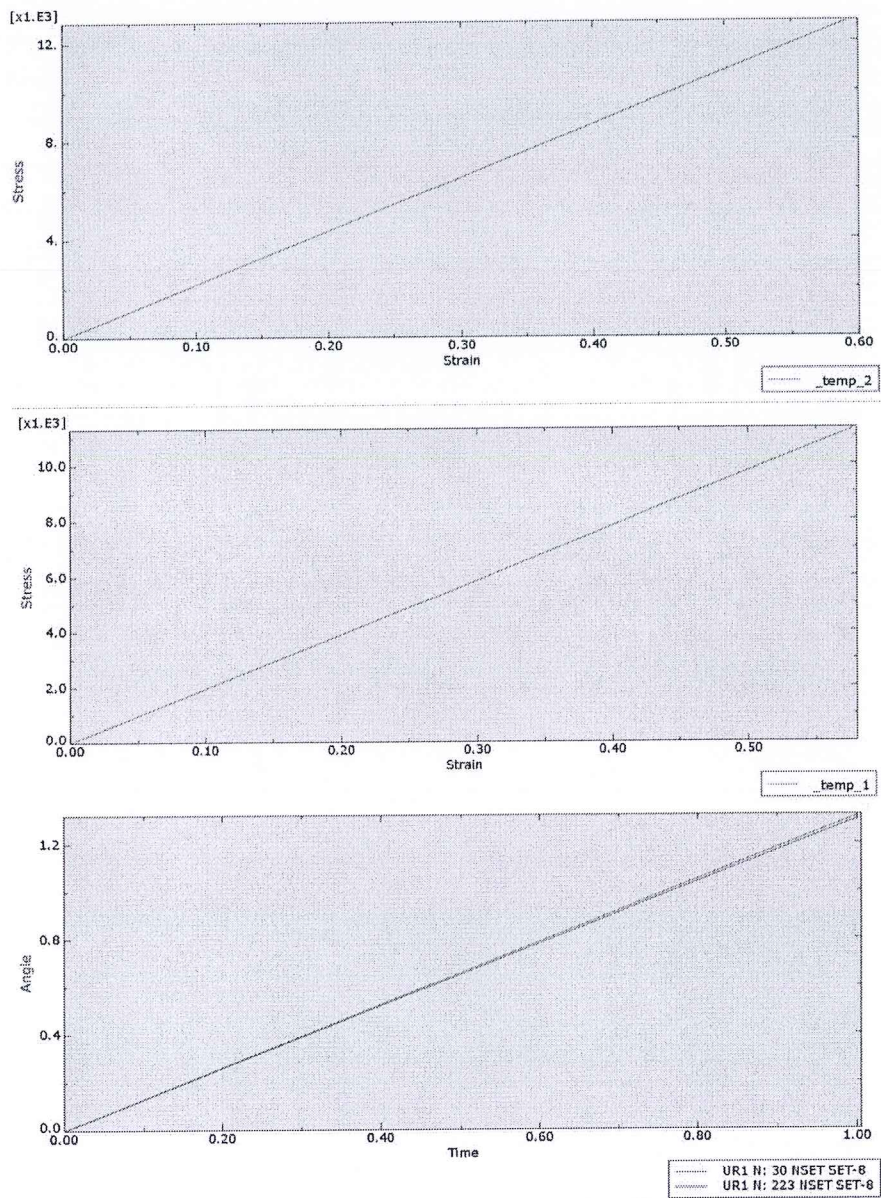


Figure 33 Diagram of stresses and manifested rotations in the key nodes of the considered steel box girder cross-section under asymmetrical loading - pure steel and composite node



## 6. CONCLUSIONS

---

This thesis is dedicated to investigating the behavior of composite box girders when subjected to asymmetric loading, leading to distortion. The complexity of this problem, coupled with the scarcity of studies addressing the distinct responses of composite girders, primarily stemming from differences in stiffness between pure and composite nodes, served as the driving force behind this analysis. To comprehensively understand the structural behavior, two distinct analytical methods were employed. One approach utilizes classical formulations, while the other relies on a mathematical model grounded in the finite element method.

By developing analysis methods, which are primarily rooted in analytical formulations for bending, torsion, and distortion, it becomes evident that despite the inherent simplifications and the complexity of the physical phenomenon, these approaches can offer greater relevance and clarity in the preliminary design phase. This is in contrast to finite element or surface element methods, which entail handling a substantial amount of data, thereby introducing a higher potential for errors.

The examination of bending, warping torsion, and distortion phenomena, including the specialized principles enabling the analysis of composite girders, and the utilization of solutions grounded in solving the fundamental equilibrium equation using the beam on elastic foundation analogy, which considers the influences of the structural stiffness characteristics of the box girder frame, highlights the importance of these phenomena in shaping the overall longitudinal and transverse behavior of the structure, both within and outside the plane of the girder itself.

Through the application of the proposed analytical method to a composite box girder cross-section under asymmetric loading, segmented into loading subsystems, and taking into account the varying stiffness characteristics between the pure steel node (web/bottom flange) and the composite node (web/top flange), on the overall stress distribution, the significant influence of these stiffness characteristics of the frame is evident. The observed differences in distortion angles, leading to distinct distortion stresses in the two nodes, reaffirm the necessity of incorporating node stiffness characteristics in the analysis of composite box girders.

To validate the analytical method and its results, a mathematical model was implemented in the "ABAQUS" software package. This model accounts for the deformations of the composite girder, including both longitudinal and transverse aspects, resulting in the determination of distortion angles, stresses, and longitudinal warping. The successful comparison between the analytical method and the results obtained through numerical simulation in "ABAQUS" confirms the accuracy and practicality of the proposed method.

In conclusion, the proposed method, which enables the calculation of distinct distortion angles for pure steel and composite nodes, proves its utility in analyzing the response of composite box girders. This approach, which considers the stiffness characteristics of the frame within the girder's cross-section, is essential due to the emergence of additional stresses resulting from distortion. These additional stresses, alongside those from transverse bending and St. Venant shear, include distortional normal stresses due to warping and transverse bending stresses caused by distortion. These stresses can be significant, and their response may rely on the deformable stiffness of the cross-section. Thus, for an accurate assessment of frame stiffness, all relevant parameters should be considered.



In summary, the method proposed in chapter 3.4.4 provides a practical analytical approach for defining the distortion behavior of composite box girders. It allows for a better understanding of stress distribution within composite box girders by considering the varying stiffness provided by the concrete slab.

Since the definition of the distortion angle is crucial in the definition of the distortional stiffness of the frame, the integration of the derivatives of the basic differential equation for the distortion problem is proposed for the bending curve of the top concrete and the bottom steel flange. The equation, on which the proposed method is based, described in chapter 3.4.4.5, was solved through the analogy- "Beam of Elastic Foundation".

To further validate the accuracy of the proposed method, a laboratory test using a 3D model at an appropriate scale is suggested. This test would provide the actual distortional deformation of the box girder and serve as additional confirmation of the reliability of the simplified analytical method for predicting the girder's response under distortion.



## LITERATURE

- [1] B.S.I. BS 5400 - Steel, concrete and composite bridges. Part 3: Code of practice for design of steel bridges (2004).
- [2] B.S.I. BS 5400 - Steel, concrete and composite bridges. Part 5: Code of practice for design of composite bridges (2005).
- [3] Bathe, K. J. (2016). ADINA System. ADINA R&D Inc.
- [4] Bebiano, R., Gonçalves, R., & Camotim, D. (2015). A cross-section analysis procedure to rationalise and automate the performance of GBT-based structural analyses. *Thin-Walled Structures*, 92, 29–47.
- [5] Benscoter, S. U. (1954). A theory of torsion bending for multicell beams. *Journal of Applied Mechanics*, 21(1), 25–34.
- [6] Brazão Farinha, J. S., & Correia dos Reis, A. (1993). *Tabelas Técnicas*. P.O.B.
- [7] Calgaro, J. A. Virlogeux, M. (1988). *Projet Et Construction Des Ponts: Analyse Structurale Des Tabliers de Ponts*. Paris. Presses de l'Ecole Nationale des Ponts et Chaussées.
- [8] Camotim, D., Basaglia, C., & Silvestre, N. (2010). GBT buckling analysis of thin-walled steel frames: a state-of-the-art report. *Thin-Walled Structures*, 48(10), 726–743
- [9] Castro, J. M., Elghazouli, A. Y., & Izzuddin, B. A. (2007). Assessment of effective slab widths in composite beams. *Journal of Constructional Steel Research*, 63(10), 1317–1327.
- [10] Chapman, J.C. Dowlin, P.J. Lim, P.T.K. and Billington, C.J. "The Structural Behaviour of Steel and Concrete Box" Girder Bridges. *The Structural Engineer*, Vol.49, March, 1971
- [11] Chen, Y. S., & Yen, B. T. (1980). *Analysis of Composite Box Girders*, March 1980. Fritz Laboratory Reports. Paper 447.
- [12] European Committee For Standardization. EN 1990:2002-A1. Eurocode - Basis of structural design. (2005).
- [13] European Committee For Standardization. NP EN 1990. Eurocódigo - Bases para o projeto de estruturas. Instituto Português da Qualidade (2009).
- [14] European Committee For Standardization. NP EN 1991-2. Eurocódigo 1 - Acções em estruturas. Parte 2: Acções de tráfego em pontes. Instituto Português da Qualidade (2005).
- [15] Fan, Z. T., & Helwig, T. A (2002). Distortional Loads and Brace Forces in Steel Box Girders. *Journal of Structural Engineering*, 128(6), 710–718.
- [16] Gonçalves, R. (2014). *Apresentações Power Point da Unidade Curricular de Lajes e Cascas*. Faculdade de Ciências e Tecnologias, Universidade Nova de Lisboa.
- [17] Gonçalves, R., Bebiano, R., & Camotim, D. (2014). On the Shear Deformation Modes in the Framework of Generalised Beam Theory. *Thin-Walled Structures*, 84, 325–334.
- [18] Gonçalves, R., & Camotim, D. (2010). Steel-concrete composite bridge analysis using Generalised Beam Theory. *Steel and Composite Structures*, 10(3), 223–243.
- [19] Gonçalves, R., Ritto-Corrêa, M., & Camotim, D. (2010). A new approach to the calculation of 81
- [20] cross-section deformation modes in the framework of generalized beam theory. *Computational Mechanics*, 46(5), 759–781.





- [21]Henriques, D., Gonçalves, R., & Camotim, D. (2015). A physically non-linear GBT-based finite element for steel and steel-concrete beams including shear lag effects. *Thin-Walled Structures*, 90, 202–215.
- [22]Hetenyi, M. (1979). *Beams on elastic foundation: Theory with applications in the fields of civil and mechanical engineering* (11th ed.). The University of Michigan Press.
- [23]Kollbrunner, C.F., & Basler, K. (1969). *Torsion in Structures*. Berlin/Heidelberg: Springer-Verlag.
- [24]Křístek, V. (2004). A Shear Lag Analysis for Composite Box Girders with Deformable Connectors. *Acta Polytechnica*, 44(5-6).
- [25]Kristek, V. "Theory of box girders, Wiley, New York, N.Y., USA, 1979.
- [26]Lamas, A. R. G. (1982). O problema do "shear lag" na análise de estruturas. Seminário 286. Lisboa.
- [27]Maisel, B. I., & Roll, F. (1974). Methods of analysis and design of concrete box beams with side cantilevers. Cement and Concrete Association. London. (No. 42.494 Tech Rpt.).
- [28]Mensinger M., Ndogmo J., Guoqing L. "Analysis on the distortional behavior of composite box girders", Germany, 2015.
- [29]Murray, Noel W. (1984). *Introduction to the theory of thin-walled structures*. Oxford [Oxfordshire] : Clarendon Press.
- [30]Nakai, H. and Yoo, C. H. "Analysis and Design of Curved Steel Bridges". McGraw-Hill Book Co., Inc., New York, N.Y., USA, 1988.
- [31]Pedro, J. J. O. (1995). *Distorção em tabuleiros de pontes em caixão. Influência no comportamento longitudinal*. Tese de Mestrado. Universidade Técnica de Lisboa.
- [32]Salama, T., & Nassif, H. H. (2011). Effective flange width for composite steel beams. *Journal of Engineering Research*, 8(1), 28–43.
- [33]Schardt, R. (1989). *Verallgemeinerte Technische Biegetheorie (Teoria Generalizada de Vigas)*. Berlin: Springer-Verlag.
- [34]Schlaich, J., & Scheef, H. (1982). *Concrete Box-Girder Brides*. Structural Engineering Documents IABSE, Stuttgart.
- [35]Silvestre, N., & Camotim, D. (2002). First-order generalised beam theory for arbitrary orthotropic materials. *Thin-Walled Structures*, 40(9), 791–820.
- [36]The MathWorks Inc. (2014). MATLAB (R2014b). The MathWorks Inc. Massachusetts.
- [37]Vlasov, V. Z. (1961). *Tonkostenye sterjni*, 2nd edn. Moscow, Russia (French translation: "Pièces Longues en Voiles Mince", Éditions Eyrolles, Paris, France, 1962): Fizmatgiz.
- [38]Wright, R. N., Abdel-Samed, S. R., & Robinson, A. R. (1968). BEF Analogy for Analysis of Box Girder Bridges. *Journal of the Structural Division*, 94.
- [39]Y.K.Cheung. (1976). *Finite Strip Method in Structural Analysis* (1st ed.). Pergamon Press.
- [40]Zienkiewicz, O. C., Taylor, R. L., & Zhu, J. Z. (2005). *The Finite Element Method Set*. Oxford: Butterworth-Heinemann.



## APPENDICES

### Appendix 1 Software output

An overview of the essential modeling steps and the results obtained from the analysis conducted in the "ABAQUS" software package is provided. The results focus on key nodes that are analyzed due to their varying stiffness characteristics.

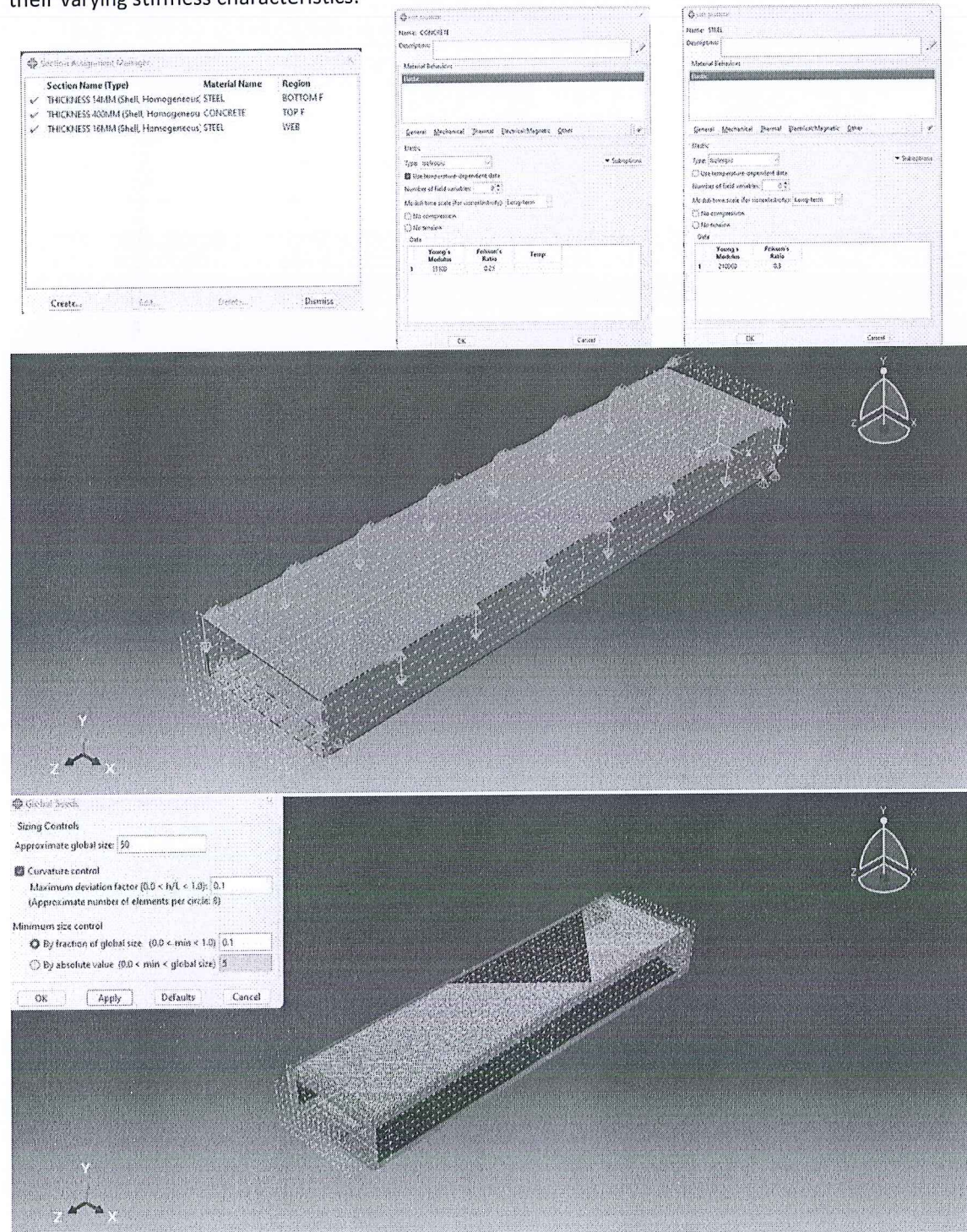


Figure 34 Input parameters, load and network formation for the mathematical model

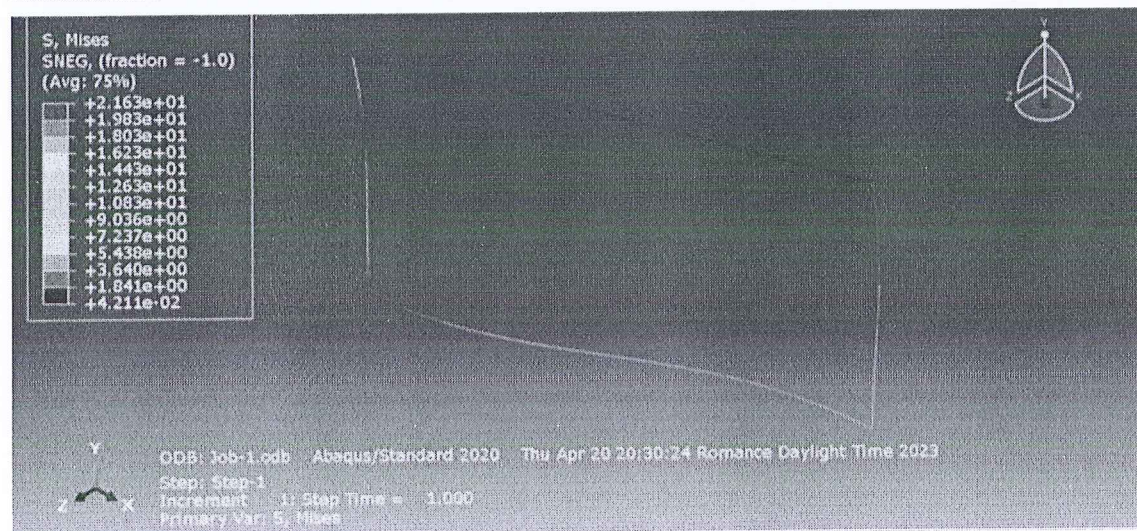
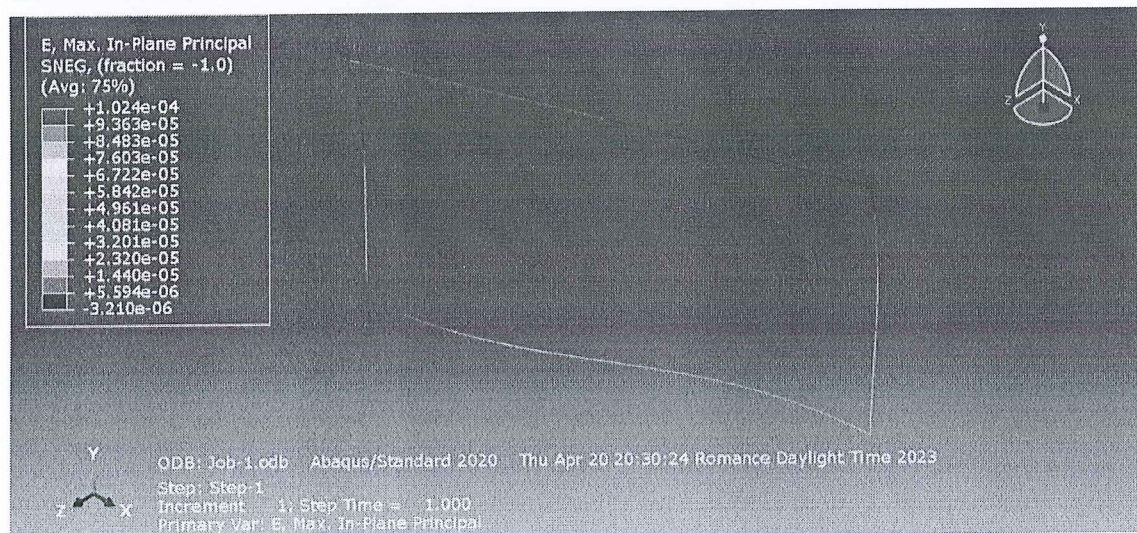
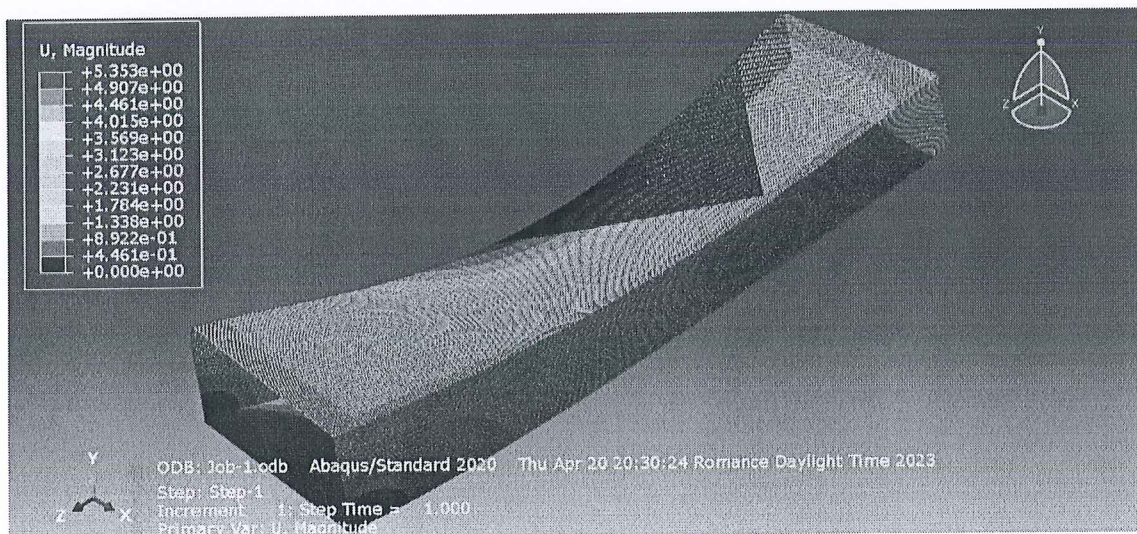


Figure 35 Girder response to the asymmetrical loading-longitudinal deflection, manifested strains and deformations at the cross-sectional level within its own plane



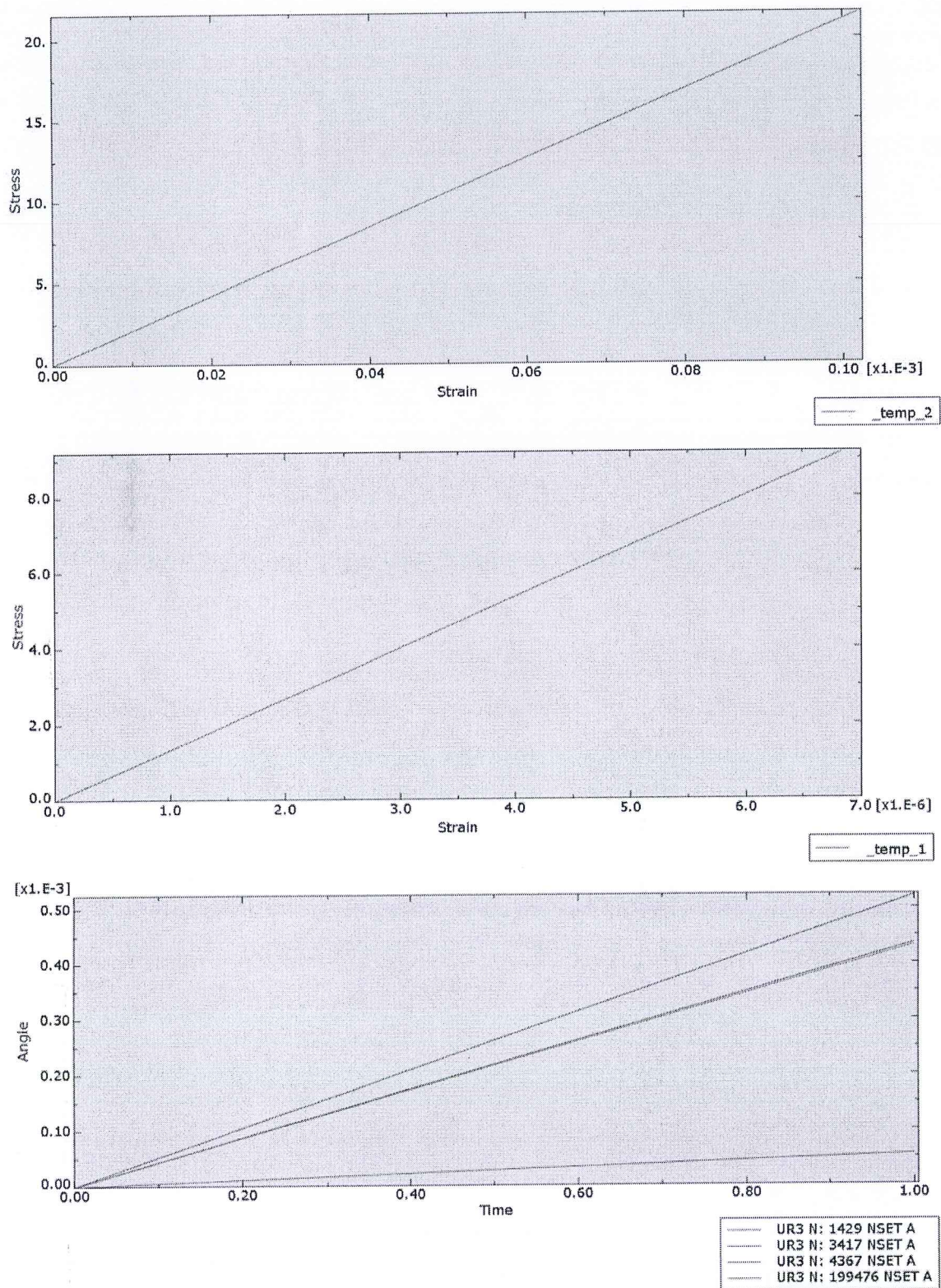


Figure 36 Diagram of stresses and manifested rotations in the key nodes of the considered steel box girder cross-section under asymmetrical loading - pure steel and composite node



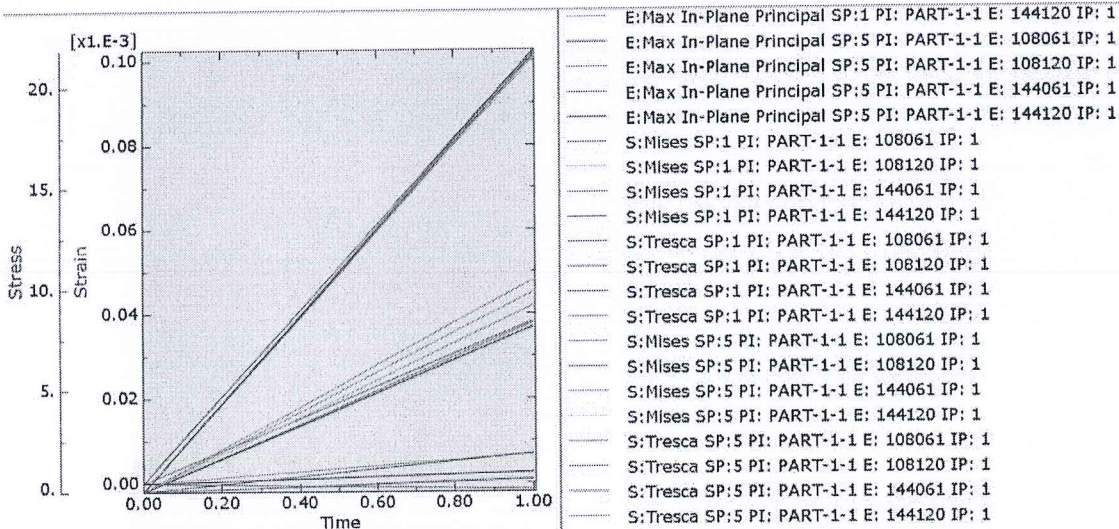
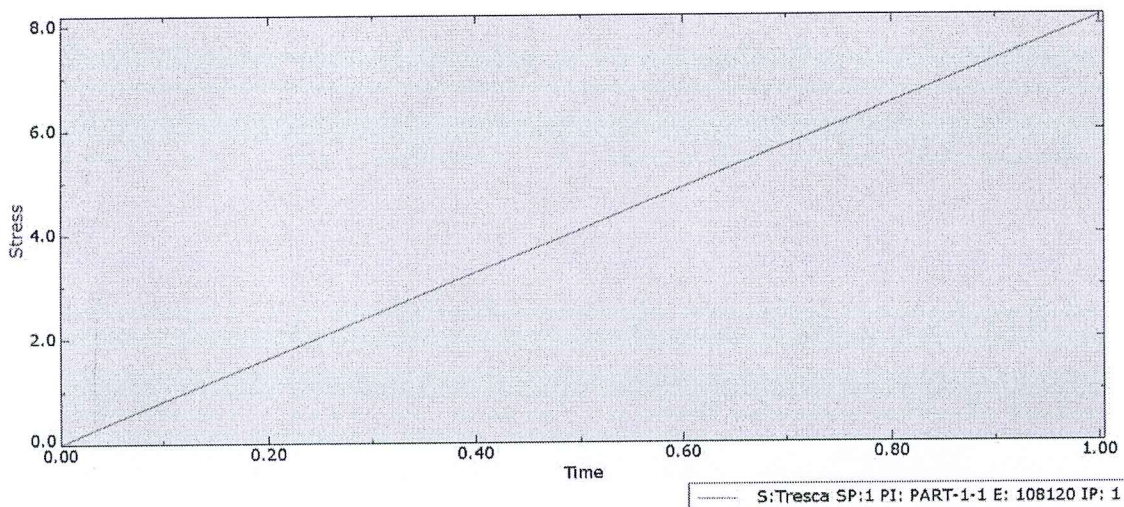
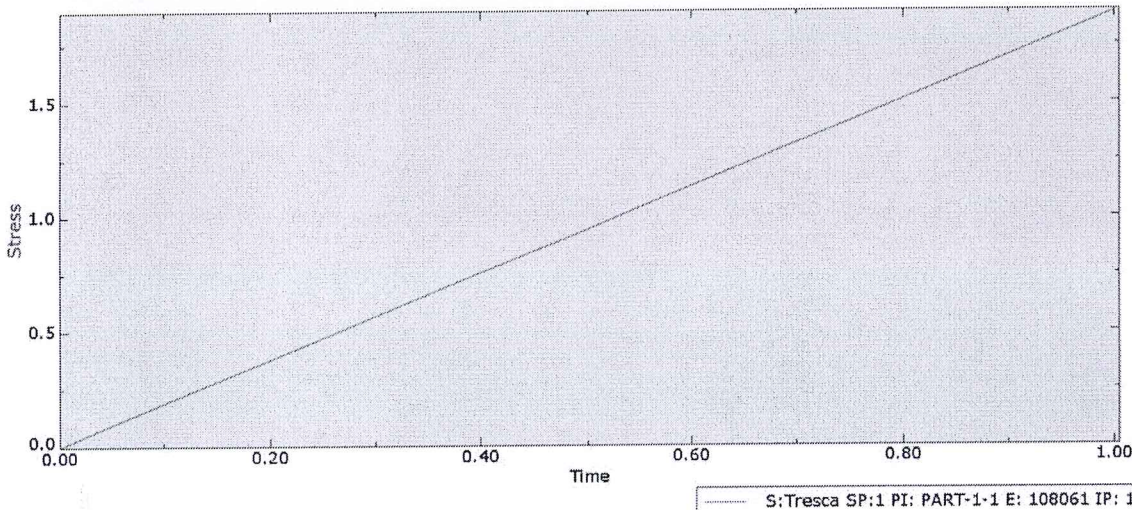


Figure 37 Diagram of stresses and manifested rotations and strains in the key nodes of the considered steel box girder cross-section under asymmetrical loading - pure steel and composite node



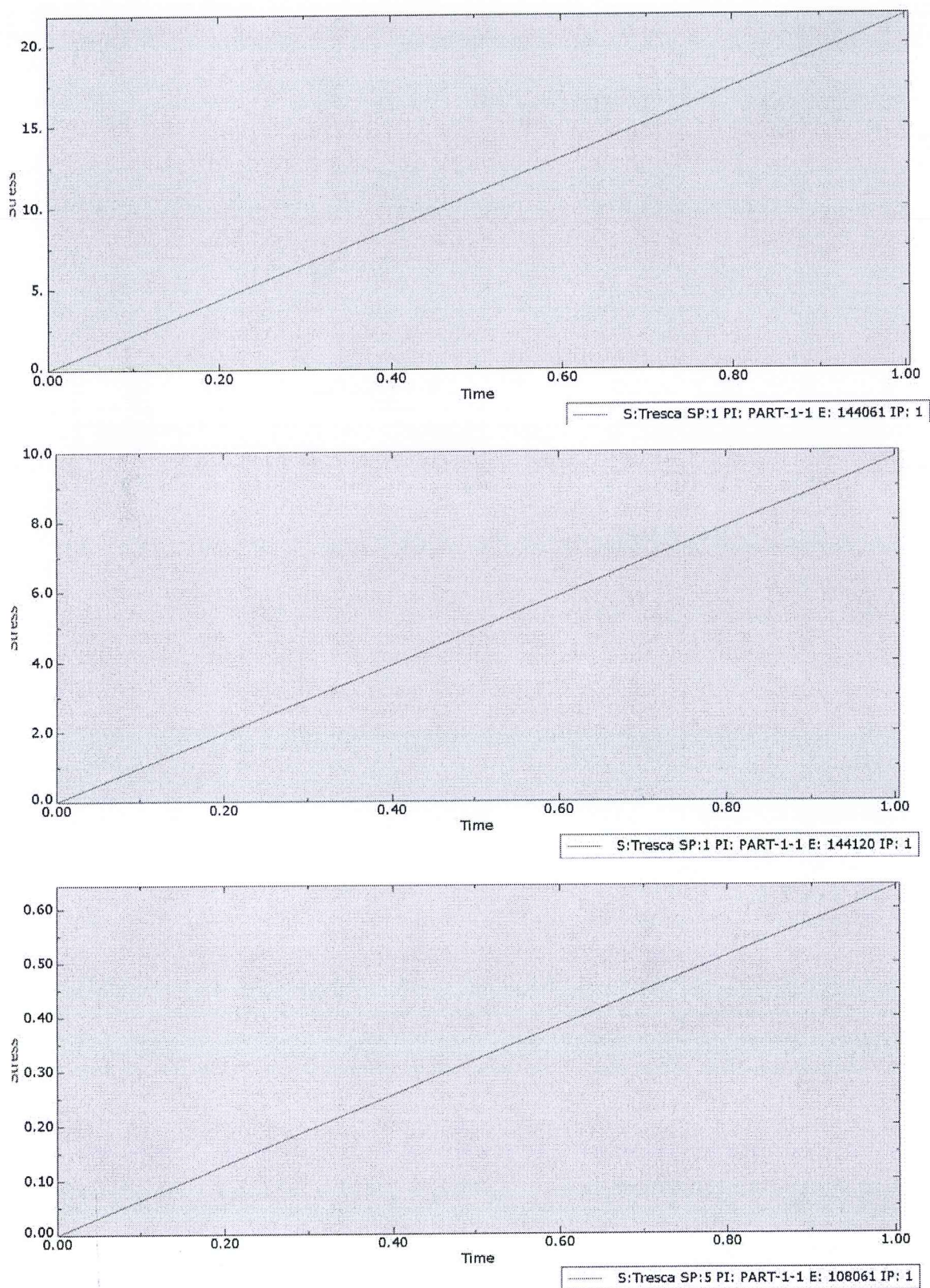


Figure 38 Diagram of shear stresses in the key nodes of the considered steel box girder cross-section under asymmetrical loading - pure steel and composite node



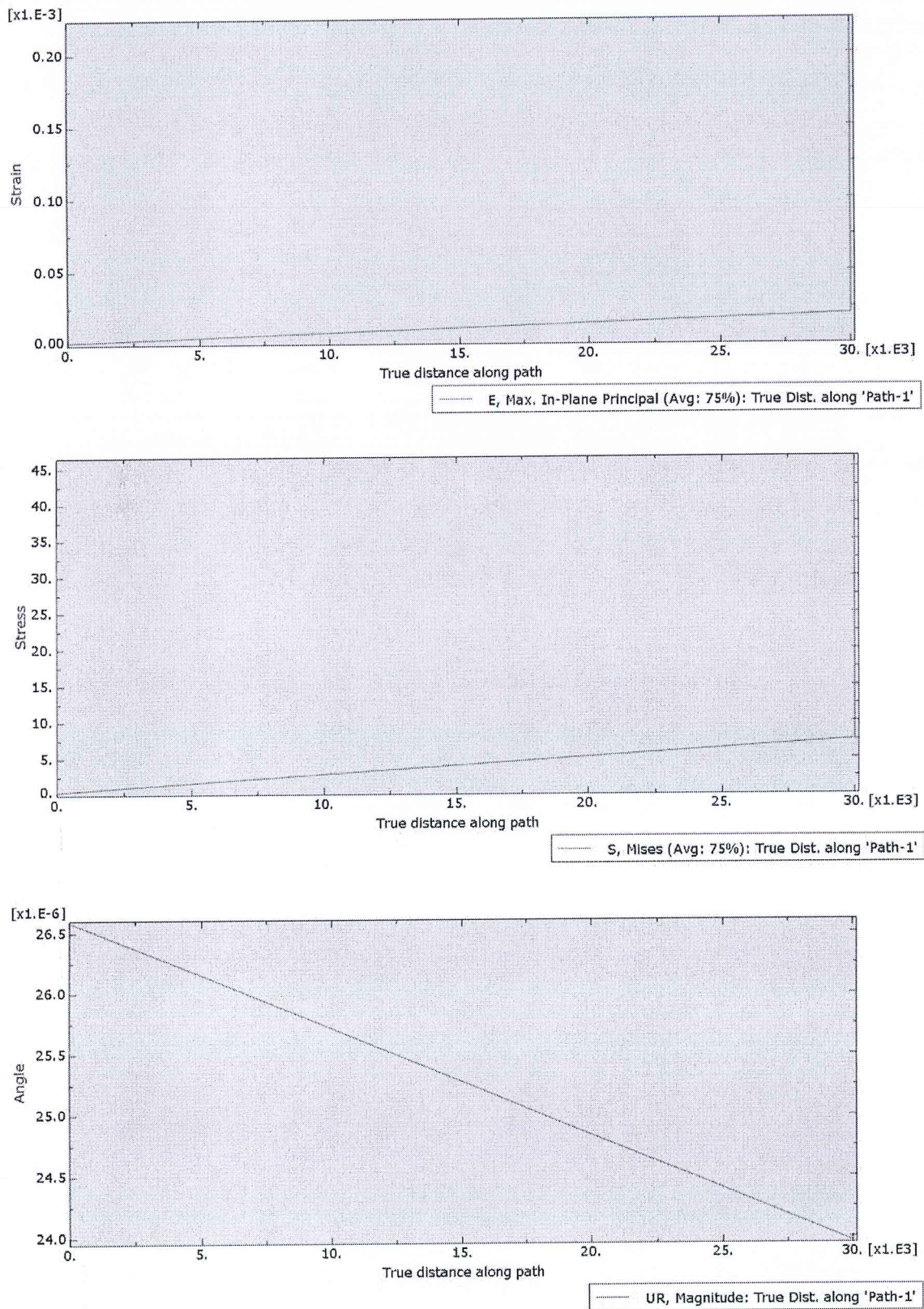


Figure 39 Diagram of the strain change, stresses and rotations in the node-steel flange/steel web along the length of the span of the considered steel box girder cross-section under asymmetrical loading



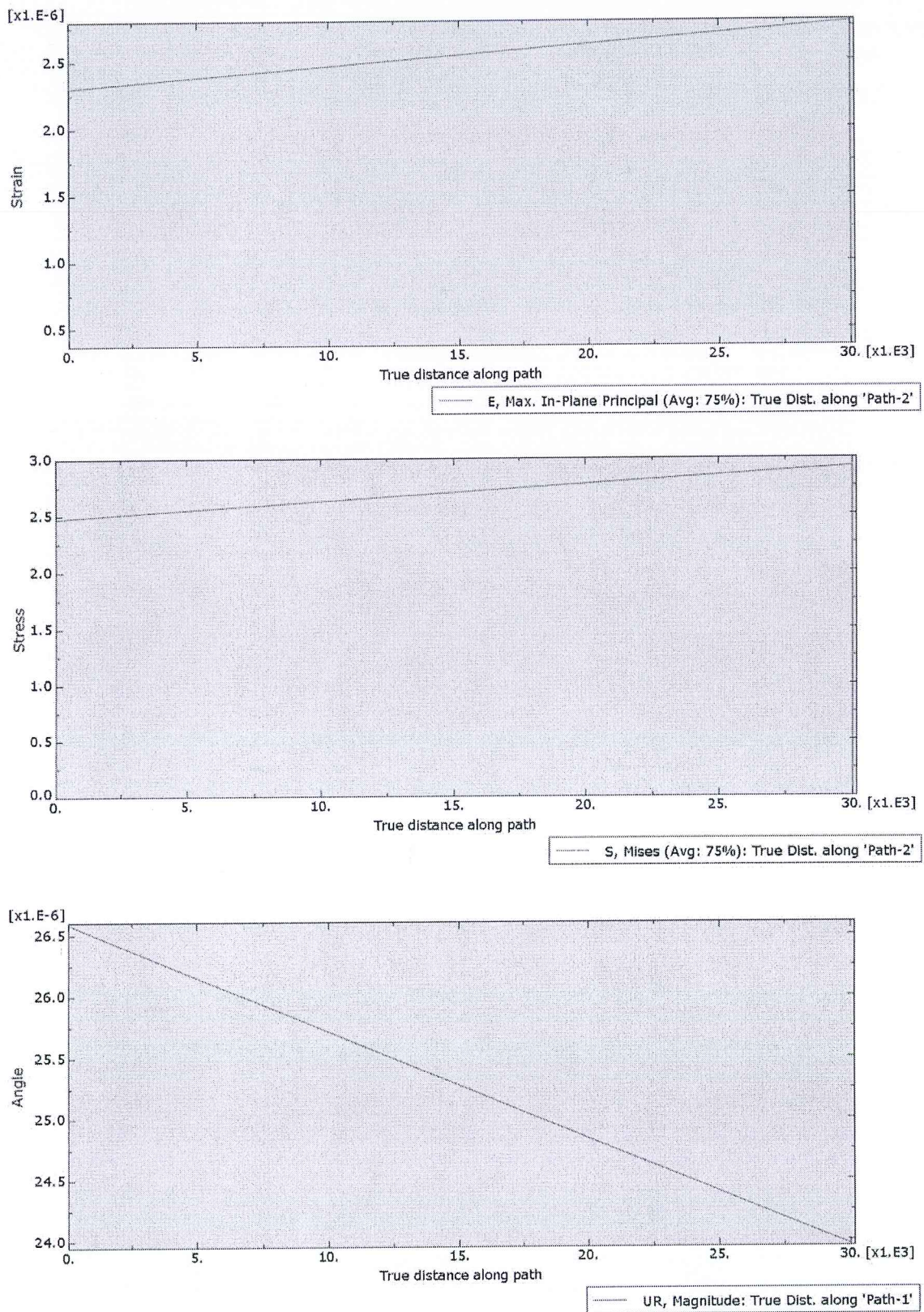


Figure 40 Diagram of the strain change, stresses and rotations in a node-concrete flange/steel web along the length of the span of the considered steel box girder cross-section under asymmetrical loading






Дека овој превод кој ми е поднесен на македонски јазик правилно и точно е преведен на англиски јазик тврдам со својот потпис и службен печат:

In witness that this translation of the above document which was originally submitted to me in Macedonian is correct I do affix my seal and signature:

Овластен Преведувач/ Certified Translator

  
Анета Трпковска/ Aneta Trpkovska



Датум/Date

11.09.2023

Скопје/Skopje

Овластен судски преведувач со решение бр. 08/1-1810/2002-2 издадено од Министерство за Правда – Скопје, Република Македонија и решение бр. 08-933/2 од 19.02.2020 издадено од Министерство за Правда, Република Северна Македонија

Certified court translator by the Decision No. 08/1-1810/2002-2 issued by the Ministry of Justice – Skopje, Republic of Macedonia, and Decision No. 08-933/2 as of 19.02.2020 issued by the Ministry of Justice, Republic of North Macedonia

Јас, НОТАР Снежана Видовска  
за подрачјето на основните судови на градот Скопје

Потврдувам дека овој превод е извршен од  
овластен судски преведувач Анета Трпковска, решение  
бр. 08/1-1810/2002-2 од Македонски јазик на Англиски  
јазик.

Нотарската такса за заверка по тарифен број 10  
т. 3 од Законот за судски такси во износ од 50 денари  
наплатена и поништена на примерокот кој останува за  
архивирање.

Нотарската награда е пресметана во износ од  
100 денари.

Број УЗП 6853/2023

Во Скопје 13.09.2023

